Boundary Integral Equations in Kinetic Plasma Theory

Dissertation

zur Erlangung des Grades des
Doktors der Naturwissenschaften (Dr. rer. nat.)
der Fakultät für Mathematik und Informatik
der Universität des Saarlandes

eingereicht von

Torsten Keßler, M. Sc.

Saarbrücken
2021

Tag des Kolloquiums:	13. Januar 2022
Dekan der Fakultät:	Prof. Dr. Thomas Schuster
Vorsitzender:	Prof. Dr. Martin Fuchs
1. Berichterstatter:	Prof. Dr. Sergej Rjasanow
2. Berichterstatterin:	Prof. Dr. Irene M. Gamba
3. Berichterstatter:	Prof. Dr. Eric Sonnendrücker
Akademischer Beisitzer:	Dr. Andreas Buchheit

Für meine Eltern, Dorette und Rainer,
und meinen Bruder Patrick

Abstract

In this thesis, we use boundary integral equations (BIE) as a powerful tool to gain new insights into the dynamics of plasmas. On the theoretical side, our work provides new results regarding the oscillation of bounded plasmas. With the analytical computation of the frequencies for a general ellipsoid we contribute a new benchmark for numerical methods. Our results are validated by an extensive numerical study of several three-dimensional problems, including a particle accelerator with complex geometry and mixed boundary conditions. The use of Boundary Element Methods (BEM) reduces the dimension of the problem from three to two, thus drastically reducing the number of unknowns. By employing hierarchical methods for the computation of the occurring nonlocal sums and integral operators, our method scales linearly with the number of particles and the number of surface triangles, where the error decays exponentially in the expansion parameter. Furthermore, our method allows the pointwise evaluation of the electric field without loss of convergence order. As we are able to compute the occurring boundary integrals analytically, we can precisely predict the electric field near the boundary. This property makes our method exceptionally well suited for the numerical simulation of plasma sheaths near irregular boundaries or of plasma-surface interaction such as etching of semiconductors.

Zusammenfassung

In der vorliegenden Arbeit nutzen wir Randintegralgleichungen als ein mächtiges Werkzeug, um neue Einsichten in die Dynamik von Plasmen zu gewinnen. Auf theoretischer Seite entwickelt diese Arbeit neue Resultate bezüglich der Oszillation beschränkter Plasmen. Durch die analytische Berechnung der Frequenzen im Fall eines allgemeinen Ellipsoids stellen wir ein neues Testbeispiel für numerische Methoden bereit. Unsere Resultate werden durch umfangreiche numerische Untersuchen dreidimensionaler Beispiele validiert, etwa einen Partikelbeschleuniger mit komplexer Geometrie und gemischten Randwerten. Mithilfe der Randelementmethode reduziert sich die Dimension des Problems von drei auf zwei, womit sich die Anzahl der Unbekannten drastisch reduziert. Dank der Nutzung hierarchischer Methoden zur Berechnung der auftauchenden nichtlokalen Summen und Integraloperatoren skaliert unsere Methode linear mit der Anzahl der Partikel und der Anzahl der Oberflächendreiecken, wobei der Fehler exponentiell im Entwicklungsparameter abfällt. Des Weiteren erlaubt unsere Methode die Berechnung des elektrischen Felds ohne Verringerung der Konvergenzordnung. Da wir die auftretenden Randintegrale analytisch berechnen können, können wir präzise Aussagen über das elektrische Feld nahe des Rands treffen. Dank dieser Eigenschaft ist unsere Methode außergewöhnlich gut geeignet, um Plasmaränder nahe irregulärer Ränder oder Plasma-Oberflächen-Interaktionen, etwa das Ätzen von Halbleitern, zu simulieren.

Contents

Preface

> Wer kann was Dummes, wer was Kluges denken, das nicht die Vorwelt schon gedacht?[1]
>
> *(Johann Wolfgang von Goethe)*

A plasma is a mixture of positively charged ions, electrons and neutral atoms that, unlike in neutrally charged gases, are able to move freely in space. Most of the observable mass in the universe is in the state of a plasma. In our solar system, the largest accumulation of plasma is the sun. At enormous temperature and pressure in its core atomic nuclei fuse, thus producing energy in form of electromagnetic waves that illuminate the earth. Regularly, the sun erupts plasma that is caught by the magnetic field of the earth and pushed towards the poles. There, the plasma interacts with the gas in the atmosphere and light at specific wavelengths is emitted, giving rise to the characteristic aurora. In August and September 1859, the earth was hit by an extreme eruption of plasma [35]. Auroras were observable over all of Europe, North America and as south as Cuba and Hawaii [36]. This solar storm massively disturbed the then recently established telegraphy system.

If used in a controlled environment, however, plasmas contributed to major scientific and technological breakthroughs in the last 150 years. With the invention of a powerful induction coil (an early transformer) by Rühmkorff in the 1850s [127, p. 69], scientists were able to investigate gas discharge plasmas that form between two coils. Without knowing that he was working with plasma, von Siemens found in 1857 that the discharge produced ozone when oxygen or air flows between coils. In his apparatus, the coils are placed outside the glass tube filled with gas, hence giving his method the name silent discharge [96].

Today, gas discharge plasmas are employed in a wide range of applications [11]: Surface modification such as etching in the semiconductor industry, different kind of lasers, e.g. the He-Ne laser, electrodeless lamps with long lifetime, and, until a few years ago, in plasma display panels. The ozone synthesised with von Siemens' method is used to purify water, e.g. if it is biologically contaminated. This invention marks the beginning of plasma medicine, a branch of clinical medicine that is concerned with applications of plasmas for medical treatment [163]. In plasma spectroscopy [103] one exploits that the constituents of a particle beam emit light at characteristic wavelengths when directly injected in a plasma, making it possible to determine composition of the particle beam.

Perhaps the most challenging problem nowadays in plasma physics is the controlled fusion inside a hydrogen plasma with the ultimate goal to produce energy. To that end, it is necessary to confine the plasma by strong magnetic fields and to heat it to several million Kelvin. The understanding of a plasma under these extreme conditions and the ability to control it require the joint effort of theoretical and experimental physicists as well as engineers around the world. Supported by 35 countries, scientists work at ITER in Saint-Paul-lès-Durance, France,[2] the world's

[1] "Who can think something stupid, who can think something smart that previous generations did not already think?"

[2] `https://www.iter.org/`

largest nuclear fusion reactor of tokamak type, with the aim to produce more electric power than it consumes. At the same time, different fusion reactor designs are investigated, most notably the stellarator Wendelstein 7-X (W7-X), located in Greifswald, Germany.[3] In recent experiments with W7-X, the hydrogen plasma reached a temperature of around twenty million Kelvin and lasted more than one hundred seconds [117].

A curious application of plasmas are loudspeaker. Usually, the sound is generated by an oscillating membrane. Owing to the large inertia of the membrane compared to air, the produced tones are smeared over neighbouring frequencies. Plasma speakers mitigate this unpleasant effect. The oscillation of a membrane is replaced by a plasma with direct contact to the surrounding air. By applying an alternating current of varying frequency, the plasma oscillates, hence thrusting the nearby air. We notice these density variations of the air as sound. A pioneer in this field was the Saarlander Otto Braun.[4] His "High-fidelity-Studio" in Saarbrücken, where he was working on his plasma speakers since the 1960s, was well known to audio enthusiasts beyond Saarland. A regular visitor of Braun's studio in the 1980s I spoke with praised the outstanding audio quality of the plasma speaker, saying that he had never experienced such a clear replay of music with other devices.

The wide range of applications of plasmas presented above make it impossible to treat them all with a single model. In this thesis, we focus on the Vlasov–Poisson system, a mathematical model for plasmas with typical speed much smaller than the speed of light and where the generated magnetic fields are negligible. For its theoretical analysis and numerical treatment, we combine two well-established tools from different fields, namely the particle discretisation for kinetic equations and boundary integral equations for the solution of (elliptic) boundary value problems. As we shall see, this approach provides new ways for the theoretical study of plasmas and enriches the family of numerical methods for the Vlasov–Poisson system, in particular, if effects near the boundary are important.

[3] `https://www.ipp.mpg.de/w7x`

[4] Otto Braun was born on 10 July 1928 and died on 23 July 2020, aged 92 years [157].

List of Publications and Joint Publication Statement

This thesis is a revised version of the publication

> [95] T. Keßler, S. Rjasanow, and S. Weißer. "Vlasov–Poisson System Tackled by Particle Simulation Utilizing Boundary Element Methods". In: *SIAM J. Sci. Comput.* 42 (2020), B299–B326,

except for the work on plasma oscillations in Chapter 5 and Section 6.1, which has not been published yet. Furthermore, I have published two articles together with my supervisor Prof. Sergej Rjasanow in the field of kinetic equations,

> [93] T. Keßler and S. Rjasanow. "Fully conservative spectral Galerkin-Petrov method for the inhomogeneous Boltzmann equation". In: *Kinet. Relat. Mod.* 12 (2019), pp. 507–549,
>
> [94] T. Keßler and S. Rjasanow. "Limit model for the Vlasov–Maxwell system with strong magnetic fields via gyroaveraging". In: *St. Petersb. Math. J.* 32 (2021), pp. 753–765,

and two articles together with my colleague Andreas Buchheit, regarding the connection between sums and integrals over functions with singularities,

> [26] A. A. Buchheit and T. Keßler. *Singular Euler–Maclaurin expansion.* 2020. arXiv: 2003.12422 [math.NA]. In review,
>
> [27] A. A. Buchheit and T. Keßler. *Singular Euler–Maclaurin expansion on multidimensional lattices on multidimensional lattices.* 2021. arXiv: 2102.10941 [math.NA]. In review.

The results of [26] are summarised in an invited blog posting on Wolfram Blog.[1]

In accordance to the Plagiarism Policy of the Faculty of Mathematics and Computer Science of Saarland University, Revision 2020-01-15, I now discuss the individual contributions to [95]: The initial idea to combine the particle discretisation with Boundary Element Methods (BEM) is due to Sergej Rjasanow. I developed a first three-dimensional implementation of the method and wrote an initial draft of the paper. Steffen Weißer and I discussed possible test cases and jointly interpreted the results. Furthermore, Steffen Weißer wrote most of the section on BEM in the final version of the article. I wrote the remaining part of the article, following the advice of Prof. Sergej Rjasanow and Steffen Weißer. The research on plasma oscillations is motivated by a conversation with Giovanni Manfredi who, without a proof, told me that a ball of electronic plasma oscillates with a frequency of $\omega_p/\sqrt{3}$, where ω_p denotes the plasma frequency.

[1] https://blog.wolfram.com/2021/06/30/the-singular-euler-maclaurin-expansion-a-new-twist-to-a-centuries-old-problem/

Acknowledgements

I am indebted to Sergej Rjasanow for giving me the possibility to pursue a PhD under his supervision. With his great experience he guided my development to an independent researcher, encouraging me to publish and to present my work early on. In our joint teaching and the organisation of conferences he taught me what is additionally important to be successful in academics.

I thank Richards Grzibovskis and Christian Michel for their superb teaching of Boundary Element Methods and hierarchical methods that went far beyond what is found in textbooks.

I am grateful to Steffen Weißer for the time he devoted to my mathematical education since my undergraduate studies and for the fantastic collaboration on our joint publication.

I thank Andreas Buchheit and Daniel Seibel for reading all or parts of my thesis and for making valuable suggestions as well as for their friendship that was deepened by the collaboration on joint publications and joint travel to conferences in various European cities.

I owe thanks to several people outside Saarland University: To George Wilkie for insightful discussions on plasma physics and numerical methods for kinetic equations, to Giovanni Manfredi for drawing my attention to plasma oscillations, to Stefan Steinerberger for helpful discussions on the concavity of the Newton potential and for pointing me to the Fraenkel asymmetry and to Jan Dillenkofer for his help on multithreading.

I am grateful to Irene Gamba for inviting me to Oden Institute in Austin, Texas, USA and for her great hospitality. I thank Irene Gamba and Michael Abdelmalik for many inspiring discussions on numerical methods for the Boltzmann equation during my time in Austin and via video chat afterwards.

Finally, I owe my family my immense gratitude for their support and their interest in my work. I appreciate every attempt of my parents, my brother, my aunts, my uncle or my grandmothers to grasp the content of the thesis. I hope that after reading the Abstract and the Preface and maybe the Introduction you understand a good deal of my work!

1. Introduction

> Den Hrn. D'Alembert halte ich für einen grossen mathematicum in abstractis; aber wenn er einen incursum macht in mathesin applicatam, so höret alle estime bey mir auf [...] und wäre es oft besser für den realen physicam, wenn keine Mathematik auf der Welt wäre.[1]
>
> *(Daniel Bernoulli [60])*

By heating a gas, the negative and positive charges comprising the neutral atoms are separated and a new state of matter arises, a plasma. Owing to the conservation of electric charge, the plasma has total charge equal to zero. If the length scale on which we observe the plasma, e.g. the width of an electric trap used to confine the plasma, is much larger then its internal length scale, known as Debye length, the plasma is almost neutral locally, meaning that the charge densities of the positively and negatively charged constituents are almost equal in most of the parts of the plasma. This condition is known as quasineutrality. The resulting nonvanishing charge density ϱ gives rise to an electric field $\boldsymbol{E}$ according to Gauß' law,

$$\operatorname{div} \boldsymbol{E} = \frac{1}{\varepsilon_0}\varrho,$$

with the vacuum permittivity ε_0. In the absence of boundaries the electric field reads

$$\boldsymbol{E}(\boldsymbol{x}) = \frac{1}{4\pi\varepsilon_0}\int_{\mathbb{R}^3} \frac{\boldsymbol{x}-\boldsymbol{y}}{|\boldsymbol{x}-\boldsymbol{y}|^3}\varrho(\boldsymbol{y})\,\mathrm{d}\boldsymbol{y}, \quad \boldsymbol{x} \in \mathbb{R}^3,$$

if we ignore the magnetic field generated by electric current. The form of $\boldsymbol{E}$ highlights the second important property of a plasma, namely its collective behaviour [31, Chapter 1]. For a bounded subset Ω of the plasma with total charge Q and centre of charges $\boldsymbol{x}_0$, the electric field in the farfield reads

$$\boldsymbol{E}_\infty(\boldsymbol{x}) = \frac{Q}{4\pi\varepsilon_0}\frac{\boldsymbol{x}-\boldsymbol{x}_0}{|\boldsymbol{x}-\boldsymbol{x}_0|^3}, \quad \boldsymbol{x} \in \mathbb{R}^3 \setminus \Omega.$$

Now, the average of $\boldsymbol{E}_\infty$ over a solid angle $A \subseteq S^2$ is constant,

$$\frac{1}{|A|}\int_A r^2 \boldsymbol{E}_\infty(\boldsymbol{x}_0 + r\boldsymbol{e})\,\mathrm{d}S_{\boldsymbol{e}} = \frac{Q}{4\pi\varepsilon_0}\frac{1}{|A|}\int_A \boldsymbol{e}\,\mathrm{d}S_{\boldsymbol{e}},$$

for any radius $r > 0$. Therefore, a change in the charge distribution in B affects all parts of the plasma. In contrast to the interaction of neutral particles which is short-ranged and is thus local in space, the interaction of the charged particles inside the plasma is nonlocal.

[1] "I consider Mr. D'Alembert to be a great mathematicum in abstractis; but if he makes an incursum in mathesin applicatam, then all esteem stops with me [...] and it would often be better for the real physicam if there were no mathematics in the world."

There are numerous mathematical models for the evolution of plasmas. Fluid models are among the most most accessible descriptions of plasma dynamics. Here, the state of the plasma is described by few macroscopic quantities such as (number) density, velocity and temperature. Their time evolution is governed by conservation laws similar to those of classical fluid dynamics. The inherent problem of fluid models is that the equations involve quantities such as the diffusion coefficients which cannot be computed within the model but need to be provided by a general theory, the kinetic theory. In contrast to the fluid models, the state of the plasma comprising the species S is described by a scalar function f_s for each $s \in S$, called (particle) distribution function of the species s. For a time $t > 0$ it is defined on the six-dimensional phase space $\mathbb{R}^3 \times \mathbb{R}^3$ of positions $\boldsymbol{x} \in \mathbb{R}^3$ and velocities $\boldsymbol{v} \in \mathbb{R}^3$,

$$f_s : (0,\infty) \times \mathbb{R}^3 \times \mathbb{R}^3 \to [0,\infty),\ (t,\boldsymbol{x},\boldsymbol{v}) \mapsto f_s(t,\boldsymbol{x},\boldsymbol{v}).$$

For a region $A \times B \subseteq \mathbb{R}^3 \times \mathbb{R}^3$ in phase space, the integral

$$\int_A \int_B f_s(t,\boldsymbol{x},\boldsymbol{v}) \,\mathrm{d}\boldsymbol{v}\,\mathrm{d}\boldsymbol{x}$$

equals the number of particles of species s in A with velocities in B at the time $t > 0$. Consequently,

$$\varrho(t,\boldsymbol{x}) = \sum_{s\in S} q_s \int_{\mathbb{R}^3} f_s(t,\boldsymbol{x},\boldsymbol{v})\,\mathrm{d}\boldsymbol{v}, \quad \boldsymbol{j}(t,\boldsymbol{x}) = \sum_{s\in S} q_s \int_{\mathbb{R}^3} \boldsymbol{v}\, f_s(t,\boldsymbol{x},\boldsymbol{v})\,\mathrm{d}\boldsymbol{v},$$

are the total charge and current density of the plasma, where q_s denotes the particle charge of species s. The distribution function evolves according to a collisionless Boltzmann equation,

$$\partial_t f_s + \boldsymbol{v}\cdot\nabla_{\boldsymbol{x}} f_s + \frac{1}{m_s}\boldsymbol{F}_s(t,\boldsymbol{x},\boldsymbol{v})\cdot\nabla_{\boldsymbol{v}} f_s = 0, \tag{1.1}$$

where m_s is the particle mass of species s and $\boldsymbol{F}_s$ is the Lorentz force exerted by all particles in the plasma on particles of species s,

$$\boldsymbol{F}_s(t,\boldsymbol{x},\boldsymbol{v}) = q_s\big(\boldsymbol{E}(t,\boldsymbol{x}) + \boldsymbol{v}\times\boldsymbol{B}(t,\boldsymbol{x})\big),$$

for the particle charge q_s. The electromagnetic fields $(\boldsymbol{E},\boldsymbol{B})$ are computed from $(\varrho,\boldsymbol{j})$ by Maxwell's equations or approximations thereof, most notably the Darwin approximation [43] and the electrostatic approximation [42]. For the latter, $\boldsymbol{B} = \boldsymbol{0}$ and $\boldsymbol{E} = -\nabla\phi$, where the electric potential ϕ is the solution of

$$-\Delta\phi = \frac{1}{\varepsilon_0}\varrho, \tag{1.2}$$

supplied with the decay condition $\phi(\boldsymbol{x}) \to 0$ for $|\boldsymbol{x}| \to \infty$. Equations (1.1) and (1.2) constitute the Vlasov–Poisson system. In case the plasma is confined to a bounded domain, the system is augmented with boundary conditions for the distribution function and the electric potential. We discuss this in Section 2.3. The Vlasov–Poisson system first appeared in the works of Jeans on the dynamics of star clusters at the beginning of the 20th century and was independently applied by Vlasov to plasma physics at the end of the 1930s [84]. Writing N for the total number of particles,

$$N = \sum_{s\in S} \int_{\mathbb{R}^3}\int_{\mathbb{R}^3} f_s(t,\boldsymbol{x},\boldsymbol{v})\,\mathrm{d}\boldsymbol{v}\,\mathrm{d}\boldsymbol{x},$$

which is a conserved quantity under time evolution, the electric field reads

$$\boldsymbol{E}(t,\boldsymbol{x}) = N\frac{1}{N}\sum_{s\in S}\frac{q_s}{4\pi\varepsilon_0}\int_{\mathbb{R}^3}\int_{\mathbb{R}^3}\frac{\boldsymbol{x}-\boldsymbol{y}}{|\boldsymbol{x}-\boldsymbol{y}|^3}f_s(t,\boldsymbol{x},\boldsymbol{v})\,\mathrm{d}\boldsymbol{v}\,\mathrm{d}\boldsymbol{y}.$$

Here, the term

$$\frac{q_s}{4\pi\varepsilon_0}\frac{\boldsymbol{x}-\boldsymbol{y}}{|\boldsymbol{x}-\boldsymbol{y}|^3}f_s(t,\boldsymbol{y},\boldsymbol{v})$$

is the electric field density generated by particles of the species s at $\boldsymbol{y}$ with velocity $\boldsymbol{v}$, evaluated at $\boldsymbol{x}$. Consequently, $\boldsymbol{E}$ is proportional to the average over the electric fields of the particles in the plasma. That is why the Vlasov–Poisson system is known as the mean field limit of the particle dynamics. We shall review this in more detail in Section 2.3. Since the interaction $(\boldsymbol{x}-\boldsymbol{y})|\boldsymbol{x}-\boldsymbol{y}|^{-3}$ is only weakly singular, i.e. the negative power of the singularity for $\boldsymbol{x}=\boldsymbol{y}$ is smaller than the space dimension, the integral average is well-defined at all points, in particular where the field of an individual particle would be not defined. Therefore, the mean-field limit of the electric field provides a regularisation for the nearfield with the assumption of quasineutrality, however, without sacrificing the long-range character of the interaction and hence the collective behaviour of the plasma.

Owing to the quadratic nonlinearity in the Vlasov–Poisson system, analytic solutions are rare. We thus have to rely on numerical approximations, see [44] for a review. To represent f in a computer[2] at a fixed time $t>0$, we would first sample $f(t,\boldsymbol{x},\cdot)$ in each direction at 200 points. Storing the result as floating point numbers with double precision requires 8×200^3 B ≈ 61 MiB, which is unproblematic on today's hardware. To obtain full information on f at time t, we need to repeat the sampling procedure at several points in space. Using 200 points per direction, the total size sums up to 8×200^6 B $= 476\,837$ GiB. This raises our memory requirements from the cell phone in our pocket to the world's largest supercomputers like *Stampede2*, operated by the Texas Advanced Computing Center in Austin, TX, USA. Its 4200 Intel Xeon Phi Knights Landing compute nodes provide in total 470 400 GiB [153, Table 1], so that a typical discretisation of f at one time point occupies all of *Stampede2*'s memory.

This unfavourable memory scaling is a major problem for semi-Lagrangian schemes [143], see [128] for a recent review and [100] for a discussion of semi-Lagrangian schemes with applications on supercomputers, where the numerical approximation of the distribution function is interpolated on a grid in phase space after advection steps in space and velocity. One remedy is to split the six-dimensional advection steps into several lower-dimensional ones [52, 53]. Another possibility is to exploit low-rank tensor approximations of the particle density function on the computational grid that reduce the memory requirements of the scheme [99, 101], see also [50].

Discontinuous Galerkin methods [45, 83, 111] use piecewise polynomials to approximate the distribution function in phase space. By varying the grid size and the polynomial degree, a reduction of degrees of freedom is possible in regions where the distribution function is smooth. Moreover, the update rule per time step is local in phase space and thus is scalable on massively parallel devices, e.g. GPUs [51].

Since the Vlasov–Poisson system is the mean field limit of the particle dynamics in the plasma, it is tempting to approximate the distribution function by a finite sample of computational particles, known as macroparticles. The use of particle methods for the numerical simulation of plasmas can be traced back to as early as 1962 [38], see [39] for a historic and [160] for a

[2]Here and in the following, we suppress the species indices.

more recent review. In contrast to real particles, macroparticles represent the motion of a large collection of real particles. Their interaction should be consistent with the long-range interaction in the plasma and, at the same time, with the regularisation introduced by the mean field limit. This is usually accomplished via the particle-in-cell method [9]. Here, the macroparticles evolve according to Newton's laws[3] and only the acceleration of each particle needs to be computed. To that end, a grid in space is introduced on which the electric field is computed, thus reducing the six-dimensional phase space to a three-dimensional problem. This grid acts as moderator between the particles. First, the charges of the particles are interpolated on the grid by evaluating a rescaled (first order) B-spline at the grid points. This amounts to the regularisation of the Dirac distribution, the singular point charge distribution, by a spline function. The scaling is chosen such that in the limit of vanishing grid size, the Dirac distribution is recovered. Owing to the compact support of the B-splines, this regularisation is local in space. In a next step, the electric field is approximated on the grid by a standard solver for the Poisson equation, e.g. finite difference, finite element or spectral methods. Implicit in this step is the global influence of the local charge distribution, as the computation involves the solution of a linear system of equations, or in case of Fourier-based spectral methods, the use of global basis functions. Afterwards, the electric field is extrapolated from the grid onto the particle positions.

The use of boundary integral equations and their numerical approximation by Boundary Element Methods (BEM) for the solution of the Poisson equation makes the regularisation in the nearfield and the long-range character of the interaction explicit [34, 95]. In Fig. 1.1, we sketch

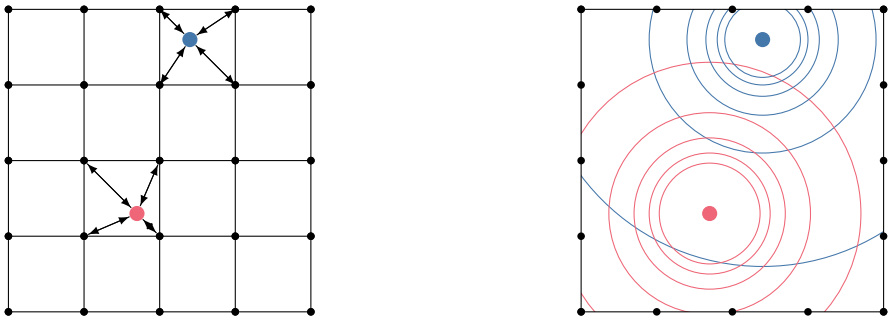

Figure 1.1.: Schematic comparison of the computation of the electric field for the particle-in-cell method on the left and using BEM on the right. In the particle-in-cell method, the interaction of the particles is moderated by the grid and the electric field is interpolated from nearby grid points. In case of BEM, the particles interact via a regularised Coulomb force and a harmonic correction to the field is constructed only requiring the values of the particle field on the boundary.

the different approaches to the field computation for the particle-in-cell method and for the field computation using BEM. The electric potential ϕ is sought as a superposition of the regularised particle fields plus a harmonic function ϕ_0 to account for boundary conditions,

$$\phi(\boldsymbol{x}) = \frac{1}{4\pi\varepsilon_0} \sum_{i=1}^{n_p} q_i \int_{\mathbb{R}^3} \frac{\delta^\sigma_{\boldsymbol{x}_i}(\boldsymbol{y})}{|\boldsymbol{x}-\boldsymbol{y}|} \,\mathrm{d}\boldsymbol{y} + \phi_0(\boldsymbol{x}). \tag{1.3}$$

Here, n_p denotes the total number of particles and q_i the charge of the ith particle at $\boldsymbol{x}_i$. Its regularised charge distribution is given by $\delta^\sigma_{\boldsymbol{x}_i}$, a function with integral equals one and,

[3] For f given by a sum of Dirac distributions, the Vlasov equation is equivalent to Newton's laws, see Lemma 2.1.

additionally, such that for $\sigma \to 0$, it converges to the Dirac distribution supported at $\boldsymbol{x}_i$. It is noteworthy that ϕ is always a (weak) solution of the Poisson equation,

$$-\Delta\phi = \frac{1}{\varepsilon_0} \sum_{i=1}^{n_p} q_i \delta^\sigma_{\boldsymbol{x}_i},$$

so the only approximation error of BEM is in the traces of ϕ on the boundary.

If $\delta^\sigma_{\boldsymbol{x}_i}$ has compact support and is rotationally invariant around $\boldsymbol{x}_i$, the integrals on the right hand side of (1.3) agree with the Coulomb potential,

$$\frac{q_i}{|\boldsymbol{x} - \boldsymbol{x}_i|}, \quad i = 1, \dots, n_p,$$

outside any sufficiently large ball centred at $\boldsymbol{x}_i$,[4] so the regularisation of the Coulomb field obeys the same scaling in the farfield as the field of point charges. If furthermore, $\delta^\sigma_{\boldsymbol{x}_i}$ is square-integrable, the regularised Coulomb potential is continuous.[5] In Lemma 3.43 we review a particular choice of $\delta^\sigma_{\boldsymbol{x}}$ for which is regularised Coulomb interaction is Lipschitz continuous.

It is crucial that the correction ϕ_0 can be computed using solely the data of the potential on the boundary. First, this means that we only have to discretise the boundary, thus reducing the dimension of the problem from three to two. Second, as we shall later see, $\nabla\phi_0$ obeys a similar scaling as the regularised Coulomb field of the particles,

$$|\nabla\phi_0(\boldsymbol{x})| = \mathcal{O}\big(R^{-2}\big),$$

where R denotes the distance of $\boldsymbol{x}$ to the boundary. Third, boundary formulation allows the evaluation of $\nabla\phi$ at any point in the domain with no loss of order of convergence compared to a point evaluation of ϕ. Thus BEM offer a very good accuracy per degree of freedom for the evaluation of the electric field, in particular in comparison with finite element methods.

This thesis is organised as follows. In Chapter 2 we review how the Vlasov–Poisson system is derived from the microscopic particle dynamics and discuss the possibility to write the electric potential as a function of its boundary traces by means of representation formula. Chapter 3 begins with a review of the necessary function spaces to derive the boundary integral equations discretised by BEM later in this chapter. We develop BEM with a particular emphasis on its later application to plasma dynamics. Hierarchical methods, presented in Chapter 4, are a standard approximation technique to accelerate computations while preserving the long-range character of the original formulation. Our analysis of plasma oscillations in Chapter 5 is a first example of the fruitful application of boundary integral equations in kinetic plasma theory, both from an analytical and numerical point of view. In Chapter 6, we validate our approach in a string of numerical examples. We conclude this thesis in Chapter 7 and give an outlook on future research topics.

[4] Without loss of generality we may assume $\boldsymbol{x}_0 = \boldsymbol{0}$. Outside any sufficiently large ball, the integral is a rotationally symmetric harmonic function and thus has to be of the form $C/|\boldsymbol{x}| + D$. The decay of the integral for $|\boldsymbol{x}| \to \infty$ implies $D = 0$ and $C = 1$ follows by taking the limit $|\boldsymbol{x}| \to \infty$ of $|\boldsymbol{x}|$ times the integral.

[5] In this case, the regularised Coulomb potential resides in $H^2_{\mathrm{loc}}(\mathbb{R}^3)$ by Theorem 3.40 which, by the Sobolev embedding theorem [67, p. 158], is a subspace of the continuous functions on $\mathbb{R}^3$.

2. Many Particle Dynamics

> The word "plasma" will be used to designate that portion of an arc-type discharge in which the densities of ions and electrons are high but substantially equal.
>
> *(Irving Langmuir and Lewi Tonks [156])*

To understand the assumptions that lead us to the Vlasov–Poisson system for the description of plasma dynamics, we begin with the general relativistic treatment of charged particle dynamics in Section 2.1. Afterwards, we turn to the electrostatic approximation of the Maxwell–Lorentz system in Section 2.2 where we also motivate the use of boundary integral operators to represent the electric field. The final step towards the Vlasov–Poisson system is a specific mean limit procedure discussed in Section 2.3. We close this chapter with a nondimensionalisation of the Vlasov–Poisson equation in Section 2.4.

2.1. Maxwell–Lorentz System

A system of n particles with positions $\boldsymbol{x}_1, \dots, \boldsymbol{x}_n$, charges $q_1, \dots, q_n$ and masses $m_1, \dots, m_n$ evolves according to

$$\begin{aligned} \dot{\boldsymbol{x}}_i(t) &= \frac{1}{m_i} \boldsymbol{p}_i(t), \\ \dot{\boldsymbol{p}}_i(t) &= q_i \Big(\boldsymbol{E}\big(t, \boldsymbol{x}_i(t)\big) + \boldsymbol{v}_i(t) \times \boldsymbol{B}\big(t, \boldsymbol{x}_i(t)\big) \Big), \end{aligned} \tag{2.1}$$

for any time $t > 0$ and $i = 1, \dots, n$, see [145, p. 14] or [105, § 17]. The velocities and momenta are coupled nonlinearly,

$$\boldsymbol{v}_i = \gamma(\boldsymbol{p}_i / m_i)^{-1} \frac{\boldsymbol{p}_i}{m_i}, \quad i = 1, \dots, n,$$

where γ is the Lorentz factor,

$$\gamma(\boldsymbol{p}/m) = \sqrt{1 + \frac{|\boldsymbol{p}|^2}{m^2 c_0^2}},$$

and c_0 is the speed of light. The electromagnetic fields $(\boldsymbol{E}, \boldsymbol{B})$ are the solutions of Maxwell's equations,

$$\begin{aligned} \operatorname{div} \boldsymbol{E} &= \frac{1}{\varepsilon_0} \sum_{j=1}^{n} q_j \delta_{\boldsymbol{x}_j}, \quad \operatorname{div} \boldsymbol{B} = 0, \\ \partial_t \boldsymbol{E} + \mathbf{curl}\, \boldsymbol{B} &= \boldsymbol{0}, \quad \partial_t \boldsymbol{B} + \varepsilon_0 \mu_0 \mathbf{curl}\, \boldsymbol{E} = \mu_0 \sum_{j=1}^{n} q_j \boldsymbol{v}_j \delta_{\boldsymbol{x}_j}. \end{aligned} \tag{2.2}$$

Here, ε_0, μ_0 are the vacuum permittivity and permeability, respectively. They are related to the speed of light by

$$c_0 = \frac{1}{\sqrt{\varepsilon_0 \mu_0}}.$$

With $\delta_{\boldsymbol{x}}$, $\boldsymbol{x} \in \mathbb{R}^3$, we denote the Dirac distribution which equals the point evaluation at $\boldsymbol{x}$,

$$\langle \varphi, \delta_{\boldsymbol{x}} \rangle = \varphi(\boldsymbol{x})$$

for a continuous function $\varphi : \mathbb{R}^3 \to \mathbb{R}$.

Because Maxwell's equation are linear, the collective fields are given as the sum of the individual fields $\big((\boldsymbol{E}_i, \boldsymbol{B}_i)\big)_{i=1}^n$. These are known as the Liénard–Wiechert fields [129, Chapter 19],

$$\begin{aligned} \boldsymbol{E}_i(t,\boldsymbol{x}) &= \frac{q_i}{4\pi\varepsilon_0}\Bigg((1 - \boldsymbol{v}_i^2/c_0^2)\frac{(\widehat{\boldsymbol{r}}_i - \boldsymbol{v}_i/c_0)}{(1 - \widehat{\boldsymbol{r}}_i \cdot \boldsymbol{v}_i/c_0)^3 |\boldsymbol{x} - \boldsymbol{x}_i|^2} \\ &\qquad + \frac{\widehat{\boldsymbol{r}}_i \times [(\widehat{\boldsymbol{r}}_i - \boldsymbol{v}_i/c_0) \times \dot{\boldsymbol{v}}_i/c_0]}{(1 - \widehat{\boldsymbol{r}}_i \cdot \boldsymbol{v}_i/c_0)^3 |\boldsymbol{x} - \boldsymbol{x}_i|} \Bigg)\Bigg|_{t\,=\,t_i^{\mathrm{ret}}}, \\ \boldsymbol{B}_i(t,\boldsymbol{x}) &= \frac{\widehat{\boldsymbol{r}}_i}{c_0} \times \boldsymbol{E}_i(t,\boldsymbol{x})\Big|_{t\,=\,t_i^{\mathrm{ret}}}, \end{aligned} \tag{2.3}$$

where

$$\widehat{\boldsymbol{r}}_i = \frac{\boldsymbol{x} - \boldsymbol{x}_i(t_i^{\mathrm{ret}})}{|\boldsymbol{x} - \boldsymbol{x}_i(t_i^{\mathrm{ret}})|}.$$

The retarded time t_i^{ret} is the solution of the nonlinear equation

$$t_i^{\mathrm{ret}} = t - \frac{|\boldsymbol{x} - \boldsymbol{x}_i(t_i^{\mathrm{ret}})|}{c_0},$$

which reflects the finite propagation speed of the electromagnetic fields. The computation of t_i^{ret} is very difficult and generally no closed form solution can be found. Note that t_i^{ret} may be negative, so it does not suffice to prescribe initial conditions for the positions and momenta to get a well-posed initial value problem. For the system (2.1)-(2.2) to be well-defined, the time axis has to be extended to $(-\infty, \infty)$ and, therefore, includes the whole history of the system [41]. Latter discussion excludes self-interaction, i.e. the acceleration of a particle by its own retarded electromagnetic fields. Classical electrodynamics predicts exponential divergence of the particle velocity by self-forces, incompatible with practical experience [145, Chapter 3.3]. Feynman, Leighton, and Sands [56, Chapter 28] discuss physical consequences of this singularity and review some attempts to resolve this issue.

2.2. Limit of Small Velocities

If the velocities of the particles are much smaller than c_0 and light travels the maximum distance

$$\max_{i,j=1,\dots,n} |\boldsymbol{x}_i - \boldsymbol{x}_j|$$

in a time much smaller than the typical time scale of the particle system, then

$$\gamma \approx 1, \quad t_i^{\mathrm{ret}} \approx t,\ i = 1, \dots, n.$$

This means we are ignoring all effects that are caused by the finite propagation speed of $(\boldsymbol{E}, \boldsymbol{B})$. Setting $\boldsymbol{v}_i/c_0 = \boldsymbol{0}$ in the electric field (2.3) yields

$$\boldsymbol{E}_i(t,\boldsymbol{x}) = \frac{q_i}{4\pi\varepsilon_0}\frac{\widehat{\boldsymbol{r}}_i(t)}{|\boldsymbol{x}-\boldsymbol{x}_i(t)|^2},$$

which is parallel to $\widehat{\boldsymbol{r}}_i(t)$, so

$$\boldsymbol{B}_i(t,\boldsymbol{x}) = \frac{\widehat{\boldsymbol{r}}_i(t)}{c_0} \times \boldsymbol{E}_i(t,\boldsymbol{x}) = \boldsymbol{0}$$

for all $i = 1,\dots,n$. These fields are the solution to the electrostatic approximation of Maxwell's equations,

$$\operatorname{div} \boldsymbol{E} = \frac{1}{\varepsilon_0}\sum_{j=1}^{n} q_j \delta_{\boldsymbol{x}_j}, \quad \mathbf{curl}\, \boldsymbol{E} = \boldsymbol{0}. \tag{2.4}$$

The equations of motion read

$$\begin{aligned} \dot{\boldsymbol{x}}_i(t) &= \boldsymbol{v}_i(t), \\ \dot{\boldsymbol{v}}_i(t) &= \frac{q_i}{m_i}\boldsymbol{E}(t,\boldsymbol{x}_i(t)), \end{aligned} \tag{2.5}$$

for $i = 1,\dots,n$. Because $\mathbf{curl}\, \boldsymbol{E} = \boldsymbol{0}$, there exists a scalar function ϕ, called (electric) potential, with $\boldsymbol{E} = -\nabla\phi$. Therefore, (2.4) is equivalent to

$$-\Delta\phi = \frac{1}{\varepsilon_0}\sum_{j=1}^{n} q_j \delta_{\boldsymbol{x}_j}, \quad \boldsymbol{E} = -\nabla\phi. \tag{2.6}$$

Supplemented with the decay condition

$$\phi(\boldsymbol{x}) \to 0, \quad |\boldsymbol{x}| \to \infty,$$

the unique solution of (2.6) is

$$\phi(\boldsymbol{x}) = \frac{1}{\varepsilon_0}\sum_{j=1}^{n} q_j U(\boldsymbol{x}-\boldsymbol{x}_j),$$

where U is the fundamental solution of the Laplace operator,

$$U(\boldsymbol{z}) = \frac{1}{4\pi|\boldsymbol{z}|}, \quad \boldsymbol{z} \in \mathbb{R}^3 \setminus \{\boldsymbol{0}\}.$$

If the particles are contained in a bounded domain $\Omega \subseteq \mathbb{R}^3$, the decay condition on ϕ is replaced by some boundary conditions on $\Gamma = \partial\Omega$. As a model problem, we consider a Dirichlet boundary value problem with datum g,

$$\begin{cases} -\Delta\phi = \dfrac{1}{\varepsilon_0}\displaystyle\sum_{j=1}^{n} q_j \delta_{\boldsymbol{x}_j} & \text{in } \Omega, \\ \phi = g & \text{on } \Gamma. \end{cases}$$

The solution is constructed similar to the free space equation (2.6),

$$\phi(\boldsymbol{x}) = \frac{1}{\varepsilon_0}\sum_{j=1}^{n} q_j G(\boldsymbol{x}, \boldsymbol{x}_j) + \int_\Gamma \boldsymbol{n}(\boldsymbol{y}) \cdot \nabla_{\boldsymbol{y}} G(\boldsymbol{x}, \boldsymbol{y}) g(\boldsymbol{y}) \, \mathrm{d}S_{\boldsymbol{y}}, \tag{2.7}$$

where $\boldsymbol{n}$ denotes the outward normal vector field to Ω and G is the Green function of the Laplace operator in Ω with Dirichlet boundary conditions,

$$\begin{cases} -\Delta G(\cdot, \boldsymbol{y}) = \delta_{\boldsymbol{y}} & \text{in } \Omega, \\ G(\cdot, \boldsymbol{y}) = 0 & \text{on } \Gamma. \end{cases}$$

It can be written as $G(\boldsymbol{x}, \boldsymbol{y}) = U(\boldsymbol{x} - \boldsymbol{y}) + \widetilde{U}_{\boldsymbol{y}}(\boldsymbol{x})$, where $\widetilde{U}_{\boldsymbol{y}}$ is the solution of

$$\begin{cases} -\Delta \widetilde{U}_{\boldsymbol{y}} = 0 & \text{in } \Omega, \\ \widetilde{U}_{\boldsymbol{y}} = -U(\cdot - \boldsymbol{y}) & \text{on } \Gamma. \end{cases}$$

Even though properties such as symmetry, $G(\boldsymbol{x}, \boldsymbol{y}) = G(\boldsymbol{y}, \boldsymbol{x})$ [55, p. 35] and the singular Laplacian, $-\Delta G(\cdot, \boldsymbol{y}) = \delta_{\boldsymbol{y}}$, turn G into an ideal replacement for $U(\cdot - \cdot)$ in case of bounded domains, its definition make it infeasible for a computational treatment of boundary value problems. That is because each point evaluation of G requires to solve a boundary value problem and easily computable expressions for G are available only for certain simple geometries such as balls or half spaces.

Therefore, we use an equivalent representation for ϕ, called representation formula,

$$\phi(\boldsymbol{x}) = \frac{1}{\varepsilon_0}\sum_{j=1}^{n} q_j U(\boldsymbol{x} - \boldsymbol{x}_j) + \int_\Gamma U(\boldsymbol{x} - \boldsymbol{y}) \psi(\boldsymbol{y}) \, \mathrm{d}S_{\boldsymbol{y}} + \int_\Gamma \boldsymbol{n}(\boldsymbol{y}) \cdot \nabla U(\boldsymbol{x} - \boldsymbol{y}) \, g(\boldsymbol{y}) \, \mathrm{d}S_{\boldsymbol{y}}, \tag{2.8}$$

where ψ denotes the unknown normal derivative of ϕ on Γ. We shall see in Section 3.3.5 how to solve for ψ by means of boundary integral equations. Above formulation has the advantage that the geometry enters only through the domain of integration; the rest is purely formulated in terms of the easily computable fundamental solution U. Once we know ψ, we can evaluate ϕ and its derivatives of arbitrary order inside Ω, in particular the gradient $\nabla\phi$ which we need to compute the acceleration of the particles.

2.3. Mean Field Limit and Vlasov Equation

In a real plasma, the number of particles n usually exceeds 10^{20}. This makes a direct treatment of (2.5) infeasible. Furthermore, the trajectories of every single particle are often not of interest as they do not tell us how the plasma behaves on a global (macroscopic) scale. Collective effects are hidden in the large sum (2.8) and cannot be observed by tracing the trajectories of single particles. Thus, we bundle physical particles in so-called macroparticles, or marker, such that

- the system of macroparticles has the same total mass and total charge as the original particle system,
- a macroparticle represents a specific species in the plasma, i.e. the charges and masses are the same for all physical particles represented by the macroparticle.

For our analysis, we assume that the plasma consists of a single species with charge q_0 and mass m_0. From now on, n denotes the number of macroparticles and $\big((\boldsymbol{x}_i, \boldsymbol{v}_i)\big)_{i=1}^n$ refer to the trajectories of the macroparticles. The total energy of the system of macroparticles is

$$H = \frac{1}{2}\widetilde{m}\sum_{i=1}^{n}|\boldsymbol{v}_i|^2 + \frac{1}{2\varepsilon_0}\widetilde{q}^2\sum_{\substack{i,j=1\\ j\neq i}}^{n} U(\boldsymbol{x}_i - \boldsymbol{x}_j)$$

where $\widetilde{q}, \widetilde{m}$ are the charge and mass of a macroparticle, respectively. We assume that, initially, the plasma is located in an open and bounded set $\Omega \subseteq \mathbb{R}^3$. With n_0, we denote its initial number density, i.e. the average number of particles per cubic metre. The total number of physical particles is thus given by $n_0|\Omega|$. In view of the definition of the macroparticles, we choose

$$\widetilde{q} = \frac{q_0}{n} n_0|\Omega|, \qquad \widetilde{m} = \frac{m_0}{n} n_0|\Omega|.$$

This scaling is known as pulverisation limit [123, Chapter 3]. The equations of motions are then given by

$$\begin{aligned} \dot{\boldsymbol{x}}_i &= \boldsymbol{v}_i, \\ \dot{\boldsymbol{v}}_i &= -\frac{1}{n}\frac{n_0|\Omega|q_0^2}{\varepsilon_0 m_0}\sum_{\substack{j=1\\ j\neq i}}^{n} \nabla_{\boldsymbol{x}_i} U(\boldsymbol{x}_i - \boldsymbol{x}_j), \end{aligned} \tag{2.9}$$

for $i = 1, \dots, n$. In contrast to the full particle description, the macroparticles are not accelerated by the superposition of the inner-particle field ∇U but by its arithmetic mean. That's why this procedure is also known as mean field limit [146, Chapter 5].

By introducing the empirical measure

$$\mu_n[\boldsymbol{X}, \boldsymbol{V}] = \frac{1}{n}\sum_{i=1}^{n} \delta_{\boldsymbol{x}_i} \otimes \delta_{\boldsymbol{v}_i},$$

for positions $\boldsymbol{X} = (\boldsymbol{x}_1, \dots, \boldsymbol{x}_n) \in \mathbb{R}^{3\times n}$ and velocities $\boldsymbol{V} = (\boldsymbol{v}_1, \dots, \boldsymbol{v}_n) \in \mathbb{R}^{3\times n}$ of the particles and the Hamiltonian flow $(S_t)_{t\geq 0}$ [3, Section 38],

$$S_t(\boldsymbol{X}_0, \boldsymbol{V}_0) = \text{solution of (2.9) at time } t \text{ with initial conditions } (\boldsymbol{X}_0, \boldsymbol{V}_0),$$

the solution of (2.9) can be compactly written as

$$\Psi_n = n_0|\Omega|\Big(\mu_n\big[S_t(\boldsymbol{X}_0, \boldsymbol{V}_0)\big]\Big)_{t\geq 0}.$$

The mapping Ψ_n defines a measure on $\mathbb{R}\times\mathbb{R}^3\times\mathbb{R}^3$. For $\eta : \mathbb{R}\times\mathbb{R}^3\times\mathbb{R}^3 \to \mathbb{R}$ continuous with compact support we have

$$\langle \eta, \Psi_n\rangle = n_0|\Omega|\frac{1}{n}\sum_{i=0}^{n}\int_0^\infty \eta(t, \boldsymbol{x}_i(t), \boldsymbol{v}_i(t))\,\mathrm{d}t.$$

The system of ordinary differential equations (2.9) can be recast as a scalar partial differential equation for Ψ_n.

2.1 Lemma *The measure Ψ_n is a weak solution of the initial value problem*

$$\begin{cases} \partial_t f + \boldsymbol{v} \cdot \nabla_{\boldsymbol{x}} f + \dfrac{q_0}{m_0} \boldsymbol{E}[f](t,\boldsymbol{x}) \cdot \nabla_{\boldsymbol{v}} f = 0, \\ f(0) = n_0 |\Omega| \dfrac{1}{n} \displaystyle\sum_{i=1}^{n} \delta_{\boldsymbol{x}_i^0} \otimes \delta_{\boldsymbol{v}_i^0}, \end{cases}$$

where $\boldsymbol{X}_0 = (\boldsymbol{x}_1^0, \dots, \boldsymbol{x}_n^0)$, $\boldsymbol{V}_0 = (\boldsymbol{v}_1^0, \dots, \boldsymbol{v}_n^0)$ and the electric field $\boldsymbol{E}[f]$ is given by

$$\boldsymbol{E}[f](t,\boldsymbol{x}) = -\frac{q_0}{\varepsilon_0} \int_{\mathbb{R}^3} \int_{\mathbb{R}^3} f(t,\boldsymbol{v},\boldsymbol{y}) \nabla_{\boldsymbol{x}} U(\boldsymbol{x}-\boldsymbol{y}) \, d\boldsymbol{v} \, d\boldsymbol{y}, \quad \boldsymbol{x} \in \mathbb{R}^3.$$

This means that for all $\eta : \mathbb{R} \times \mathbb{R}^3 \times \mathbb{R}^3 \to \mathbb{R}$ continuously differentiable that vanish outside a compact set we have

$$-\Big\langle \partial_t \eta + \boldsymbol{v} \cdot \nabla_{\boldsymbol{x}} \eta + \frac{q_0}{m_0} \boldsymbol{E}[\Psi_n] \cdot \nabla_{\boldsymbol{v}} \eta, \Psi_n \Big\rangle = n_0 |\Omega| \frac{1}{n} \sum_{i=1}^{n} \eta\big(0, \boldsymbol{x}_i^0, \boldsymbol{v}_i^0\big).$$

Proof. From the definition of the electric field we readily see

$$\boldsymbol{E}[\Psi_n](t, \boldsymbol{x}_i(t)) = -\frac{q_0}{\varepsilon_0} n_0 |\Omega| \frac{1}{n} \sum_{\substack{j=1 \\ j \neq i}} \nabla_{\boldsymbol{x}_i} U(\boldsymbol{x}_i(t) - \boldsymbol{x}_j(t)) = \frac{m_0}{q_0} \dot{\boldsymbol{v}}_i(t), \quad i = 1, \dots, n.$$

Therefore,

$$\begin{aligned} &- \Big\langle \partial_t \eta + \boldsymbol{v} \cdot \nabla_{\boldsymbol{x}} \eta + \frac{q_0}{m_0} \boldsymbol{E}[\Psi_n] \cdot \nabla_{\boldsymbol{v}} \eta, \Psi_n \Big\rangle \\ &= -n_0 |\Omega| \frac{1}{n} \sum_{i=1}^{n} \int_0^\infty \Big(\partial_t \eta\big(t, \boldsymbol{x}_i(t), \boldsymbol{v}_i(t)\big) + \dot{\boldsymbol{x}}_i(t) \cdot \nabla_{\boldsymbol{x}} \eta\big(t, \boldsymbol{x}_i(t), \boldsymbol{v}_i(t)\big) \\ &\qquad + \dot{\boldsymbol{v}}_i(t) \cdot \nabla_{\boldsymbol{v}} \eta\big(t, \boldsymbol{x}_i(t), \boldsymbol{v}_i(t)\big) \Big) \, \mathrm{d}t \\ &= -n_0 |\Omega| \frac{1}{n} \sum_{i=1}^{n} \int_0^\infty \frac{\mathrm{d}}{\mathrm{d}t} \Big(\eta(t, \boldsymbol{x}_i(t), \boldsymbol{v}_i(t)) \Big) \, \mathrm{d}t = n_0 |\Omega| \frac{1}{n} \sum_{i=1}^{n} \eta\big(0, \boldsymbol{x}_i^0, \boldsymbol{v}_i^0\big). \end{aligned}$$

■

The partial differential equation and the expression for the electric field in Lemma 2.1 constitute the Vlasov–Poisson system,

$$\begin{cases} \partial_t f + \boldsymbol{v} \cdot \nabla_{\boldsymbol{x}} f - \dfrac{q_0}{m_0} \nabla_{\boldsymbol{x}} \phi(t,\boldsymbol{x}) \cdot \nabla_{\boldsymbol{v}} f = 0, \\ -\Delta_{\boldsymbol{x}} \phi = \dfrac{q_0}{\varepsilon_0} \displaystyle\int_{\mathbb{R}^3} f(t,\boldsymbol{x},\boldsymbol{v}) \, \mathrm{d}\boldsymbol{v}, \\ \phi \to 0, \quad |\boldsymbol{x}| \to \infty, \\ f(0,\cdot) = f_0, \end{cases} \tag{2.10}$$

for the so-called particle distribution function $f : (0,\infty) \times \mathbb{R}^3 \times \mathbb{R}^3 \to [0,\infty)$ and an initial condition $f_0 : \mathbb{R}^3 \times \mathbb{R}^3 \to [0,\infty)$. It has the following physical interpretation: For measurable subsets A, B of $\mathbb{R}^3$ the integral

$$\int_A \int_B f(t,\boldsymbol{x},\boldsymbol{v})\,\mathrm{d}\boldsymbol{v}\,\mathrm{d}\boldsymbol{x}$$

is proportional to the number of particles contained in A with velocities from B at the time $t \geq 0$. Macroscopic quantities of the plasma are related to f by its moments in velocity space, for instance

$$n(t,\boldsymbol{x}) = \int_{\mathbb{R}^3} f(t,\boldsymbol{x},\boldsymbol{v})\,\mathrm{d}\boldsymbol{v}, \quad \boldsymbol{V}(t,\boldsymbol{x}) = \frac{1}{n(t,\boldsymbol{x})} \int_{\mathbb{R}^3} \boldsymbol{v}\, f(t,\boldsymbol{x},\boldsymbol{v})\,\mathrm{d}\boldsymbol{v}, \tag{2.11}$$

$$T(t,\boldsymbol{x}) = \frac{1}{3n(t,\boldsymbol{x})} \int_{\mathbb{R}^3} |\boldsymbol{v} - \boldsymbol{V}(t,\boldsymbol{x})|^2 f(t,\boldsymbol{x},\boldsymbol{v})\,\mathrm{d}\boldsymbol{v}, \tag{2.12}$$

for the local number density, mean velocity and temperature, respectively.

If the plasma is contained in an open, bounded set $\Omega \subseteq \mathbb{R}^3$ we furthermore have to impose boundary conditions on the distribution function f and the electric potential ϕ. Typically, $f = 0$ on $\partial\Omega$, which means that particles reaching the boundary are absorbed. Boundary conditions for ϕ are discussed in Section 3.3.

For an integrable initial condition f_0 with support in Ω and

$$\int_{\mathbb{R}^3} \int_{\mathbb{R}^3} f_0(\boldsymbol{x},\boldsymbol{v})\,\mathrm{d}\boldsymbol{v}\,\mathrm{d}\boldsymbol{x} = n_0|\Omega|,$$

we can draw a sequence of stochastically independent samples $\big((\boldsymbol{x}_i^0, \boldsymbol{v}_i^0)\big)_{i=1}^{\infty}$. From the strong law of large numbers [140, Chapter IV §3, Theorem 3] we know

$$n_0|\Omega|\frac{1}{n}\sum_{i=1}^{n} \delta_{\boldsymbol{x}_i^0} \otimes \delta_{\boldsymbol{v}_i^0} \to f_0$$

weakly for $n \to \infty$, which means for every $\eta : \mathbb{R}^3 \times \mathbb{R}^3 \to \mathbb{R}$ continuous and bounded,

$$\lim_{n\to\infty} n_0|\Omega|\frac{1}{n}\sum_{i=1}^{n} \eta\big(\boldsymbol{x}_i^0, \boldsymbol{v}_i^0\big) = \int_{\mathbb{R}^3} \int_{\mathbb{R}^3} \eta(\boldsymbol{x},\boldsymbol{v})\, f_0(\boldsymbol{x},\boldsymbol{v})\,\mathrm{d}\boldsymbol{x}\,\mathrm{d}\boldsymbol{v}.$$

This raises the question if the weak approximation of the initial condition by the independent samples implies the (weak) approximation of the Vlasov equation, that is

$$\Psi_n \to f \quad \text{weakly for } n \to \infty.$$

An affirmative answer was given by Neunzert and Wick [122] and refined in a sequence of follow-up papers [121, 120, 119], see also [62] and [164] for different proofs. Apart from higher regularity for the initial condition f_0 in order to guarantee unique solvability of (2.10), they require that (2.9) is fulfilled with a regularised fundamental solution U_σ, for instance

$$U_\sigma(\boldsymbol{z}) = \frac{1}{4\pi} \frac{1}{\sqrt{z_1^2 + z_2^2 + z_3^2 + \sigma^2}}, \quad \boldsymbol{z} \in \mathbb{R}^3,$$

with $\sigma > 0$. The regularisation parameter σ depends on time and the number of particles and vanishes for $t \to \infty$, $n \to \infty$ with a rate dictated by the initial condition. Lazarovici and Pickl [110] proved the weak convergence of the particle solution under nearly optimal conditions on σ and the regularisation U_σ. For their analysis it suffices to take $\sigma \propto n^{-1/3-\varepsilon}$ with $\varepsilon > 0$. In addition they relax the assumptions on the regularisation U_σ, allowing for

$$U_\sigma(z) = \frac{1}{4\pi} \begin{cases} \dfrac{3}{2\sigma} - \dfrac{|z|^2}{2\sigma^3}, & |z| \le \sigma, \\ \dfrac{1}{|z|}, & |z| > \sigma, \end{cases} \qquad z \in \mathbb{R}^3. \tag{2.13}$$

In this form, U_σ is the potential generated by a charged ball at $\mathbf{0}$ with radius σ and constant charge density $|B_\sigma(\mathbf{0})|^{-1} = 3/(4\pi\sigma^3)$, see Lemma 3.43.

2.4. Nondimensional Vlasov–Poisson System

In this section we discuss typical scales for the physical quantities involved in the Vlasov–Poisson system (2.10) and transform it into a system with nondimensional units.

Important quantities for the time evolution of the plasma are its characteristic temperature T_0 and its characteristic number density n_0. The former influences the strength of the drift part $\boldsymbol{v} \cdot \nabla_{\boldsymbol{x}} f$ of the Vlasov equation relative to the acceleration part $-q_0/m_0 \nabla_{\boldsymbol{x}} \phi \cdot \nabla_{\boldsymbol{v}} f$, which is controlled by the number density n_0. In equilibrium, the typical velocity V_0 is the thermal velocity,

$$V_0 = \sqrt{\frac{k_B T_0}{m_0}},$$

where k_B is the Boltzmann constant. Since f is a density function on the phase space $\mathbb{R}^3 \times \mathbb{R}^3$ it has dimension length^{-3} $\cdot$ velocity^{-3}. Therefore, we make the ansatz

$$f(t, \boldsymbol{x}, \boldsymbol{v}) = \frac{n_0}{V_0^3} \widetilde{f}\big(t/t_0, \boldsymbol{x}/L_0, \boldsymbol{v}/V_0\big),$$

with a nondimensional function $\widetilde{f}$. Here, L_0 is the typical length scale of the plasma and $t_0 = L_0/V_0$ its time scale. Plugging this into the Vlasov equation yields

$$\partial_{\tilde{t}} \widetilde{f} + \widetilde{\boldsymbol{v}} \cdot \nabla_{\tilde{\boldsymbol{x}}} \widetilde{f} - \frac{q_0 L_0}{m_0 V_0^2} \nabla_{\boldsymbol{x}} \phi \cdot \nabla_{\tilde{\boldsymbol{v}}} \widetilde{f} = 0,$$

where the electric potential is still expressed in unscaled variables. The quotient

$$\frac{m_0 V_0^2}{q_0 L_0} = \frac{k_B T_0}{q_0 L_0}$$

has the unit of the electric field and is equal to the strength of a uniform field that is needed to accelerate a particle with charge q_0 and mass m_0 from zero velocity to V_0 on the distance L_0. This motivates the nondimensional form of the electric potential,

$$\phi(t, \boldsymbol{x}) = \frac{k_B T_0}{q_0} \widetilde{\phi}\big(t/t_0, \boldsymbol{x}/L_0\big),$$

so the rescaled Vlasov equation reads

$$\partial_{\tilde{t}} \tilde{f} + \tilde{\boldsymbol{v}} \cdot \nabla_{\tilde{\boldsymbol{x}}} \tilde{f} - \nabla_{\tilde{\boldsymbol{x}}} \tilde{\phi} \cdot \nabla_{\tilde{\boldsymbol{v}}} \tilde{f} = 0.$$

Inserting this into the Poisson equation for the ϕ yields

$$-\Delta_{\tilde{\boldsymbol{x}}} \tilde{\phi} = \frac{L_0^2}{\lambda_D^2} \int_{\mathbb{R}^3} \tilde{f}(\tilde{t}, \tilde{\boldsymbol{x}}, \tilde{\boldsymbol{v}}) \, \mathrm{d}\tilde{\boldsymbol{v}},$$

where λ_D is the Debye length,

$$\lambda_D = \sqrt{\frac{\varepsilon_0 k_B T_0}{n_0 q_0^2}}.$$

In total, we obtain the nondimensional Vlasov–Poisson system,

$$\begin{cases} \partial_t f + \boldsymbol{v} \cdot \nabla_{\boldsymbol{x}} f - \nabla_{\boldsymbol{x}} \phi \cdot \nabla_{\boldsymbol{v}} f = 0, \\ -\Delta \phi = \dfrac{L_0^2}{\lambda_D^2} \displaystyle\int_{\mathbb{R}^3} f \, \mathrm{d}\boldsymbol{v}. \end{cases}$$

Here and in the following, we drop the tildes and use f and ϕ to refer to the nondimensional functions.

3. Boundary Integral Formulation

The ultimate goal of this chapter is to solve (2.8) for the unknown density ψ purely by means of a formulation of the problem on the boundary of the domain, thus avoiding a volume discretisation, see Section 3.5. This strategy is known as Boundary Element Method which we study in Section 3.4. It is based on a discretisation of of boundary integral equations discussed in Section 3.3. The involved operators are defined by means of the Newton potential whose properties are given in Section 3.2. We begin with a review of the relevant function spaces for the treatment of elliptic boundary value problems. Their use, however, is not limited to this chapter. Especially distributions are employed in several parts of this thesis.

3.1. Function Spaces

> [The existence of] a non-negative test function φ with $\varphi(0) > 0$ is all one needs to get distribution theory started.
>
> *(Lars Hörmander [87])*

For the rest of this section, let $\Omega \subseteq \mathbb{R}^d$ denote an open set. The function spaces we need for the analysis of boundary value problems are linear subspaces of the large space of distributions. In the presentation of this material, we mostly follow [87], see also [135] for more information on distributions and [58, 76, 158] for a detailed discussion on Sobolev spaces. Trèves [159] gives a general review of topological vector spaces.

3.1 Definition (Fréchet space) *A vector space X equipped with a metric d is called Fréchet or F-space if*

- *the vector addition and the scalar multiplication on X are continuous with respect to d,*
- *and (X, d) is complete, i.e. every Cauchy sequence converges.*

3.2 Lemma *For a Fréchet space (X, d) there are countably many seminorms*

$$|\cdot|_k : X \to [0, \infty), \quad k \in \mathbb{N},$$

such that the mapping

$$\widetilde{d} : X \times X \to [0, \infty),\ (x, y) \mapsto \sum_{k=0}^{\infty} \frac{1}{2^k} \frac{|x - y|_k}{1 + |x - y|_k}$$

defines a metric on X which is equivalent to d. This means that $U \subseteq X$ is open with respect to $\widetilde{d}$ if and only if it is open in (X, d).

In particular, a sequence $(x_n)_{n\in\mathbb{N}}$ converges to $x \in X$ in (X, d) if and only if

$$|x_n - x|_k \to 0, \quad n \to \infty,$$

for all $k \in \mathbb{N}$.

Fréchet spaces are generalisations of Banach and Hilbert spaces.

3.3 Definition (Banach and Hilbert spaces) *A Fréchet space* (X, d) *is a Banach space if* d *is induced by a norm* $\|\cdot\|$ *on* X*, i.e.*

$$d(x, y) = \|x - y\|, \quad x, y \in X.$$

If $\|\cdot\|$ *is induced by an inner product* $(\cdot, \cdot)$*,*

$$\|x\| = \sqrt{(x, x)}, \quad x \in X,$$

we call $(X, (\cdot, \cdot))$ *a Hilbert space.*

3.4 Remark By the Jordan–von Neumann theorem [91, Theorem 1], the norm of a Banach space $(X, \|\cdot\|)$ is induced by an inner product if and only if $\|\cdot\|$ obeys the parallelogram law,

$$\|x + y\|^2 + \|x - y\|^2 = 2\big(\|x\|^2 + \|y\|^2\big), \quad x, y \in X.$$

In this case, we say that the space X endowed with $\|\cdot\|$ is a Hilbert space.

Classical examples for Fréchet and Banach spaces are the vector spaces of (locally) integrable and differentiable functions.

3.5 Definition (Measurable functions) *Let* $M \subseteq \mathbb{R}^d$*. A function* $f : M \to \mathbb{R}$ *is called Borel-measurable if for every interval* $(a, b) \subseteq \mathbb{R}$ *there is an element* A *of the Borel* σ*-algebra on* $\mathbb{R}^d$*, called (Borel-) measurable set, such that*

$$f^{-1}[(a, b)] = A \cap M,$$

where $f^{-1}[\cdot]$ *is the preimage mapping of* f*. The function* f *is called Lebesgue-measurable if there exits* $Z \subseteq M$ *with Lebesgue measure zero such that* $f|_{M \setminus Z}$ *is Borel-measurable.*

3.6 Definition (Integrable functions) *For* $p \in [1, \infty)$ *and* $M \subseteq \mathbb{R}^d$ *Borel-measurable, the vector space of Lebesgue-measurable functions* $f : M \to \mathbb{R}$ *whose* p*-th power is integrable,*

$$\int_M |f(\boldsymbol{x})|^p \, d\boldsymbol{x} < \infty$$

is denoted by $L_p(M)$*. Equipped with the norm*

$$\|\cdot\| : L_p(M) \to [0, \infty), \; f \mapsto \left(\int_M |f(\boldsymbol{x})|^p \, d\boldsymbol{x} \right)^{1/p},$$

$L_p(M)$ *is a Banach space provided we identify functions that are equal outside sets of measure zero.*

The space of locally integrable functions $L_{p,loc}(\Omega)$ *on an open set* $\Omega \subseteq \mathbb{R}^d$ *is defined by*

$$L_{p,loc}(\Omega) = \{f : \Omega \to \mathbb{R} : f \in L_p(K) \; \forall K \subseteq \Omega \text{ compact}\}.$$

Convergence is understood with respect to the seminorms

$$|\cdot|_{K,p} : L_{p,loc}(\Omega) \to \mathbb{R}, \; f \mapsto \|f\|_{L_p(K)},$$

where $K \subseteq \Omega$ *is compact. This turns* $L_{p,loc}(\Omega)$ *into a Fréchet space.*

3.7 Remark In Definition 3.6 we define the convergence in $L_{p,\mathrm{loc}}(\Omega)$ via the convergence with respect to an uncountable number of seminorms. However, it suffices to consider a particular countable number of compact sets, called an exhaustion of Ω, defined next. The same argument applies to the spaces of differentiable functions we review in the following.

3.8 Definition (Exhaustion of open sets) *We say that the sequence $(\Omega_\ell)_{\ell\in\mathbb{N}}$ of compact subsets of Ω is an exhaustion of Ω if*

$$\Omega = \bigcup_{\ell\in\mathbb{N}} \Omega_\ell,$$

and $\Omega_\ell \subseteq \operatorname{int}\Omega_{\ell+1}$ for all $\ell \in \mathbb{N}$, where $\operatorname{int} A$ denotes the interior of $A \subseteq \mathbb{R}^d$.

3.9 Definition (Differentiable functions) *For $k \in \mathbb{N}$, the space*

$$C^k(\Omega) = \{f : \Omega \to \mathbb{R} : f \text{ has continuous derivatives of order } k\}$$

is a Fréchet space with respect to the seminorms

$$|\cdot|_{K,\boldsymbol{\alpha}} : C^k(\Omega) \to [0,\infty),\ f \mapsto \sup_{\boldsymbol{x}\in K} |D^{\boldsymbol{\alpha}} f(\boldsymbol{x})|,$$

where $K \subseteq \Omega$ compact and $\boldsymbol{\alpha} \in \mathbb{N}^d$ with $|\boldsymbol{\alpha}| \le k$ and

$$D^{\boldsymbol{\alpha}} f(\boldsymbol{x}) = \frac{\partial^{\alpha_1}}{\partial x_1^{\alpha_1}} \cdots \frac{\partial^{\alpha_d}}{\partial x_d^{\alpha_d}} f(\boldsymbol{x}), \quad \boldsymbol{x} \in \Omega.$$

3.10 Definition (Smooth functions) *We denote by $\mathcal{E}(\Omega)$ the space of infinitely differentiable functions on Ω,*

$$\mathcal{E}(\Omega) = \bigcap_{k\in\mathbb{N}} C^k(\Omega).$$

The topology on $\mathcal{E}(\Omega)$ is given by the seminorms

$$|\cdot|_{K,\boldsymbol{\alpha}} : \mathcal{E}(\Omega) \to [0,\infty),\ \varphi \mapsto \sup_{\boldsymbol{x}\in K} |D^{\boldsymbol{\alpha}}\varphi(\boldsymbol{x})|,$$

where $K \subseteq \Omega$ is compact and $\boldsymbol{\alpha} \in \mathbb{N}^d$. This turns $\mathcal{E}(\Omega)$ into a Fréchet space.

Test functions on Ω are a subspace of $\mathcal{E}(\Omega)$ with a stronger topology. Its construction is called LF-space.

3.11 Definition (LF-space) *Let X be a vector space which is the union of an increasing sequence of subspaces $(X_n)_{n\in\mathbb{N}}$,*

$$X = \bigcup_{n\in\mathbb{N}} X_n, \quad X_n \subseteq X_{n+1}, \quad n \in \mathbb{N}.$$

If all $(X_n)_{n\in\mathbb{N}}$ are Fréchet spaces such that $X_n \hookrightarrow X_{n+1}$ continuously for all $n \in \mathbb{N}$, we call X an LF-space given the following topology: A convex subset $U \subseteq X$ is a neighbourhood of zero iff $U \cap X_n$ is a neighbourhood of zero in X_n for all $n \in \mathbb{N}$. This definition is independent of the sequence of subspaces $(X_n)_{n\in\mathbb{N}}$ used in the construction of the topology. We say that X is the (strict) inductive limit of $(X_n)_{n\in\mathbb{N}}$.

3.12 Definition (Support of functions) *Let $M \subseteq \mathbb{R}^d$. For a function $f : M \to \mathbb{R}$, we call the closed set*

$$\operatorname{supp} f = \overline{\{\boldsymbol{x} \in M : f(\boldsymbol{x}) \neq 0\}}$$

the support of f.

3.13 Definition (Test functions) *For $A \subseteq \Omega$ closed let $\mathcal{D}_A$ denote the linear subspace of functions in $\mathcal{E}(\Omega)$ whose support lies in A. The space $\mathcal{D}(\Omega)$ of test functions is the inductive limit of $(\mathcal{D}_{\Omega_\ell})_{\ell\in\mathbb{N}}$ for an exhaustion $(\Omega_\ell)_{\ell\in\mathbb{N}}$. This means that a sequence $(\varphi_n)_{n\in\mathbb{N}}$ in $\mathcal{D}(\Omega)$ converges to 0 if there is a compact subset K such that $\operatorname{supp}\varphi_n \subseteq K$ for all $n \in \mathbb{N}$ and*

$$D^{\boldsymbol{\alpha}}\varphi_n \to 0, \quad n \to \infty$$

uniformly on all $K \subseteq \Omega$ compact and $\boldsymbol{\alpha} \in \mathbb{N}^d$.

Sometimes we need smooth functions with compact support that do not vanish on the boundary.

3.14 Definition (Test functions on closed sets) *For $A \subseteq \mathbb{R}^d$ closed, we set*

$$\mathcal{D}(A) = \{u|_A : u \in \mathcal{D}(\mathbb{R}^d)\}.$$

Here, $\mathbb{R}^d$ in the definition may be replaced by any open set that contains A.

3.15 Definition (Distributions) *The space of distributions is the dual space of $\mathcal{D}(\Omega)$ and is denoted by $\mathcal{D}'(\Omega)$. The topology on $\mathcal{D}'(\Omega)$ is the weak-$*$ topology, i.e. a sequence $(u_n)_{n\in\mathbb{N}}$ converges to 0 if*

$$\langle\varphi, u_n\rangle \to 0, \quad n \to \infty$$

for all $\varphi \in \mathcal{D}(\Omega)$.

3.16 Example For $\boldsymbol{x_0} \in \Omega$ the Dirac distribution

$$\delta_{\boldsymbol{x}_0} : \mathcal{D}(\Omega) \to \mathbb{R}, \varphi \mapsto \varphi(\boldsymbol{x_0})$$

lies in $\mathcal{D}'(\Omega)$. In general, every locally integrable function f defines a distribution via

$$\varphi \mapsto \int_\Omega \varphi\, f \,\mathrm{d}\boldsymbol{x} = \langle\varphi, T_f\rangle.$$

Moreover, the inclusion

$$L_{1,\mathrm{loc}}(\Omega) \hookrightarrow \mathcal{D}'(\Omega), f \mapsto T_f$$

is injective and with dense image. Distributions of this type are called regular. Irregular distributions are often called singular [65, p. 4]. The Dirac distribution is an example for a singular distribution.

By duality, we can extend differentiation, multiplication and change of variables to distributions.

3.17 Definition (Basic operations on distributions) *Assume $u \in \mathcal{D}'(\Omega)$.*

(a) For $\psi \in \mathcal{E}(\Omega)$ we define the product ψu by

$$\langle\varphi, \psi u\rangle = \langle\varphi\psi, u\rangle, \quad \varphi \in \mathcal{D}(\Omega).$$

(b) For $\boldsymbol{\alpha} \in \mathbb{N}^d$ the derivative $D^{\boldsymbol{\alpha}}u$ is given by

$$\langle\varphi, D^{\boldsymbol{\alpha}}u\rangle = (-1)^{|\boldsymbol{\alpha}|}\langle D^{\boldsymbol{\alpha}}\varphi, u\rangle, \quad \varphi \in \mathcal{D}(\Omega).$$

(c) *Suppose $\widetilde{\Omega} \subseteq \mathbb{R}^d$ open and $\chi : \widetilde{\Omega} \to \Omega$ a C^∞-diffeomorphism. The distribution $u \circ \chi$ on $\widetilde{\Omega}$ is defined by*

$$\langle \widetilde{\varphi}, u \circ \chi \rangle = \langle |\det D\chi|^{-1} \widetilde{\varphi}, u \rangle, \quad \widetilde{\varphi} \in \mathcal{D}(\widetilde{\Omega}),$$

where $D\chi$ denotes the Jacobi matrix of χ, $(D\chi)_{i,j} = \partial_j \chi_i$, for $i, j = 1, \ldots, d$.

3.18 Remark Above definitions are consistent with the usual for smooth functions. In particular, we have for all $\psi \in \mathcal{E}(\Omega)$, $\varphi \in \mathcal{D}(\Omega)$ and $\boldsymbol{\alpha} \in \mathbb{N}^d$:

$$\langle \varphi, D^{\boldsymbol{\alpha}} T_\psi \rangle = (-1)^{|\boldsymbol{\alpha}|} \int_\Omega D^{\boldsymbol{\alpha}} \varphi \psi \, \mathrm{d}\boldsymbol{x} = \int_\Omega \varphi \, D^{\boldsymbol{\alpha}} \psi \, \mathrm{d}\boldsymbol{x} = \langle \varphi, T_{D^{\boldsymbol{\alpha}} \psi} \rangle$$

and $\psi T_\varphi = T_{\psi \varphi}$.

The notion of supports extends to distributions.

3.19 Definition (Support of distributions) *A distribution $u \in \mathcal{D}'(\Omega)$ is said to vanish outside a closed set $F \subseteq \Omega$ if*

$$\varphi \in \mathcal{D}(\Omega), \operatorname{supp} \varphi \subseteq \Omega \setminus F \implies \langle \varphi, u \rangle = 0.$$

The support is then defined as

$$\operatorname{supp} u = \bigcap_{\substack{F \subseteq \Omega \text{ closed} \\ u \text{ vanishes outside } F}} F.$$

3.20 Lemma *The distributions with compact support are exactly the elements of $\mathcal{E}'(\Omega)$, the dual space of $\mathcal{E}(\Omega)$.*

The convolution of functions, or generally distributions, is an important concept for the integral operators discussed later in this chapter.

3.21 Definition (Convolution) *For $u, v \in \mathcal{D}'(\mathbb{R}^d)$, where one has compact support, the convolution $u * v \in \mathcal{D}'(\mathbb{R}^d)$, is defined by*

$$\langle \varphi, u * v \rangle = u_{\boldsymbol{x}}(v_{\boldsymbol{y}}(\varphi(\boldsymbol{x} + \boldsymbol{y}))), \quad \varphi \in \mathcal{D}(\mathbb{R}^d),$$

where the indices on u and v indicate the variable they are acting on. If u and v are regular, so is $u * v$,

$$(u * v)(\boldsymbol{x}) = \int_{\mathbb{R}^d} u(\boldsymbol{x} - \boldsymbol{y}) v(\boldsymbol{y}) \, d\boldsymbol{y}, \quad \boldsymbol{x} \in \mathbb{R}^d.$$

The following properties are direct consequences of the definition.

3.22 Lemma *For $u, v \in \mathcal{D}'(\mathbb{R}^d)$ with one having compact support, the convolution is symmetric, $u * v = v * u$, and derivatives can be exchanged between the two distributions,*

$$D^{\boldsymbol{\alpha}}(u * v) = (D^{\boldsymbol{\alpha}} u) * v = u * (D^{\boldsymbol{\alpha}} v), \quad \boldsymbol{\alpha} \in \mathbb{N}^d.$$

To study the smoothness of distributions we define Sobolev space of arbitrary order. The key to their definition is the Fourier transform whose natural domain of definition are Schwartz functions.

3.23 Definition (Schwartz functions) *With $\mathcal{S}(\mathbb{R}^d)$, we denote the space of rapidly decaying elements of $\mathcal{E}(\mathbb{R}^d)$, called Schwartz functions,*

$$\varphi \in \mathcal{S}(\mathbb{R}^d) \iff \forall \boldsymbol{\alpha}, \boldsymbol{\beta} \in \mathbb{N}^d : |\varphi|_{\boldsymbol{\alpha},\boldsymbol{\beta}} = \sup_{\boldsymbol{x}\in\mathbb{R}^d} |\boldsymbol{x}^{\boldsymbol{\beta}} D^{\boldsymbol{\alpha}}\varphi(\boldsymbol{x})| < \infty.$$

The Fréchet space topology on $\mathcal{S}(\mathbb{R}^d)$ is induced by the family of seminorms $(|\cdot|_{\boldsymbol{\alpha},\boldsymbol{\beta}})_{\boldsymbol{\alpha},\boldsymbol{\beta}\in\mathbb{N}^d}$.

3.24 Definition (Fourier transform) *For $\varphi \in \mathcal{S}(\mathbb{R}^d)$, the Fourier transform $\widehat{\varphi} \in \mathcal{S}(\mathbb{R}^d)$ is defined by*

$$\widehat{\varphi}(\boldsymbol{\xi}) = \mathcal{F}[\varphi](\boldsymbol{\xi}) = \int_{\mathbb{R}^d} \exp(\mathrm{i}\,\boldsymbol{x}\cdot\boldsymbol{\xi})\,\varphi(\boldsymbol{x})\,d\boldsymbol{x},$$

and continuously maps Schwartz functions onto Schwartz functions. We have $\widehat{\widehat{\varphi}} = (2\pi)^d \breve{\varphi}$ with $\breve{\varphi}(\boldsymbol{x}) = \varphi(-\boldsymbol{x})$, $\boldsymbol{x} \in \mathbb{R}^d$. Therefore, the inverse operation of $\mathcal{F}$ is

$$\mathcal{F}^{-1}[\widehat{\varphi}](\boldsymbol{x}) = (2\pi)^{-d} \int_{\mathbb{R}^d} \exp(-\mathrm{i}\,\boldsymbol{x}\cdot\boldsymbol{\xi})\,\widetilde{\varphi}(\boldsymbol{\xi})\,d\boldsymbol{\xi}.$$

Clearly, $\mathcal{D}(\mathbb{R}^d) \subseteq \mathcal{S}(\mathbb{R}^d)$. Thus, the dual space of $\mathcal{S}(\mathbb{R}^d)$ is a subspace of $\mathcal{D}'(\mathbb{R}^d)$ and contains those distributions to which we can extend Fourier transform while keeping most of its properties.

3.25 Definition (Tempered distributions) *The tempered distributions $\mathcal{S}'(\mathbb{R}^d)$ are the dual space of $\mathcal{S}(\mathbb{R}^d)$, equipped with the weak-$*$ topology.*

3.26 Lemma *The Fourier transform continuously extends from $\mathcal{S}(\mathbb{R}^d)$ to $\mathcal{S}'(\mathbb{R}^d)$. For $u \in \mathcal{S}'(\mathbb{R}^d)$ the Fourier transform $\widehat{u} \in \mathcal{S}'(\mathbb{R}^d)$ is defined by*

$$\langle \varphi, \widehat{u} \rangle = \langle \widehat{\varphi}, u \rangle$$

for $\varphi \in \mathcal{S}(\mathbb{R}^d)$.

3.27 Lemma *For all $\varphi, \psi \in \mathcal{S}(\mathbb{R}^d)$, $\boldsymbol{a} \in \mathbb{R}^d$ and $\boldsymbol{\alpha} \in \mathbb{N}^d$, we have*

(a) $\mathcal{F}[\varphi(\cdot - \boldsymbol{a})](\boldsymbol{\xi}) = \exp(\mathrm{i}\,\boldsymbol{a}\cdot\boldsymbol{\xi})\widehat{\varphi}(\boldsymbol{\xi})$,

(b) $\mathcal{F}[D^{\boldsymbol{\alpha}}\varphi](\boldsymbol{\xi}) = (-\mathrm{i})^{|\boldsymbol{\alpha}|}\boldsymbol{\xi}^{\boldsymbol{\alpha}}\widehat{\varphi}(\boldsymbol{\xi})$,

(c) $\mathcal{F}[\boldsymbol{x}^{\boldsymbol{\alpha}}\varphi](\boldsymbol{\xi}) = \mathrm{i}^{|\boldsymbol{\alpha}|}\, D^{\boldsymbol{\alpha}}\widehat{\varphi}(\boldsymbol{\xi})$,

(d) $\mathcal{F}[\varphi * \psi] = \widehat{\varphi}\,\widehat{\psi}$,

(e) $\mathcal{F}[\varphi\,\psi] = (2\pi)^{-d}\,\widehat{\varphi} * \widehat{\psi}$,

(f) $\displaystyle\int_{\mathbb{R}^d} \varphi\,\psi\,d\boldsymbol{x} = (2\pi)^{-d} \int_{\mathbb{R}^d} \widehat{\varphi}\,\widehat{\psi}\,d\boldsymbol{\xi}$ *(Parseval's identity)*

3.28 Remark The first three properties in Lemma 3.27 also hold for tempered distributions and (d) and (e) hold if one of the factors is a tempered distribution.

The spaces and their duals we defined so far embed continuously as

$$\mathcal{D}(\mathbb{R}^d) \subseteq \mathcal{S}(\mathbb{R}^d) \subseteq \mathcal{E}(\mathbb{R}^d)$$

and

$$\mathcal{E}'(\mathbb{R}^d) \subseteq \mathcal{S}'(\mathbb{R}^d) \subseteq \mathcal{D}'(\mathbb{R}^d).$$

The class of Sobolev spaces are subspaces of $\mathcal{S}'(\mathbb{R}^d)$ whose elements are characterised by the decay behaviour of their Fourier transform.

3.29 Definition (Sobolev spaces in $\mathbb{R}^d$) *For $s \in \mathbb{R}$ we define the Sobolev space of orders s on $\mathbb{R}^d$,*

$$H^s(\mathbb{R}^d) = \left\{ u \in \mathcal{S}'(\mathbb{R}^d) : \langle\cdot\rangle^s \, \hat{u} \in L_2(\mathbb{R}^d) \right\},$$

where $\langle\boldsymbol{\xi}\rangle^s = (1 + |\boldsymbol{\xi}|^2)^{s/2}$ for $\boldsymbol{\xi} \in \mathbb{R}^d$. Endowed with the inner product

$$(u, v)_s = (2\pi)^{-d} \int_{\mathbb{R}^d} \langle\boldsymbol{\xi}\rangle^{2s} \hat{u}(\boldsymbol{\xi}) \hat{v}(\boldsymbol{\xi}) \, d\boldsymbol{\xi}, \quad u, v \in H^s(\mathbb{R}^d),$$

this space is a Hilbert space. Furthermore, $\mathcal{S}(\mathbb{R}^d) \hookrightarrow H^s(\mathbb{R}^d)$ with dense image.

3.30 Theorem ([58, Theorem 9.3.2]) *Given the identification of $(L_2(\mathbb{R}^d))' = L_2(\mathbb{R}^d)$, the dual space of $H^s(\mathbb{R}^d)$ is isometrically isomorphic to the Sobolev space of opposite order,*

$$(H^s(\mathbb{R}^d))' \cong H^{-s}(\mathbb{R}^d).$$

The definition of the inner product on $H^s(\mathbb{R}^d)$ is nonlocal. However, if s is a positive integer, $(\cdot,\cdot)_s$ admits an alternative presentation in L_2-norms of derivatives:

3.31 Theorem ([158, Remark 25.2], [87, p. 241]) *For $s \geq 0$ of the form $s = m + \mu$ with $m \in \mathbb{N}$ and $\mu \in [0, 1)$, we have*

$$u \in H^s(\mathbb{R}^d) \implies \forall \boldsymbol{\alpha} \in \mathbb{N}^d, |\boldsymbol{\alpha}| \leq m : D^{\boldsymbol{\alpha}} u \in L_2(\mathbb{R}^d)$$

and furthermore if $\mu > 0$,

$$\int_{\mathbb{R}^d} \int_{\mathbb{R}^d} \frac{|D^{\boldsymbol{\alpha}} u(\boldsymbol{x}) - D^{\boldsymbol{\alpha}} u(\boldsymbol{y})|^2}{|\boldsymbol{x} - \boldsymbol{y}|^{d+2\mu}} \, d\boldsymbol{x} \, d\boldsymbol{y} < \infty$$

for all $\boldsymbol{\alpha} \in \mathbb{N}^d$ with $|\boldsymbol{\alpha}| = m$. An equivalent inner product on $H^s(\mathbb{R}^d)$ is given by

$$\begin{aligned}(u, v) = &\sum_{\substack{\boldsymbol{\alpha} \in \mathbb{N}^d \\ |\boldsymbol{\alpha}| \leq m}} (D^{\boldsymbol{\alpha}} u, D^{\boldsymbol{\alpha}} v)_{L_2(\mathbb{R}^d)} \\ &+ \sum_{\substack{\boldsymbol{\alpha} \in \mathbb{N}^d \\ |\boldsymbol{\alpha}| = m}} \int_{\mathbb{R}^d} \int_{\mathbb{R}^d} \frac{(D^{\boldsymbol{\alpha}} u(\boldsymbol{x}) - D^{\boldsymbol{\alpha}} u(\boldsymbol{y}))(D^{\boldsymbol{\alpha}} v(\boldsymbol{x}) - D^{\boldsymbol{\alpha}} v(\boldsymbol{y}))}{|\boldsymbol{x} - \boldsymbol{y}|^{d+2\mu}} \, d\boldsymbol{x} \, d\boldsymbol{y},\end{aligned}$$

for $u, v \in H^s(\mathbb{R}^d)$. The sum in the last line is dropped in case of $\mu = 0$.

We continue with the definition of Sobolev on Ω. To this end, we fix an exhaustion $(\Omega_\ell)_{\ell\in\mathbb{N}}$ for Ω with $\Omega_\ell \subseteq \operatorname{int}\Omega_{\ell+1}$ for all $\ell \in \mathbb{N}$ and $(\chi_\ell)_{\ell\in\mathbb{N}} \subseteq \mathcal{D}(\Omega)$ such that $0 \le \chi_\ell \le 1$, $\chi_\ell = 1$ on Ω_ℓ and $\operatorname{supp}\chi_\ell \subseteq \operatorname{int}\Omega_{\ell+1}$ for all $\ell \in \mathbb{N}$.

For distributions in $H^s(\mathbb{R}^d)$ with compact support in Ω, we can naturally define Sobolev spaces on Ω. This is similar to Definition 3.13. For a closed set $A \subseteq \mathbb{R}^d$ we define

$$H^s_A = \left\{u \in H^s(\mathbb{R}^d) : \operatorname{supp} u \subseteq A\right\},$$

a closed subspace of $H^s(\mathbb{R}^d)$ and therefore a Hilbert (and consequently a Fréchet) space when endowed with the subspace topology.

3.32 Definition (Sobolev spaces on subsets I) *The space $H^s_{comp}(\Omega)$ is defined as the inductive limit of $(H^s_{\Omega_\ell})_{\ell\in\mathbb{N}}$. We have*

$$H^s_{comp}(\Omega) = \bigcup_{\ell\in\mathbb{N}} H^s_{\Omega_\ell} = \bigcup_{\substack{K\subseteq\Omega\\ K \text{ compact}}} H^s_K.$$

Clearly, $H^s_{comp}(\Omega) \subseteq \mathcal{E}'(\Omega)$ continuously. Furthermore, $\mathcal{D}(\Omega)$ is dense in $H^s_{comp}(\Omega)$.

3.33 Example For $\alpha \in \mathbb{N}^d$ and $\boldsymbol{x_0} \in \Omega$, the Fourier transform of $D^{\boldsymbol{\alpha}}\delta_{\boldsymbol{x}_0}$ is

$$\mathcal{F}(D^{\boldsymbol{\alpha}}\delta_{\boldsymbol{x}_0})(\boldsymbol{\xi}) = (-\mathrm{i})^{|\boldsymbol{\alpha}|}\boldsymbol{\xi}^{\boldsymbol{\alpha}}\exp(\mathrm{i}\,\boldsymbol{x}_0\cdot\boldsymbol{\xi}), \quad \boldsymbol{\xi} \in \mathbb{R}^d,$$

which is regular and grows like $\langle\boldsymbol{\xi}\rangle^{|\boldsymbol{\alpha}|}$. Therefore $\langle\cdot\rangle^m\mathcal{F}(D^{\boldsymbol{\alpha}}\delta_{\boldsymbol{x}_0})$ is square-integrable if and only if m is smaller than $-|\alpha| - d/2$. This means $D^{\boldsymbol{\alpha}}\delta_{\boldsymbol{x}_0} \in H^{-|\alpha|-d/2-\varepsilon}_{\text{comp}}(\Omega)$ for all $\varepsilon > 0$.

We obtain a second family of Sobolev spaces via localisation.

3.34 Definition (Sobolev spaces on subsets II) *For $s \in \mathbb{R}$, we define the space*

$$H^s_{loc}(\Omega) = \left\{u \in \mathcal{D}'(\Omega) : \forall\varphi \in \mathcal{D}(\Omega) : \varphi u \in H^s(\mathbb{R}^d)\right\},$$

endowed with topology induced by the seminorms

$$|\cdot|_{s,\ell} : H^s_{loc}(\Omega) \to [0,\infty), \quad u \mapsto \|\chi_\ell u\|_s, \quad \ell \in \mathbb{N}.$$

This turns $H^s_{loc}(\Omega)$ into a Fréchet space. Moreover, $\mathcal{E}(\Omega)$ is dense in $H^s_{loc}(\Omega)$.

The two family of Sobolev spaces on Ω are linked via their dual spaces.

3.35 Theorem ([76, Remark 6.26], [158, p. 228]) *For $s \in \mathbb{R}$ it holds*

$$(H^s_{loc}(\Omega))' \cong H^{-s}_{comp}(\Omega), \quad (H^s_{comp}(\Omega))' \cong H^{-s}_{loc}(\Omega).$$

3.2. The Newton Potential

> Zur bequemern Handhabung der dazu dienenden Untersuchungen werden wir uns erlauben, dieses V mit einer besondern Benennung zu belegen, und diese Gröſse das *Potential* der Massen, worauf sie sich bezieht, nennen.[1]
>
> *(Carl Friedrich Gauß [63])*

For the rest of this section we fix an open set $\Omega \subseteq \mathbb{R}^3$.

[1] "For a more convenient handling of the investigations, we will take the liberty to assign a special designation to this V, and call this quantity the *potential* of the masses to which it refers."

3.36 Definition (Fundamental solution) *The function*

$$U : \mathbb{R}^3 \setminus \{\mathbf{0}\} \to (0,\infty),\ \boldsymbol{z} \mapsto \frac{1}{4\pi|\boldsymbol{z}|}$$

is the fundamental solution for the Laplacian $-\Delta$. This means

$$-\Delta U = \delta_{\mathbf{0}},$$

if $U \in L_{1,loc}(\mathbb{R}^3)$ is considered as a distribution on $\mathbb{R}^3$.

3.37 Definition (Newton potential) *The linear mapping $\mathcal{N} : \mathcal{D}(\Omega) \to \mathcal{E}(\mathbb{R}^3)$,*

$$\mathcal{N}\varphi(\boldsymbol{x}) = U * \varphi(\boldsymbol{x}) = \int_\Omega U(\boldsymbol{x}-\boldsymbol{y})\varphi(\boldsymbol{y})\,d\boldsymbol{y}, \quad \boldsymbol{x} \in \mathbb{R}^3,$$

is called Newton potential. It is continuous and extends to a continuous mapping between $\mathcal{E}'(\mathbb{R}^3)$ and $\mathcal{D}'(\Omega)$ by duality,

$$\langle \varphi, \mathcal{N}u\rangle = \langle \mathcal{N}\varphi, u\rangle,$$

for $u \in \mathcal{E}'(\mathbb{R}^3)$ and $\varphi \in \mathcal{D}(\Omega)$.

The Newton potential is the inverse of the Laplace operator on $\mathcal{E}'(\Omega)$.

3.38 Lemma *For $u \in \mathcal{E}'(\mathbb{R}^3)$ it holds*

$$-\Delta\mathcal{N}u = \mathcal{N}(-\Delta u) = u|_\Omega.$$

Proof. For $\varphi \in \mathcal{D}(\Omega)$, we have

$$\begin{aligned}\langle \varphi, -\Delta\mathcal{N}u\rangle &= \langle \mathcal{N}(-\Delta)\varphi, u\rangle \\ &= \langle U * (-\Delta\varphi), u\rangle = \langle (-\Delta U) * \varphi, u\rangle \\ &= \langle \delta_{\mathbf{0}} * \varphi, u\rangle = \langle \varphi, u\rangle\end{aligned}$$

and analogously for $\mathcal{N}(-\Delta u)$. ∎

3.39 Example As a first example, we consider the Newton potential of $\delta_{\boldsymbol{x}_0}$, $\boldsymbol{x}_0 \in \Omega$. Then $\delta_{\boldsymbol{x}_0} \in \mathcal{E}'(\Omega)$ and for the convolution we get

$$U * \delta_{\boldsymbol{x}_0} = U(\cdot - \boldsymbol{x}_0) = \frac{1}{4\pi|\cdot - \boldsymbol{x}_0|}.$$

Thus,

$$\mathcal{N}\delta_{\boldsymbol{x}_0} = \frac{1}{4\pi|\cdot - \boldsymbol{x}_0|}.$$

The spaces $\mathcal{E}'(\Omega)$ and $\mathcal{D}'(\Omega)$ are too large in order to examine the smoothing properties of the Newton potential. Furthermore, we wish to study the mapping properties of the Newton potential in stronger topologies. Our first example with a Dirac distribution already shows that for a sequence $(\boldsymbol{x}_n)_{n\in\mathbb{N}}$ in Ω which converges to $\boldsymbol{x} \in \Omega$, we have

$$\frac{1}{4\pi|\cdot - \boldsymbol{x}_n|} \to \frac{1}{4\pi|\cdot - \boldsymbol{x}|}, \quad n \to \infty \tag{3.1}$$

in $L_{2,\mathrm{loc}}(\mathbb{R}^3)$, which means that the convergence of $(\delta_{\boldsymbol{x}_n})_{n\in\mathbb{N}}$ to $\delta_{\boldsymbol{x}}$ in the weak-$*$ topology implies the stronger convergence of $(\mathcal{N}\delta_{\boldsymbol{x}_n})_{n\in\mathbb{N}}$ in $L_{2,\mathrm{loc}}(\mathbb{R}^3)$. In general, $\mathcal{N}$ smoothes by two orders.

3.40 Theorem ([138, Theorem 3.1.2], [88]) *For $s \in \mathbb{R}$,*

$$\mathcal{N} : H^s_{comp}(\Omega) \to H^{s+2}_{loc}(\mathbb{R}^3)$$

continuously.

3.41 Example From Example 3.33 we know that $\delta_{\boldsymbol{x}_0} \in H^{-3/2-\varepsilon}_{\mathrm{comp}}(\Omega)$ for $\boldsymbol{x}_0 \in \Omega$ and $\varepsilon > 0$. Consequently, $\mathcal{N}\delta_{\boldsymbol{x}_0} \in H^{1/2-\varepsilon}_{\mathrm{loc}}(\Omega)$. For the particular choice of $\varepsilon = 1/2$, we recover our observation (3.1).

In our case the Dirac distribution $\delta_{\boldsymbol{x}_0}$ is an idealised representation of a charged particle placed at $\boldsymbol{x}_0$. Albeit calculations with convolution operators are drastically simplified by this charge model, the singularity at $\boldsymbol{x}_0$ causes theoretical and numerical problems. Since $\delta_{\boldsymbol{x}_0} \notin \widetilde{H}^{-1}(\Omega)$, the well-developed L_2-theory for the numerical solution of the Poisson equation on Lipschitz domains by Finite Element Methods does not apply. For instance, we observe in Example 3.93 that the numerical approximations converge with a suboptimal rate.

In the theoretical study of the mean field limit as reviewed in Section 2.3 the regularisation is mitigated by different regularisations. The singular $\mathcal{N}\delta_{\boldsymbol{x}_0}$ is replaced by

$$\widetilde{U}_\sigma(\boldsymbol{x}-\boldsymbol{x}_0) = \frac{1}{4\pi}\frac{1}{\sqrt{(x_1-x_{0,1})^2+(x_2-x_{0,2})^2+(x_3-x_{0,3})^2+\sigma^2}}, \quad \boldsymbol{x} \in \mathbb{R}^3,$$

see Neunzert [119], or

$$U_\sigma(\boldsymbol{x}-\boldsymbol{x}_0) = \frac{1}{4\pi}\begin{cases} \dfrac{3}{2\sigma} - \dfrac{|\boldsymbol{x}-\boldsymbol{x}_0|^2}{2\sigma^3}, & |\boldsymbol{x}-\boldsymbol{x}_0| \le \sigma, \\ \dfrac{1}{|\boldsymbol{x}-\boldsymbol{x}_0|}, & \text{else}, \end{cases} \qquad \boldsymbol{x} \in \mathbb{R}^3. \tag{3.2}$$

used by Lazarovici and Pickl [110]. The latter is the rescaled Newton potential of $B_\sigma(\boldsymbol{x}_0)$, the ball of radius σ centred at $\boldsymbol{x}_0$.

3.42 Lemma *The family of functions in $H^{1/2-\varepsilon}_{comp}(\mathbb{R}^3)$,*

$$\delta^\sigma_{\boldsymbol{x}_0} = \frac{1}{|B_\sigma(\boldsymbol{x}_0)|}\mathbb{1}_{B_\sigma(\boldsymbol{x}_0)},$$

converges to $\delta_{\boldsymbol{x}_0}$ as $\sigma \to 0$ in $H^{-3/2-\varepsilon}_{comp}(\mathbb{R}^3)$ for any $\varepsilon > 0$. Here, $\mathbb{1}_{B_\sigma(\boldsymbol{x}_0)}$ denotes the indicator function of $B_\sigma(\boldsymbol{x}_0)$.

Proof. We first prove that $\delta^\sigma_{\boldsymbol{x}_0} \in H^{1/2-\varepsilon}_{\mathrm{comp}}(\mathbb{R}^3)$ for all $\varepsilon > 0$. To that end, it suffices to consider the case $\boldsymbol{x}_0 = \boldsymbol{0}$ as the Fourier transforms only differ by a constant factor, cf. Lemma 3.27. The Fourier transform of $\delta^\sigma_{\boldsymbol{0}}$ reads

$$\begin{aligned}
\mathcal{F}\big[\delta^\sigma_{\boldsymbol{0}}\big](\boldsymbol{\xi}) &= \frac{1}{|B_\sigma(\boldsymbol{0})|}\int\limits_{B_\sigma(\boldsymbol{0})} \exp(\mathrm{i}\,\boldsymbol{x}\cdot\boldsymbol{\xi})\,\mathrm{d}\boldsymbol{x} \\
&= \frac{1}{|B_\sigma(\boldsymbol{0})|}\int\limits_0^\sigma 2\pi r^2 \int\limits_{-1}^1 \exp(\mathrm{i}\,|\boldsymbol{\xi}|r\zeta)\,\mathrm{d}\zeta\,\mathrm{d}r \\
&= \frac{3}{\sigma^3}\int\limits_0^\sigma r\frac{\sin(|\boldsymbol{\xi}|r)}{|\boldsymbol{\xi}|}\,\mathrm{d}r = \frac{3}{\sigma^2|\boldsymbol{\xi}|^2}\left(\frac{\sin(\sigma|\boldsymbol{\xi}|)}{\sigma|\boldsymbol{\xi}|} - \cos(\sigma|\boldsymbol{\xi}|)\right), \quad \boldsymbol{\xi} \in \mathbb{R}^3.
\end{aligned}$$

The term in brackets is bounded on $\mathbb{R}^3$ and thus $\langle\cdot\rangle^s \mathcal{F}\left[\delta_{\mathbf{0}}^\sigma\right]$ is square-integrable if and only if

$$2(s-2)+2<-1,$$

that is $s<1/2$. By expanding the trigonometric functions into their Taylor series around zero it follows

$$\lim_{\sigma\to\mathbf{0}} \mathcal{F}\left(\delta_{\mathbf{0}}^\sigma\right)(\boldsymbol{\xi}) = 1 = \mathcal{F}(\delta_{\mathbf{0}})(\boldsymbol{\xi}), \quad \boldsymbol{\xi}\in\mathbb{R}^3.$$

Together with the dominated convergence theorem [106, Theorem 5.8 Chapter VI],

$$\int_{\mathbb{R}^3} \langle\boldsymbol{\xi}\rangle^{-3-2\varepsilon} |\mathcal{F}\left[\delta_{\boldsymbol{x}_0}^\sigma\right](\boldsymbol{\xi}) - \mathcal{F}[\delta_{\mathbf{0}}](\boldsymbol{\xi})|^2 \,\mathrm{d}\boldsymbol{\xi} \to 0, \quad \sigma\to 0,$$

that is

$$\delta_{\boldsymbol{x}_0}^\sigma \to \delta_{\boldsymbol{x}_0}, \quad \sigma\to 0$$

in $H_{\mathrm{comp}}^{-3/2-\varepsilon}$ for all $\varepsilon>0$. ■

3.43 Lemma *With the notation of Lemma 3.42 it holds*

$$\mathcal{N}\delta_{\boldsymbol{x}_0}^\sigma = U_\sigma(\cdot-\boldsymbol{x}_0),$$

where U_σ is given by (3.2).

Proof. We first note that

$$\mathcal{N}\delta_{\boldsymbol{x}_0}^\sigma(\boldsymbol{z}) = \frac{1}{|B_\sigma(\boldsymbol{x}_0)|}\int_{B_\sigma(\boldsymbol{x}_0)} \frac{1}{4\pi|\boldsymbol{z}-\boldsymbol{y}|}\,\mathrm{d}\boldsymbol{y}, \quad \boldsymbol{z}\in\mathbb{R}^3,$$

so by the mean value property of harmonic functions [55, p. 25]

$$\mathcal{N}\delta_{\boldsymbol{x}_0}^\sigma(\boldsymbol{z}) = \frac{1}{4\pi|\boldsymbol{z}-\boldsymbol{x}_0|}$$

for $\boldsymbol{z}\in\mathbb{R}^3$ outside $\overline{B}_\sigma(\boldsymbol{x}_0)$. If $\boldsymbol{z}$ lies inside the ball $B_\sigma(\boldsymbol{x}_0)$, then

$$\begin{aligned}
\mathcal{N}\delta_{\boldsymbol{x}_0}^\sigma(\boldsymbol{z}) &= \frac{3}{4\pi\sigma^3} 2\pi\sigma^3 \int_0^1\int_{-1}^1 \frac{1}{4\pi} r^2 \left[r^2 - 2\frac{|\boldsymbol{z}-\boldsymbol{x}_0|}{\sigma} r\zeta + \frac{|\boldsymbol{z}-\boldsymbol{x}_0|^2}{\sigma^2}\right]^{-\frac{1}{2}} \mathrm{d}\zeta\,\mathrm{d}r \\
&= \frac{1}{4\pi}\frac{3}{2}\int_0^1 \frac{\sigma}{|\boldsymbol{z}-\boldsymbol{x}_0|} r\left(\frac{|\boldsymbol{z}-\boldsymbol{x}_0|}{\sigma} + r - \left|\frac{|\boldsymbol{z}-\boldsymbol{x}_0|}{\sigma} - r\right|\right)\mathrm{d}r \\
&= \frac{1}{4\pi}\left(\frac{3}{2\sigma} - \frac{|\boldsymbol{z}-\boldsymbol{x}_0|^2}{2\sigma^3}\right),
\end{aligned}$$

concluding the proof. ■

The Newton potential of $\delta_{\boldsymbol{x}_0}^\sigma$ agrees with that of a point charge outside $B_\sigma(\boldsymbol{x}_0)$ and only regularises the singularity in zero. Furthermore, $\mathcal{N}\delta_{\boldsymbol{x}_0}^\sigma$ is constant on $\partial B_\sigma(\boldsymbol{x}_0)$. By the following result due to Fraenkel [57, Theorem 1.1] (see also [132]) this uniquely characterises $\delta_{\boldsymbol{x}_0}^\sigma$ up to a constant factor.

3.44 Theorem *If the Newton potential of an open and bounded set $\Omega\subseteq\mathbb{R}^3$ is constant on $\partial\Omega$, then Ω is a ball, $\Omega = B_\sigma(\boldsymbol{x}_0)$ for some $\sigma>0$ and $\boldsymbol{x}_0\in\mathbb{R}^3$.*

3.3. Boundary Value Problems

> Partial differential equations are made by God, the boundary conditions by the Devil.
>
> *(Alan Turing)*

Although the Newton potential is primarily defined to study solutions of the free space equation

$$-\Delta u = f \quad \text{in } \mathbb{R}^3,$$

we shall see in this section that it is a versatile tool to analyse boundary value problems of the form

$$\begin{cases} -\Delta u = f & \text{in } \Omega, \\ u = g_D & \text{on } \Gamma_D, \\ \boldsymbol{n} \cdot \nabla u = g_N & \text{on } \Gamma_N, \end{cases} \tag{3.3}$$

with a bounded domain $\Omega \subseteq \mathbb{R}^3$ whose boundary $\Gamma = \partial\Omega$ with outward normal vector field $\boldsymbol{n}$ is decomposed in an open Dirichlet part Γ_D and an open Neumann part Γ_N such that

$$\overline{\Gamma}_D \cup \overline{\Gamma}_N = \Gamma, \quad \Gamma_D \cap \Gamma_N = \varnothing,$$

and given right hand side f, Dirichlet datum g_D and Neumann datum g_N.

Before we discuss the application of $\mathcal{N}$ to (3.3) we need a precise notion of the boundary values appearing in (3.3). To that end, we review Sobolev spaces on Lipschitz manifolds and relate them to the domain by means of trace operators. Finally, we give a representation of u purely by its traces on the boundary and the volume term f and discuss the mapping properties of the involved operators.

3.3.1. Sobolev Spaces and Lipschitz Boundaries

The Sobolev spaces $H^s_{\mathrm{loc}}(\Omega)$ and $H^s_{\mathrm{comp}}(\Omega)$, we have discussed so far, are well suited for the investigation of convolution-type operators. The Newton potential from the previous section is a typical example. However, these spaces are either too small or too large to sufficiently describe values on the boundary. In case of $H^s_{\mathrm{comp}}(\Omega)$, all elements have zero trace on Γ, whereas $H^s_{\mathrm{loc}}(\Omega)$ contains the functions from $\mathcal{E}(\Omega)$ that generally can not be extended to $\overline{\Omega}$. Therefore, we need to further restrict the set of admissible functions. Since we need results for both Ω ($d = 3$) and Γ ($d = 2$), we present the theory for general dimension d, $\Omega \subseteq \mathbb{R}^d$. Most of the material is taken from [113, Chapter 3].

3.45 Definition (Sobolev spaces on subsets III) *For $s \in \mathbb{R}$, we define the Sobolev space $H^s(\Omega)$ of order s on Ω as the quotient space*

$$H^s(\Omega) = H^s(\mathbb{R}^d)/H^s_{\Omega^c},$$

where $u_1, u_2 \in H^s(\mathbb{R}^d)$ are equivalent if $u_1 - u_2 \in H^s_{\Omega^c}$, i.e. u_1 and u_2 coincide on Ω. Together with the quotient norm

$$\|[u]\| = \inf_{v \in H^s_{\Omega^c}} \|u - v\|_s, \quad [u] \in H^s(\Omega),$$

$H^s(\Omega)$ is a Hilbert space. Here, $[\cdot]$ denotes the equivalent classes in $H^s(\Omega)$.

3.46 Remark There is a one-to-one correspondence between the equivalence classes in $H^s(\Omega)$ and the restriction of elements in $H^s(\mathbb{R}^d)$ on Ω. Specifically, for $u_1, u_2 \in [u]$ with $[u] \in H^s(\Omega)$,

$$u_1|_\Omega = u_2|_\Omega + (u_1 - u_2)|_\Omega = u_2|_\Omega,$$

since $u_1 = u_2$ on Ω. Thus, $[u]$ is uniquely described by $u_1|_\Omega$ and instead of working with equivalence classes, we can think of $H^s(\Omega)$ as a space of certain restricted distributions. An equivalent norm on $H^s(\Omega)$ is

$$\|[u]\| = \inf_{\substack{\widetilde{u} \in H^s(\mathbb{R}^d) \\ \widetilde{u}|_\Omega = u}} \|\widetilde{u}\|_s, \quad [u] \in H^s(\Omega).$$

3.47 Remark Several properties that hold for $H^s(\mathbb{R}^d)$ or $H^s_{\mathrm{comp}}(\Omega)$ do not hold for $H^s(\Omega)$ for a general open set $\Omega \subseteq \mathbb{R}^d$. They crucially depend on the smoothness of the boundary $\partial\Omega$, for instance:

- In general, it is not possible to continuously select an element of the equivalence class for $u \in H^s(\Omega)$, i.e. an extension of u from Ω to $\mathbb{R}^d$.
- Even though $\mathcal{D}(\mathbb{R}^d)$ is dense in $H^s(\mathbb{R}^d)$, it is generally not true that $\mathcal{D}\big(\overline{\Omega}\big)$ is dense in $H^s(\Omega)$. However, $\mathcal{E}(\Omega) \cap H^s(\Omega)$ is always dense in $H^s(\Omega)$. This follows by a slight generalisation of the classical paper "$H = W$" by Meyers and Serrin [115].

For the characterisation of the dual space of $H^s(\Omega)$, we need a second class of Sobolev spaces on Ω.

3.48 Definition (Sobolev spaces on subsets IV) *For $s \in \mathbb{R}$, $\widetilde{H}^s(\Omega)$ is defined as the completion of $\mathcal{D}(\Omega)$ in $H^s(\mathbb{R}^d)$,*

$$\widetilde{H}^s(\Omega) = \overline{\mathcal{D}(\Omega)}^{H^s(\mathbb{R}^d)}.$$

From the definition we see

$$\widetilde{H}^s(\Omega) \subseteq H^s_{\overline{\Omega}},$$

since $H^s_{\overline{\Omega}}$ is a closed subspace of $H^s(\mathbb{R}^d)$ that contains $\mathcal{D}(\Omega)$. For $s \geq 0$ of the form $s = m + \mu$ with $m \in \mathbb{N}$ and $\mu \in [0, 1)$, we conclude by Theorem 3.31:

$$\begin{gathered} D^{\boldsymbol{\alpha}} u \in L_2(\Omega) \quad \forall \boldsymbol{\alpha} \in \mathbb{N}^d : |\boldsymbol{\alpha}| \leq m, \\ \int_\Omega \int_\Omega \frac{(D^{\boldsymbol{\alpha}} u(\boldsymbol{x}) - D^{\boldsymbol{\alpha}} u(\boldsymbol{y}))^2}{|\boldsymbol{x} - \boldsymbol{y}|^{d+2\mu}} \, \mathrm{d}\boldsymbol{x} \, \mathrm{d}\boldsymbol{y} < \infty, \quad \forall \boldsymbol{\alpha} \in \mathbb{N}^d : |\boldsymbol{\alpha}| = m. \end{gathered} \tag{3.4}$$

for all $u \in H^s(\Omega)$. To establish the converse inclusion, respectively, implication, we need Lipschitz regularity of the boundary Γ.

3.49 Definition (Lipschitz boundary) *An open set $\Omega \subseteq \mathbb{R}^d$ has a Lipschitz boundary if for all $\boldsymbol{x} \in \Gamma = \partial\Omega$, there exist $a_1, \ldots, a_d > 0$, an open neighbourhood V and a Lipschitz continuous function*

$$\zeta : \prod_{j=1}^{d-1} [-a_j, a_j] \to \mathbb{R}$$

such that after a rigid motion, i.e. a rotation and translation, in a new coordinate system $(y_1, \dots, y_d)$*, we have*

$$V = \{(y_1, \dots, y_d) : -a_j < y_j < a_j,\ j = 1, \dots, d\} = V' \times [-a_d, a_d]$$

and

$$\begin{aligned} |\zeta(\boldsymbol{y}')| &\le \frac{a_n}{2} \quad \forall\, \boldsymbol{y}' \in V', \\ \Omega \cap V &= \{(\boldsymbol{y}', y_d) \in V : y_d < \zeta(\boldsymbol{y}')\}, \\ \Gamma \cap V &= \{(\boldsymbol{y}', y_d) \in V : y_d = \zeta(\boldsymbol{y}')\}. \end{aligned}$$

If Γ *is unbounded, we additionally require that the Lipschitz constants of the local parametrisations* ζ *are uniformly bounded.*

3.50 Remark Every open set whose boundary is a smooth manifold has a Lipschitz boundary. Moreover, the following holds [73, Corollary 1.2.2.3]:

3.51 Lemma *Let* $\Omega \subseteq \mathbb{R}^d$ *be a bounded open convex set. Then* Ω *has a Lipschitz boundary.*

For open sets with Lipschitz boundary, the extension and density properties from Remark 3.47 hold true:

3.52 Lemma *Let* Ω *have a Lipschitz boundary. Then* $\mathcal{D}(\bar{\Omega})$ *is dense in* $H^s(\Omega)$ *for all* $s \in \mathbb{R}$.

3.53 Lemma *Suppose that* Ω *has Lipschitz boundary. Then for all* $s \ge 0$ *there exists a continuous operator, called Stein's extension operator [147, p. VI.23],*

$$\mathfrak{E} : H^s(\Omega) \to H^s(\mathbb{R}^d)$$

such that $(\mathfrak{E}u)|_\Omega = u$ *for all* $u \in H^s(\Omega)$*. For smooth functions, also the values on the boundary are preserved:*

$$(\mathfrak{E}\varphi)|_{\bar{\Omega}} = \varphi, \quad \varphi \in \mathcal{D}(\bar{\Omega}).$$

3.54 Proposition *If* Ω *has Lipschitz boundary, then*

$$\widetilde{H}^s(\Omega) = H^s_{\bar{\Omega}}$$

for all $s \in \mathbb{R}$*. Furthermore, if* $s = m + \mu$ *with* $m \in \mathbb{N}$ *and* $\mu \in [0, 1)$*, then*

$$H^m(\Omega) = \left\{u \in L_2(\Omega) : \forall \boldsymbol{\alpha} \in \mathbb{N}^d : |\boldsymbol{\alpha}| \le m : D^{\boldsymbol{\alpha}} u \in L_2(\Omega)\right\}$$

and if $\mu > 0$*,*

$$H^s(\Omega) = \{u \in H^m(\Omega) : \forall \boldsymbol{\alpha} \in \mathbb{N}^d : |\boldsymbol{\alpha}| = m : |D^{\boldsymbol{\alpha}} u|_{\mu,\Omega} < \infty\},$$

where the seminorm $|\cdot|_{\mu,\Omega}$ *is given by*

$$|v|^2_{\mu,\Omega} = \int_\Omega \int_\Omega \frac{(v(\boldsymbol{x}) - v(\boldsymbol{y}))^2}{|\boldsymbol{x} - \boldsymbol{y}|^{d+2\mu}}\, d\boldsymbol{x}\, d\boldsymbol{y}, \quad v \in H^\mu(\Omega).$$

An equivalent norm on $H^s(\Omega)$ *is*

$$\|u\|^2_{s,\Omega} = \sum_{\substack{\boldsymbol{\alpha} \in \mathbb{N}^d \\ |\boldsymbol{\alpha}| \le m}} \|D^{\boldsymbol{\alpha}} u\|^2_{L_2(\Omega)} + \sum_{\substack{\boldsymbol{\alpha} \in \mathbb{N}^d \\ |\boldsymbol{\alpha}| = m}} |D^{\boldsymbol{\alpha}} u|^2_{\mu,\Omega}, \quad u \in H^s(\Omega),$$

where the sum over the seminorms is dropped if $\mu = 0$.

Sobolev spaces on Lipschitz domains admit an easy characterisation of their dual spaces.

3.55 Proposition *For $s \in \mathbb{R}$ and an open set $\Omega \subseteq \mathbb{R}^d$ with Lipschitz boundary,*

$$(H^s(\Omega))' \cong \widetilde{H}^{-s}(\Omega), \quad (\widetilde{H}^s(\Omega))' \cong H^{-s}(\Omega).$$

3.3.2. Sobolev Spaces on Manifolds

By virtue of the local parametrisation for the Lipschitz boundary Γ, we can identify functions on Γ with those on $\mathbb{R}^{d-1}$. For the sake of convenience, the assume that the boundary Γ is compact. Thus, there are open cubes $V_1, \dots, V_n \subseteq \mathbb{R}^d$ together with rigid motions $R_1, \dots, R_n$ on $\mathbb{R}^d$ and Lipschitz continuous functions $\zeta_1, \dots, \zeta_n$ defined on $V_1', \dots, V_n'$ such that

$$\Gamma \subseteq \bigcup_{i=1}^{n} R_i V_i$$

and for all $\boldsymbol{x} \in \Gamma$ there exist $i \in \{1, \dots, n\}$ and $\widetilde{\boldsymbol{x}} \in V_i'$ with $\boldsymbol{x} = R_i(\widetilde{\boldsymbol{x}}, \zeta_i(\widetilde{\boldsymbol{x}}))$. For a partition of unity $(\chi_i)_{i=1}^n$ of Γ subordinate $(R_i V_i)_{i=1}^n$, we can rewrite every function $u : \Gamma \to \mathbb{R}$ as

$$\widetilde{u}(\widetilde{\boldsymbol{x}}) = \sum_{i=1}^{n} (\chi_i u) \circ R_i(\widetilde{\boldsymbol{x}}, \zeta_i(\widetilde{\boldsymbol{x}})), \quad \widetilde{\boldsymbol{x}} \in \mathbb{R}^{d-1}.$$

By Rademacher's theorem [131], Lipschitz continuous functions are almost everywhere differentiable. We can therefore define the surface gradient ∇_Γ as the gradient of above representation. The space $H^1(\Gamma)$ consists of those functions u on Γ for which $\widetilde{u}$ is in $H^1_{\mathrm{loc}}(\mathbb{R}^{d-1})$. For spaces $H^s(\Gamma)$ with $s \in (0,1)$, we use the characterisation from Theorem 3.31. This motivates the following definition:

3.56 Definition (Sobolev spaces on manifolds) *For $s \in (0,1)$, we define the Sobolev space of order s on Γ as*

$$H^s(\Gamma) = \{u \in L_2(\Gamma) : |u|_{s,\Gamma} < \infty\},$$

with

$$|u|^2_{s,\Gamma} = \int_\Gamma \int_\Gamma \frac{(u(\boldsymbol{x}) - u(\boldsymbol{y}))^2}{|\boldsymbol{x} - \boldsymbol{y}|^{d-1+2s}} \, dS_{\boldsymbol{y}} \, dS_{\boldsymbol{x}}.$$

Endowed with the norm

$$\|u\|^2_{s,\Gamma} = \|u\|^2_{L_2(\Gamma)} + |u|^2_{s,\Gamma}, \quad u \in H^s(\Gamma),$$

this normed space is a Hilbert space. Furthermore, we set $H^0(\Gamma) = L_2(\Gamma)$ and

$$H^1(\Gamma) = \{u \in L_2(\Gamma) : \|\nabla_\Gamma u\|_{L_2(\Gamma)} < \infty\},$$

which is a Hilbert space with respect to the norm

$$\|u\|^2_{1,\Gamma} = \|u\|^2_{L_2(\Gamma)} + \|\nabla_\Gamma u\|^2_{L_2(\Gamma)}, \quad u \in H^1(\Gamma).$$

Sobolev spaces of negative order are defined as the dual space of the respective Sobolev space,

$$H^{-s}(\Gamma) = (H^s(\Gamma))', \quad s \in [0,1].$$

3.57 Remark By construction of the Sobolev spaces on Γ, the inclusion

$$\iota : H^s(\Gamma) \hookrightarrow L_2(\Gamma)$$

is continuous with dense image for all $s \in [0, 1]$. Therefore, the adjoint

$$\iota' : H^{-s}(\Gamma) \to L_2(\Gamma)'$$

is continuous and injective. Because $H^s(\Gamma)$ is reflexive, ι' has a dense image [23, Chapter 5, Remark 3]. Under the identification $(L_2(\Gamma))' = L_2(\Gamma)$, we have

$$H^s(\Gamma) \hookrightarrow L_2(\Gamma) \hookrightarrow H^{-s}(\Gamma)$$

with dense inclusions. This situation is known as Gelfand triple [66, Chapter I, Section 4.2] or rigged Hilbert spaces, frequently utilised in Quantum Mechanics, see the dissertation [112] and the references cited therein.

In particular, for all $\Phi \in H^{-s}(\Gamma)$ there exists $(\phi_n)_{n\in\mathbb{N}}$ in $L_2(\Gamma)$ such that

$$\sup_{\substack{u\in H^s(\Gamma)\\ u\neq 0}} \frac{|\langle u, \phi_n\rangle_\Gamma - \Phi(u)|}{\|u\|_{s,\Gamma}} \to 0, \quad n \to \infty,$$

where $\langle\cdot,\cdot\rangle_\Gamma$ denotes the $L_2(\Gamma)$-pairing

$$L_2(\Gamma) \times L_2(\Gamma) \to \mathbb{R}, \ (u, v) \mapsto \int_\Gamma u\, v \,\mathrm{d}S.$$

Another application of Rademacher's theorem shows that we can uniquely define an outward normal vector almost everywhere on Γ.

3.58 Lemma *Let $\Omega \subseteq \mathbb{R}^d$ open with Lipschitz boundary Γ. There exits a measurable function*

$$\boldsymbol{n} : \Gamma \to S^{d-1}$$

which almost everywhere is the unique outward normal vector to Γ. Here, S^{d-1} denotes the unit sphere in $\mathbb{R}^d$.

Proof. After rotation and translation and a partition of unity, we can assume that Ω has the form

$$\Omega = \{(\boldsymbol{y}', y_d) \in V : y_d < \zeta(\boldsymbol{y}')\}$$

and furthermore

$$\Gamma = \{(\boldsymbol{y}', y_d) \in V : y_d = \zeta(\boldsymbol{y}')\},$$

where $V = [-a_1, a_1] \times \cdots \times [-a_d, a_d] = V' \times [-a_d, a_d]$ for $a_1, \ldots, a_d > 0$ and $\zeta : V' \to \mathbb{R}$ is Lipschitz continuous. Since $\boldsymbol{y} \mapsto y_d - \zeta(\boldsymbol{y}')$ equals zero on Γ and is almost everywhere differentiable, Γ has a unique tangent plane for almost all $\boldsymbol{y}' \in V'$ with normal vector

$$\boldsymbol{n} = \frac{1}{\sqrt{1 + |\nabla\zeta(\boldsymbol{y}')|^2}} \begin{pmatrix} -\zeta(\boldsymbol{y}') \\ 1 \end{pmatrix}$$

By definition, $\boldsymbol{y} \to y_d - \zeta(\boldsymbol{y}')$ is negative on Ω and positive on $\overline{\Omega}^c$, so, because the gradient points into the direction of the steepest ascent, the vector $\boldsymbol{n}(\boldsymbol{y})$ is the outward normal vector of Γ at $\boldsymbol{y}$. ∎

3.3.3. Trace Operators

Sobolev spaces on Γ naturally arise in the discussion of boundary values. An important result is Gagliardo's trace lemma [61], in the version of Costabel [37]:

3.59 Lemma *For all $s \in (1/2, 3/2)$, there is a unique continuous extension of*

$$\gamma_0 : \mathcal{E}(\mathbb{R}^d) \to H^{s-1/2}(\Gamma),\ \varphi \mapsto \varphi|_\Gamma$$

to $H^s_{loc}(\mathbb{R}^d)$ for all open sets $\Omega \subseteq \mathbb{R}^d$ with Lipschitz boundary.

The range $(1/2, 3/2)$ in the formulation in the trace lemma cannot be extended in general, see Mikhailov [116]:

3.60 Lemma *There is no bounded extension of the trace operator γ_0 from $H^{1/2}_{loc}(\mathbb{R}^d)$ to $L_2(\Gamma)$ for an open set $\Omega \subseteq \mathbb{R}^d$ with Lipschitz boundary.*

3.61 Lemma *If $s > 3/2$ and $\Omega \subseteq \mathbb{R}^d$ is an open set with Lipschitz boundary, then*

$$\gamma_0 : H^s_{loc}(\mathbb{R}^d) \to H^1(\Gamma)$$

is continuous.

For $s \in (1/2, 3/2)$, we loose $1/2$ order of regularity when applying the trace operator. This result is sharp:

3.62 Lemma *Let Ω be a bounded Lipschitz domain. For $s \in (1/2, 3/2)$, the trace operator*

$$\gamma_0 : H^s_{loc}(\mathbb{R}^d) \to H^{s-1/2}(\Gamma)$$

is surjective. There exits a continuous linear operator

$$\mathfrak{E} : H^{s-1/2}(\Gamma) \to H^s_{loc}(\mathbb{R}^d),$$

called extension operator, such that

$$\gamma_0 \mathfrak{E} u = u, \quad \forall u \in H^{s-1/2}(\Gamma).$$

With the definition of γ_0 for Sobolev spaces, we proceed with the definition of the normal derivative. For the ease of presentation, we restrict us to Sobolev spaces of integral order, namely $H^2(\Omega)$ and $H^1(\Omega)$.

For $u \in H^2(\Omega)$, we have $\nabla u \in H^1(\Omega)^d$. Therefore, its componentwise trace $\gamma_0(\nabla u)$ is well-defined. We set

$$\gamma_1 u = \boldsymbol{n} \cdot \gamma_0(\nabla u),$$

where $\boldsymbol{n}$ is the outward normal vector to Γ, the boundary of the Lipschitz set $\Omega \subseteq \mathbb{R}^d$. Clearly, this defines a continuous operator

$$\gamma_1 : H^2(\Omega) \to L_2(\Gamma).$$

For our purposes, the definition of γ_1 is too strict. First, we wish to study boundary values problems and the associated integral operators in more generality. Second, the range of the adjoint $\gamma_1' : L_2(\Gamma) \to \widetilde{H}^{-2}(\Omega)$ is too large.

Thus, we extend above definition of γ_1 from $H^2(\Omega)$ to a larger space. The crucial observation is that we only need information on the normal trace of the gradient which can be defined for less regularity than $\boldsymbol{u} \in H^1(\Omega)$.

3.63 Definition (Special Sobolev spaces) *Let $\Omega \subseteq \mathbb{R}^d$ be open. With $H(\operatorname{div}, \Omega)$ we denote the space of functions $\boldsymbol{u} \in L_2(\Omega)^d$ such that the distributional divergence $\operatorname{div} \boldsymbol{u}$ lies in $L_2(\Omega)$,*

$$\int_\Omega \operatorname{div} \boldsymbol{u}\, \varphi \, d\boldsymbol{x} = -\int_\Omega \boldsymbol{u} \cdot \nabla \varphi \, d\boldsymbol{x}, \quad \varphi \in \mathcal{D}(\Omega).$$

Endowed with the graph norm

$$\|\boldsymbol{u}\|^2_{\Omega,\operatorname{div}} = \|\boldsymbol{u}\|^2_{0,\Omega} + \|\operatorname{div} \boldsymbol{u}\|^2_{0,\Omega}, \quad \boldsymbol{u} \in H(\operatorname{div}, \Omega),$$

this space is a Hilbert space.

For $v \in \mathcal{D}\big(\bar{\Omega}\big)$ and $\boldsymbol{u} \in \mathcal{D}\big(\bar{\Omega}\big)^d$, the divergence of the product $v\boldsymbol{u}$ is given by

$$\operatorname{div}(v\boldsymbol{u}) = \nabla v \cdot \boldsymbol{u} + \boldsymbol{v} \operatorname{div} \boldsymbol{u},$$

so an application of Gauß' theorem the left hand side after integration over Ω yields

$$\int_\Gamma v\, \boldsymbol{u} \cdot \boldsymbol{n} \, \mathrm{d}S_{\boldsymbol{x}} = \int_\Omega \Big(\nabla v \cdot \boldsymbol{u} + v \operatorname{div} \boldsymbol{u} \Big) \, \mathrm{d}\boldsymbol{x}.$$

Now, the right hand side is a continuous bilinear form on $H(\operatorname{div}, \Omega) \times H^1(\Omega)$, so the left hand side can be uniquely extended to

$$\Big(\gamma_0 H^1(\Omega)\Big)' \times \gamma_0 H^1(\Omega) = H^{-1/2}(\Gamma) \times H^{1/2}(\Gamma).$$

Therefore, it holds:

3.64 Lemma *The normal trace*

$$\gamma_n : \mathcal{D}\big(\bar{\Omega}\big)^d \to L_2(\Gamma), \boldsymbol{u} \mapsto \boldsymbol{n} \cdot \gamma_0 \boldsymbol{u}$$

has a unique, surjective linear continuous extension to

$$\gamma_n : H(\operatorname{div}, \Omega) \to H^{-1/2}(\Gamma).$$

Since the normal derivative is the normal trace of the gradient, the additional requirement for $u \in H^1(\Omega)$ to have a well-defined normal derivative is $\nabla u \in H(\operatorname{div}, \Omega)$, so

$$\operatorname{div}\big(\nabla u\big) = \Delta u \in L_2(\Omega).$$

The space of such functions is denoted by $H^1_\Delta(\Omega)$,

$$H^1_\Delta(\Omega) = \{u \in H^1(\Omega) : \Delta u \in L_2(\Omega)\}.$$

It is a Hilbert space if equipped with the graph norm,

$$\|u\|^2 = \|u\|^2_{1,\Omega} + \|\Delta u\|^2_{0,\Omega}, \quad u \in H^1_\Delta(\Omega).$$

3.65 Lemma (Normal derivative) *For $\Omega \subseteq \mathbb{R}^d$ open and bounded with Lipschitz boundary Γ, the continuous linear mapping*

$$\gamma_1 : H^1_\Delta(\Omega) \to H^{-1/2}(\Gamma),$$

defined by

$$\gamma_1 u = \gamma_n \nabla u, \quad u \in H^1_\Delta(\Omega),$$

is surjective and extends the normal derivative for $u \in H^2(\Omega)$, i.e.

$$\gamma_1 u = \boldsymbol{n} \cdot \gamma_0(\nabla u).$$

For $u \in H^1_\Delta(\Omega)$ and $v \in H^1(\Omega)$ we have by the definition of γ_1,

$$\langle \gamma_0 v, \gamma_1 u \rangle_\Gamma = \langle \nabla v, \nabla u \rangle_\Omega + \langle v, \Delta u \rangle_\Omega. \tag{3.5}$$

This relation is known as Green's first identity.

3.66 Lemma *Let $\Omega \subseteq \mathbb{R}^d$ be open and bounded with Lipschitz boundary Γ. The normal derivative*

$$\gamma_1 : H^1_\Delta(\Omega) \to H^{-1/2}(\Gamma)$$

is continuous and surjective if $H^1_\Delta(\Omega)$ is endowed with the graph norm

$$\|u\|^2_{H^1_\Delta(\Omega)} = \|u\|^2_{1,\Omega} + \|\Delta u\|^2_{0,\Omega}, \quad u \in H^1_\Delta(\Omega).$$

3.3.4. Representation Formula

For the rest of the section we shall focus on three-dimensional boundary value problems. To that end, we fix an open, bounded set $\Omega \subseteq \mathbb{R}^3$ with Lipschitz boundary. With Green's first identity (3.5),

$$\begin{aligned} \langle \gamma_0 v, \gamma_1 u \rangle_\Gamma &= \langle \nabla v, \nabla u \rangle_\Omega + \langle v, \Delta u \rangle_\Omega, \\ \langle \gamma_0 u, \gamma_1 v \rangle_\Gamma &= \langle \nabla u, \nabla v \rangle_\Omega + \langle u, \Delta v \rangle_\Omega, \end{aligned}$$

for $u, v \in H^1_\Delta(\Omega)$. Subtracting the second from the first equation, we get

$$\langle v, \Delta u \rangle_\Omega - \langle \Delta v, u \rangle_\Omega = \langle \gamma_0 v, \gamma_1 u \rangle_\Gamma - \langle \gamma_0 u, \gamma_1 v \rangle_\Gamma. \tag{3.6}$$

This is Green's second identity. We now apply this result to boundary value problems of the form (3.3),

$$\begin{cases} -\Delta u = f & \text{in } \Omega, \\ \gamma_0 u = g_D & \text{on } \Gamma_D, \\ \gamma_1 u = g_N & \text{on } \Gamma_N, \end{cases} \tag{3.7}$$

where $f \in L_2(\Omega)$, $g_D \in H^{1/2}(\Gamma_D)$, $g_N \in H^{-1/2}(\Gamma_N)$ and the open sets $\Gamma_D, \Gamma_N \subseteq \Gamma$ comprise a partition of Γ,

$$\Gamma_D \cap \Gamma_N = \varnothing, \quad \overline{\Gamma}_D \cup \overline{\Gamma}_N = \Gamma.$$

Here, Sobolev spaces on open subsets Γ_1 of Γ are defined by

$$\widetilde{H}^s(\Gamma_1) = \left\{ u \in H^s(\Gamma) : \operatorname{supp} u \subseteq \overline{\Gamma}_1 \right\}, \quad s \in [-1, 1],$$

and similar to Definition 3.45,

$$H^s(\Gamma_1) = H^s(\Gamma)/\widetilde{H}^s(\Gamma \setminus \overline{\Gamma}_1) \cong \left\{u|_{\Gamma_1} : u \in H^s(\Gamma)\right\}, \quad s \in [-1, 1].$$

With Green's second identity (3.6), we see

$$\langle -\Delta v, u\rangle_\Omega = \langle \gamma_0 v, \gamma_1 u\rangle_\Gamma - \langle \gamma_0 u, \gamma_1 v\rangle_\Gamma + \langle v, f\rangle_\Omega \quad \forall v \in H^1_\Delta(\Omega),$$

where we have used that $-\Delta u = f$ in Ω. Rewriting the equation by the use of adjoints yields

$$\langle -\Delta v, u\rangle_\Omega = \langle v, \gamma_0'\gamma_1 u\rangle_\Omega - \langle v, \gamma_1'\gamma_0 u\rangle_\Omega + \langle v, f\rangle_\Omega \quad \forall v \in H^1_\Delta(\Omega).$$

Applying the Newton potential, we get Green's third identity or representation formula:

3.67 Theorem ([113, Theorem 6.10], [138, Theorem 3.1.6]) *For the solution u of the boundary value problem* (3.7) *holds the following representation by the Cauchy datum $(\gamma_0 u, \gamma_1 u)$ and right hand side f:*

$$u = (\mathcal{N}\gamma_0')\gamma_1 u - (\mathcal{N}\gamma_1')\gamma_0 u + \mathcal{N} f. \tag{3.8}$$

Proof. We start with the consequence from Green's second identity,

$$\langle -\Delta v, u\rangle_\Omega = \langle v, \gamma_0'\gamma_1 u\rangle_\Omega - \langle v, \gamma_1'\gamma_0 u\rangle_\Omega + \langle v, f\rangle_\Omega \quad \forall v \in H^1_\Delta(\Omega).$$

From Lemma 3.38, we know that the Newton potential is the inverse of the negative Laplacian, so

$$\langle v, u\rangle_\Omega = \langle v, \mathcal{N}\gamma_0'\gamma_1 u\rangle_\Omega - \langle v, \mathcal{N}\gamma_1'\gamma_0 u\rangle_\Omega + \langle v, \mathcal{N} f\rangle_\Omega \quad \forall v \in H^1_\Delta(\Omega),$$

This shows

$$u = (\mathcal{N}\gamma_0')\gamma_1 u - (\mathcal{N}\gamma_1')\gamma_0 u + \mathcal{N} f,$$

which concludes the proof. ∎

In the following, the study the mapping properties of $\mathcal{N}\gamma_0'$, $\mathcal{N}\gamma_1'$.

3.68 Definition (Single-layer potential) *The single-layer potential $\mathcal{V} = \mathcal{N}\gamma_0'$ is a linear continuous mapping*

$$\mathcal{V} : H^{-1/2}(\Gamma) \to H^1_{loc}(\mathbb{R}^3),$$

in particular,

$$\mathcal{V} : H^{-1/2}(\Gamma) \to H^1(\Omega).$$

The function $\mathcal{V}\psi$ is harmonic in $\Omega \cup \overline{\Omega}^c$ for all $\psi \in H^{-1/2}(\Gamma)$. If $\psi : \Gamma \to \mathbb{R}$ is bounded and measurable,

$$\mathcal{V}\psi(\boldsymbol{x}) = \frac{1}{4\pi}\int_\Gamma \frac{1}{|\boldsymbol{x} - \boldsymbol{y}|}\psi(\boldsymbol{y})\, dS_{\boldsymbol{y}}, \quad \boldsymbol{x} \in \mathbb{R}^3.$$

Proof. From Lemma 3.59 we know

$$\gamma_0 : H^1_{\text{loc}}(\mathbb{R}^3) \to H^{1/2}(\Gamma)$$

continuously. Thus with Theorem 3.35

$$\gamma_0' : H^{-1/2}(\Gamma) \to H^{-1}_{\text{comp}}(\mathbb{R}^3).$$

Composing this with the Newton potential $\mathcal{N}$,

$$\mathcal{N} : H^{-1}_{\mathrm{loc}}(\mathbb{R}^3) \to H^{1}_{\mathrm{loc}}(\mathbb{R}^3),$$

yields

$$\mathcal{V} : H^{-1/2}(\Gamma) \to H^{1}_{\mathrm{loc}}(\mathbb{R}^3) \hookrightarrow H^{1}(\Omega)$$

continuously. To show that $\mathcal{V}\psi$ is harmonic on $\Omega \cup \bar{\Omega}^c = \mathbb{R}^3 \setminus \Gamma$, let $\varphi \in \mathcal{D}(\mathbb{R}^3 \setminus \Gamma)$. Then,

$$\langle -\Delta\varphi, \mathcal{V}\psi\rangle_\Omega = -\langle \mathcal{N}\Delta\varphi, \gamma_0'\psi\rangle_\Omega = \langle \varphi, \gamma_0'\psi\rangle_\Omega = \langle \gamma_0\varphi, \psi\rangle_\Gamma = 0,$$

where the ultimate equality follows from $\gamma_0\varphi = 0$ since $\operatorname{supp}\varphi$ is a proper subset of $\mathbb{R}^3 \setminus \Gamma$. ■

3.69 Definition (Double-layer potential) *The double-layer potential $\mathcal{W} = \mathcal{N}\gamma_1'$ is a linear continuous mapping*

$$\mathcal{W} : H^{1/2}(\Gamma) \to H^{1}(\Omega),$$

with

$$\mathcal{W}\varphi(\boldsymbol{x}) = \frac{1}{4\pi}\int_\Gamma \frac{(\boldsymbol{x}-\boldsymbol{y})\cdot\boldsymbol{n}(\boldsymbol{y})}{|\boldsymbol{x}-\boldsymbol{y}|^3}\varphi(\boldsymbol{y})\,dS_{\boldsymbol{y}}, \quad \boldsymbol{x} \in \Omega \cup \bar{\Omega}^c$$

for $\varphi \in H^{1/2}(\Gamma)$. Furthermore, $\mathcal{W}\varphi$ is harmonic in Ω.

Proof. The mapping property of $\mathcal{W}$ follows from that of $\mathcal{V}$, $\mathcal{N}$ and the regularity of the solution for the boundary value problem (3.7) [37, Theorem 1]. The harmonicity of $\mathcal{W}\varphi$ for $\varphi \in H^{1/2}(\Gamma)$ is proved similar to that of $\mathcal{V}$, where γ_0 is replaced by γ_1. ■

3.3.5. Boundary Integral Operators

With the single- and double-layer potential, we can rewrite the representation formula (3.8) as

$$u = \mathcal{V}\gamma_1 u - \mathcal{W}\gamma_0 u + \mathcal{N} f.$$

Applying γ_0 and γ_1 on above equation gives us a system of coupled boundary integral equations,

$$\begin{pmatrix}\gamma_0 u\\ \gamma_1 u\end{pmatrix} = \begin{pmatrix}\frac{1}{2} - \mathsf{K} & \mathsf{V}\\ \mathsf{W} & \frac{1}{2} + \mathsf{K}'\end{pmatrix}\begin{pmatrix}\gamma_0 u\\ \gamma_1 u\end{pmatrix} + \begin{pmatrix}\mathsf{N}_0 f\\ \mathsf{N}_1 f\end{pmatrix}, \tag{3.9}$$

where $\mathsf{N}_0, \mathsf{N}_1$ are the Dirichlet and Neumann traces of $\mathcal{N}$, respectively, and V is the single-layer operator, K is the double-layer operator and W is the hypersingular operator. Below, we collect some of their properties [148, Chapter 6]:

3.70 Definition (Single-layer operator) *The linear mapping*

$$\mathsf{V} = \gamma_0\mathcal{V} : H^{-1/2}(\Gamma) \to H^{1/2}(\Gamma)$$

is called single-layer operator. It is continuous, self-adjoint and coercive, i.e. there is $c_{\mathsf{V}} > 0$ such that

$$\forall\psi \in H^{-1/2}(\Gamma) : \langle \mathsf{V}\psi, \psi\rangle_\Gamma \geq c_{\mathsf{V}}\|\psi\|^2_{-1/2,\Gamma}.$$

For $\psi : \Gamma \to \mathbb{R}$ bounded and measurable,

$$\mathsf{V}\psi(\boldsymbol{x}) = \frac{1}{4\pi}\int_\Gamma \frac{1}{|\boldsymbol{x}-\boldsymbol{y}|}\psi(\boldsymbol{y})\,dS_{\boldsymbol{y}}, \quad \boldsymbol{x} \in \Gamma.$$

3.71 Definition (Double-layer operator) *The linear mapping*

$$\frac{1}{2} + \mathsf{K} = \gamma_0 \mathcal{W} : H^{1/2}(\Gamma) \to H^{1/2}(\Gamma)$$

is continuous. For $\varphi : \Gamma \to \mathbb{R}$ measurable and bounded the double-layer operator K has the representation

$$\mathsf{K}\varphi(\boldsymbol{x}) = \frac{1}{4\pi} \lim_{\varepsilon \to 0} \int_{\Gamma \setminus B_\varepsilon(\boldsymbol{x})} \frac{(\boldsymbol{x} - \boldsymbol{y}) \cdot \boldsymbol{n}(\boldsymbol{y})}{|\boldsymbol{x} - \boldsymbol{y}|^3} \varphi(\boldsymbol{y})\, dS_{\boldsymbol{y}}, \quad \boldsymbol{x} \in \Gamma.$$

3.72 Definition (Hypersingular operator) *The linear mapping*

$$\mathsf{W} = -\gamma_1 \mathcal{W} : H^{1/2}(\Gamma) \to H^{-1/2}(\Gamma),$$

called hypersingular operator, is continuous and self-adjoint. It is semi-coercive, i.e. there is $c_{\mathsf{W}} > 0$ such that

$$\forall \varphi \in H^{1/2}(\Gamma) : \langle \varphi, \mathsf{W}\varphi \rangle_\Gamma \geq c_{\mathsf{W}} |\varphi|^2_{1/2,\Gamma}.$$

Restricted on $\widetilde{H}^{1/2}(\Gamma_1)$, where $\Gamma_1 \subseteq \Gamma$ is open such that $\Gamma \setminus \Gamma_1$ is not a null set, W is coercive,

$$\forall \varphi \in \widetilde{H}^{1/2}(\Gamma_1) : \langle \varphi, \mathsf{W}\varphi \rangle_\Gamma \geq \widetilde{c}_{\mathsf{W}} \|\varphi\|^2_{1/2,\Gamma},$$

with a constant $\widetilde{c}_{\mathsf{W}} > 0$. If Γ is piecewise smooth, then for $\varphi, \psi \in C(\Gamma)$ that are piecewise smooth,

$$\langle \psi, \mathsf{W}\varphi \rangle_\Gamma = \frac{1}{4\pi} \int_\Gamma \int_\Gamma \frac{\boldsymbol{curl}_\Gamma\, \psi(\boldsymbol{x}) \cdot \boldsymbol{curl}_\Gamma\, \varphi(\boldsymbol{y})}{|\boldsymbol{x} - \boldsymbol{y}|}\, dS_{\boldsymbol{y}}\, dS_{\boldsymbol{x}}.$$

Here $\boldsymbol{curl}_\Gamma$ denotes the surface rotation,

$$\boldsymbol{curl}_\Gamma = \boldsymbol{n} \times \nabla_\Gamma.$$

3.73 Proposition *The continuous linear mapping*

$$\mathsf{C} : H^{1/2}(\Gamma) \times H^{-1/2}(\Gamma) \to H^{1/2}(\Gamma) \times H^{-1/2}(\Gamma), \begin{pmatrix} \varphi \\ \psi \end{pmatrix} \mapsto \begin{pmatrix} \frac{1}{2} - \mathsf{K} & \mathsf{V} \\ \mathsf{W} & \frac{1}{2} + \mathsf{K}' \end{pmatrix} \begin{pmatrix} \varphi \\ \psi \end{pmatrix}$$

is called Calderón projector and is indeed a projection, $\mathsf{C}^2 = \mathsf{C}$.

With the Calderón projector we can express N_1 in terms of N_0 and the single- and double-layer potential. This is especially useful in numerical applications.

3.74 Lemma *In the situation of* (3.9)*, it holds*

$$\mathsf{N}_1 f = \mathsf{V}^{-1} \left(-\frac{1}{2} + \mathsf{K} \right) \mathsf{N}_0 f = \left(-\frac{1}{2} + \mathsf{K}' \right) \mathsf{V}^{-1} \mathsf{N}_0 f.$$

Proof. We have

$$\begin{pmatrix} \gamma_0 u \\ \gamma_1 u \end{pmatrix} = \mathsf{C} \begin{pmatrix} \gamma_0 u \\ \gamma_1 u \end{pmatrix} + \begin{pmatrix} \mathsf{N}_0 f \\ \mathsf{N}_1 f \end{pmatrix},$$

Applying C on both sides yields

$$\mathsf{C} \begin{pmatrix} \gamma_0 u \\ \gamma_1 u \end{pmatrix} = \mathsf{C}^2 \begin{pmatrix} \gamma_0 u \\ \gamma_1 u \end{pmatrix} + \mathsf{C} \begin{pmatrix} \mathsf{N}_0 f \\ \mathsf{N}_1 f \end{pmatrix}.$$

Because of the projection property $\mathsf{C}^2 = \mathsf{C}$ this means

$$\mathsf{C}\begin{pmatrix}\mathsf{N}_0 f\\ \mathsf{N}_1 f\end{pmatrix} = \begin{pmatrix}0\\0\end{pmatrix}.$$

Inspecting the first equation of above system,

$$\mathsf{V}\mathsf{N}_1 f + \left(\frac{1}{2} - \mathsf{K}\right)\mathsf{N}_0 f = 0,$$

shows

$$\mathsf{N}_1 f = \mathsf{V}^{-1}\left(-\frac{1}{2} + \mathsf{K}\right)\mathsf{N}_0 f.$$

By the projection property of the Calderón projector, $\mathsf{C}^2 = \mathsf{C}$, it follows

$$\mathsf{V}\mathsf{K}' = \mathsf{K}\mathsf{V},$$

and therefore

$$\mathsf{V}^{-1}\left(-\frac{1}{2} + \mathsf{K}\right)\mathsf{N}_0 f = \left(-\frac{1}{2} + \mathsf{K}'\right)\mathsf{V}^{-1}\mathsf{N}_0 f,$$

which proves the alternative formulation. ■

From (3.7) the traces of u are known only on parts of the boundary. By choosing extensions $(\overline{g}_D, \overline{g}_N) \in H^{1/2}(\Gamma) \times H^{-1/2}(\Gamma)$ of g_D and g_N, respectively, we can write

$$\begin{aligned}\gamma_0 u &= \overline{g}_D + \widetilde{u},\\ \gamma_1 u &= \overline{g}_N + \widetilde{t}\end{aligned}$$

with unknown $\widetilde{u} \in \widetilde{H}^{1/2}(\Gamma_N)$ and $\widetilde{t} \in \widetilde{H}^{-1/2}(\Gamma_D)$. To solve for $(\widetilde{u}, \widetilde{t})$, we also need to split the operators $\{\mathsf{V}, \mathsf{K}, \mathsf{K}', \mathsf{W}\}$ into contributions on Γ_D and Γ_N, respectively. For $\mathsf{A} \in \{\mathsf{V}, \mathsf{K}, \mathsf{K}', \mathsf{W}\}$ that maps $H^{s_1}(\Gamma)$ to $H^{s_2}(\Gamma)$ with $s_1, s_2 \in [-1, 1]$, we define A_{DN} by the diagram

$$\widetilde{H}^{s_1}(\Gamma_N) \hookrightarrow H^{s_1}(\Gamma) \xrightarrow{\mathsf{A}} H^{s_2}(\Gamma) \xrightarrow{r_D} H^{s_2}(\Gamma_D),$$

where r_D is the restriction map from Γ to Γ_D. Analogously, we define A_{DD}, A_{NN} and A_{ND}. Note that the adjoint of the restriction r_D is the inclusion $\widetilde{H}^{-s_2}(\Gamma_D) \hookrightarrow H^{-s_2}(\Gamma)$, so, for instance, $(A_{DN})' = A'_{ND}$. With above notation we reformulate (3.9) into a system of equations for $(\widetilde{u}, \widetilde{t})$,

$$\begin{pmatrix}\mathsf{V}_{DD} & \mathsf{K}_{DN}\\ -\mathsf{K}'_{ND} & \mathsf{W}_{NN}\end{pmatrix}\begin{pmatrix}\widetilde{t}\\ \widetilde{u}\end{pmatrix} = \begin{pmatrix}b_1\\ b_2\end{pmatrix}, \tag{3.10}$$

where $b_1 \in H^{1/2}(\Gamma_D)$, $b_2 \in H^{-1/2}(\Gamma_N)$ with

$$b_1 = \left(\frac{1}{2} + \mathsf{K}\right)\overline{g}_D - \mathsf{V}\overline{g}_N - \mathsf{N}_0 f, \quad b_2 = \left(\frac{1}{2} - \mathsf{K}'\right)\overline{g}_N - \mathsf{W}\overline{g}_D - \mathsf{N}_1 f. \tag{3.11}$$

3.75 Theorem *If Γ_D has positive surface measure, $|\Gamma_D| > 0$, then* (3.10) *has a unique solution that continuously depends on $(f, \overline{g}_N, \overline{g}_D)$.*

Proof. Since $|\Gamma_D| > 0$, V_{DD} is coercive. We can therefore solve the first equation for $\widetilde{t}$,

$$\widetilde{t} = (\mathsf{V}_{DD})^{-1}\Big(b_1 - \mathsf{K}_{DN}\widetilde{u}\Big).$$

Inserting this in the second equations yields

$$-(\mathsf{K}_{DN})'(\mathsf{V}_{DD})^{-1}\Big(b_1 - \mathsf{K}_{DN}\widetilde{u}\Big) + \mathsf{W}_{NN}\widetilde{u} = b_2,$$

so

$$\mathsf{S}\widetilde{u} = b_2 + (\mathsf{K}_{DN})'(\mathsf{V}_{DD})^{-1}b_1,$$

where $\mathsf{S} : \widetilde{H}^{1/2}(\Gamma_N) \to H^{-1/2}(\Gamma_N)$ is the Schur complement, given by

$$\mathsf{S} = \mathsf{W}_{NN} + (\mathsf{K}_{DN})'(\mathsf{V}_{DD})^{-1}(\mathsf{K}_{DN}).$$

It is linear continuous, symmetric and coercive,

$$\langle\varphi, \mathsf{S}\varphi\rangle_\Gamma = \langle\varphi, \mathsf{W}_{NN}\varphi\rangle_\Gamma + \langle\mathsf{K}_{DN}\varphi, (\mathsf{V}_{DD})^{-1}\mathsf{K}_{DN}\varphi\rangle_\Gamma \geq \widetilde{c}_{\mathsf{W}}\|\varphi\|^2_{1/2,\Gamma}$$

for all $\varphi \in \widetilde{H}^{1/2}(\Gamma_N)$ since W_{NN} and $(\mathsf{V}_{DD})^{-1}$ are coercive, as $|\Gamma \setminus \Gamma_N| = |\Gamma_D| > 0$. To show that the solution $(\widetilde{t}, \widetilde{u})$ continuously depends on the data $(f, \overline{g}_N, \overline{g}_D)$, we first note that S^{-1} and $(\mathsf{V}_{DD})^{-1}$ are continuous, so $(\widetilde{t}, \widetilde{u})$ depends continuously on (b_1, b_2). From definition of the right hand side we see that $(f, \overline{g}_N, \overline{g}_D) \mapsto (b_1, b_2)$ is continuous and thus $(f, \overline{g}_N, \overline{g}_D) \mapsto (\widetilde{t}, \widetilde{u})$ is continuous. ∎

In preparation for a numerical treatment of (3.10) by means of a Galerkin formulation, we reformulate Theorem 3.75 as a variational formulation:

3.76 Corollary *Suppose $|\Gamma_D| > 0$. Then, the variational formulation*

$$\begin{cases} \text{Find } (\widetilde{t}, \widetilde{u}) \in \widetilde{H}^{-1/2}(\Gamma_D) \times \widetilde{H}^{1/2}(\Gamma_N) \text{ such that} \\ \qquad \langle\mathsf{V}\widetilde{t}, \varphi\rangle_\Gamma + \langle\mathsf{K}\widetilde{u}, \varphi\rangle_\Gamma - \langle\psi, \mathsf{K}'\widetilde{t}\rangle_\Gamma + \langle\psi, \mathsf{W}\widetilde{u}\rangle_\Gamma = \langle b_1, \varphi\rangle_\Gamma + \langle\psi, b_2\rangle_\Gamma \\ \text{for all } (\varphi, \psi) \in \widetilde{H}^{-1/2}(\Gamma_D) \times \widetilde{H}^{1/2}(\Gamma_N), \end{cases} \tag{3.12}$$

with (b_1, b_2) as in (3.11)*, has a unique solution that continuously depends on $(f, \overline{g}_N, \overline{g}_D)$.*

3.4. Boundary Element Methods

> In other words we want to find out whether or not crime pays; fortunately for the finite element method, it often does.
>
> *(Gilbert Strang [152])*

Corollary 3.76 shows that we can uniquely determine the unknown traces $\widetilde{t} = \gamma_1 u|_{\Gamma_D}$ and $\widetilde{u} = \gamma_0 u|_{\Gamma_N}$ in

$$\begin{cases} -\Delta u = f & \text{in } \Omega, \\ \gamma_0 u = g_D & \text{on } \Gamma_D, \\ \gamma_1 u = g_N & \text{on } \Gamma_N \end{cases}$$

with the help of the variational formulation (3.12). The solution u and its derivatives can then be evaluated by means of the representation formula (3.8),

$$u = \mathcal{V}\Big(\overline{g}_N + \widetilde{t}\Big) - \mathcal{W}\Big(\overline{g}_D + \widetilde{u}\Big) + \mathcal{N} f. \tag{3.13}$$

However, neither for (3.12) nor for (3.13) there exist closed expressions for general domains that permit the rapid evaluation of the solution u or its traces. Therefore, we have to rely on approximations of the exact solution u. The most widespread approximation scheme is called Galerkin method. Its idea is to solve (3.12) for a sequence of finite-dimensional subspaces. The variational formulation is then equivalent to the solution of a (large) linear system. In the following, we describe the Galerkin method and study its convergence properties. To that end, we set

$$H = \widetilde{H}^{-1/2}(\Gamma_D) \times \widetilde{H}^{1/2}(\Gamma_N),$$

endowed with the norm $\|(\varphi, \psi)\|^2 = \|\varphi\|^2_{-1/2,\Gamma} + \|\psi\|^2_{1/2,\Gamma}$, and define the bilinear form

$$a : H \times H \to \mathbb{R},\ ((\widetilde{t}, \widetilde{u}), (\varphi, \psi)) \mapsto \langle \mathsf{V}\widetilde{t}, \varphi\rangle_\Gamma + \langle \mathsf{K}\widetilde{u}, \varphi\rangle_\Gamma - \langle \psi, \mathsf{K}'\,\widetilde{t}\rangle_\Gamma + \langle \psi, \mathsf{W}\widetilde{u}\rangle_\Gamma,$$

as well as the linear form

$$\ell : H \to \mathbb{R},\ (\varphi, \psi) \mapsto \langle b_1, \varphi\rangle_\Gamma + \langle \psi, b_2\rangle_\Gamma.$$

The variational formulation then reads

$$\begin{cases} \text{Find } (\widetilde{t}, \widetilde{u}) \in H \text{ such that} \\ \qquad a\big((\widetilde{t}, \widetilde{u}), (\varphi, \psi)\big) = \ell\big((\varphi, \psi)\big) \\ \text{for all } (\varphi, \psi) \in \widetilde{H}^{-1/2}(\Gamma_D) \times \widetilde{H}^{1/2}(\Gamma_N), \end{cases}$$

From the previous section we know that $\ell \in H'$ and, furthermore, that a is continuous,

$$|a\big((\widetilde{t}, \widetilde{u}), (\varphi, \psi)\big)| \le c_1 \|(\widetilde{t}, \widetilde{u})\| \|(\varphi, \psi)\|,$$

for all $(\widetilde{u}, \widetilde{t}), (\varphi, \psi) \in H$ and a constant $c_1 > 0$. Furthermore, a is coercive, that is,

$$a\big((\widetilde{t}, \widetilde{u}), (\widetilde{t}, \widetilde{u})\big) \ge c_2 \|(\widetilde{t}, \widetilde{u})\|^2$$

for all $(\widetilde{t}, \widetilde{u}) \in H$ with a constant $c_2 > 0$.

We now consider a sequence of monotonically increasing finite dimensional subspaces $(H_h)_h$, indexed by a monotonically decreasing null sequence $(h_n)_{n\in\mathbb{N}}$. In addition, we require that the union of the subspaces is dense in H,

$$\overline{\bigcup_{h\in(0,1)} H_h} = H.$$

The Galerkin approximation $(t_h, v_h) \in H_h$ is the unique solution to the finite-dimensional variational formulation

$$\begin{cases} \text{Find } (t_h, u_h) \in H_h \text{ such that} \\ \qquad a\big((t_h, u_h), (\varphi_h, \psi_h)\big) = \ell\big((\varphi_h, \psi_h)\big) \\ \text{for all } (\varphi_h, \psi_h) \in H_h. \end{cases} \tag{3.14}$$

The key result for the convergence analysis of the Galerkin method is Céa's Lemma [30, Proposition 3.1] in the formulation of Birkhoff, Schultz, and Varga [10, Theorem 13]:

3.77 Lemma *The error of the Galerkin method is bounded by the best approximation error,*

$$\|(\widetilde{t},\widetilde{u})-(t_h,u_h)\| \leq \frac{c_1}{c_2}\inf_{(\varphi_h,\psi_h)\in H_h}\|(\widetilde{t},\widetilde{u})-(\varphi_h,\psi_h)\|.$$

A direct consequence of Céa's lemma is an abstract convergence result for the Galerkin method.

3.78 Lemma *The sequence of Galerkin approximations $(t_h,u_h)_h$ converges to $(\widetilde{u},\widetilde{t})$, the unique solution of* (3.12).

Proof. Let $\varepsilon>0$. By density of the subspaces $(H_h)_h$ in H, there is $h_0>0$ and $(\varphi_{h_0},\psi_{h_0})\in H_{h_0}$ such that

$$\|(\widetilde{t},\widetilde{u})-(\varphi_{h_0},\psi_{h_0})\| < \frac{c_2}{c_1}\varepsilon.$$

Since the spaces $(H_h)_h$ are nested, we obtain with Céa's Lemma

$$\|(\widetilde{t},\widetilde{u})-(t_h,u_h)\| \leq \frac{c_1}{c_2}\inf_{(\varphi_h,\psi_h)\in H_h}\|(\widetilde{t},\widetilde{u})-(\varphi_h,\psi_h)\| \leq \frac{c_1}{c_2}\frac{c_2}{c_1}\varepsilon=\varepsilon$$

for all $h\leq h_0$. ∎

This result is only of theoretical interest as the convergence speed may be arbitrarily slow, depending on the choice of the spaces $(H_h)_h$ and the regularity of the solution $(\widetilde{t},\widetilde{u})$. In numerical applications, the approximation spaces are defined by means of a discretisation of the boundary Γ into triangles. To avoid technical difficulties, we assume from now on that

$$\Omega\subseteq\mathbb{R}^3 \text{ is a Lipschitz polyhedron,}$$

defined below.

3.79 Definition (Lipschitz polyhedron) *A convex polyhedron $\Omega\subseteq\mathbb{R}^3$ is an open, bounded subset which can be written as the intersection of finitely many half-spaces of the form*

$$\{\boldsymbol{x}\in\mathbb{R}^3 : \boldsymbol{x}\cdot\boldsymbol{e}<b\},$$

with $\boldsymbol{e}\in S^2$ and $b\in\mathbb{R}$. An open, bounded and connected set $\Omega\subseteq\mathbb{R}^3$ is called Lipschitz polyhedron if it is the finite union of convex polyhedra and the resulting boundary is Lipschitz.

3.80 Remark By Lemma 3.51 convex polyhedra are Lipschitz polyhedra. However, the union of two convex polyhedra does not need to have a Lipschitz boundary. A classical counterexample are two stacked bricks, where one of them is rotated by 90 degrees:

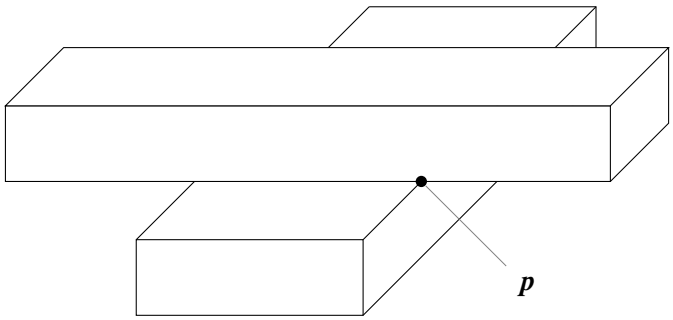

It is not possible to locally parameterise the boundary at $\boldsymbol{p}$ by two variables only. In particular, the boundary is not the graph of a Lipschitz function.

3.81 Definition (Triangulation) *A triangulation $(\mathcal{T}_h)_h$ of $\Gamma = \partial\Omega$ is a sequence of meshes, indexed by a monotonically decreasing null sequence $(h_n)_{n\in\mathbb{N}}$ such that for all $n \in \mathbb{N}$:*

- *$\mathcal{T}_{h_n}$ is a finite set of pairwise disjoint flat, open triangles in $\mathbb{R}^3$ with*

$$\bigcup_{T\in\mathcal{T}_{h_n}} \overline{T} = \Gamma,$$

- *and the diameters of all triangles in $\mathcal{T}_{h_n}$ are bounded by h_n,*

$$\sup_{T\in\mathcal{T}_{h_n}} \sup_{\boldsymbol{x},\boldsymbol{y}\in T} |\boldsymbol{x}-\boldsymbol{y}| \leq h_n.$$

The triangulation $(\mathcal{T}_h)_h$ is called regular if in addition for all $n \in \mathbb{N}$ and $T_1, T_2 \in \mathcal{T}_{h_n}$

$$\overline{T}_1 \cap \overline{T}_2 = \begin{cases} \varnothing, & \text{or} \\ \text{a common vertex}, & \text{or} \\ \text{a common edge}, & \text{or} \\ \overline{T}_1. \end{cases}$$

and the interior angles of all triangles in $(\mathcal{T}_h)_h$ are uniformly bounded from below.

3.82 Definition (Spline spaces) *Let the polyhedron Γ have flat faces $(\tau_j)_{j=1}^p$, called panels,*

$$\Gamma = \bigcup_{j=1}^{p} \overline{\tau}_j$$

and let $(\mathcal{T}_h)_h$ be a regular triangulation that conforms to the panel decomposition, i.e. each triangle in $(\mathcal{T}_h)_h$ lies completely in one of the panels $(\tau_j)_{j=1}^p$. Furthermore, let Γ_1 be the union of a subset of panels $(\tau_j)_{j=1}^p$. By $\mathcal{T}_h|\Gamma_1$, we denote the set of all triangles in $\mathcal{T}_h$ that lie in Γ_1. We set

$$S_h^0(\Gamma_1) = \{u \in L_2(\Gamma_1) : u|_T = \text{const. } \forall T \in \mathcal{T}_h|\Gamma_1\},$$

the vector space of piecewise constant splines, and

$$S_h^1(\Gamma_1) = \left\{u \in C\left(\overline{\Gamma}_1\right) : u|_T \text{ is affine linear } \forall T \in \mathcal{T}_h|\Gamma_1 \text{ and } u|_{\partial\Gamma_1} = 0\right\},$$

the vector space of continuous piecewise affine linear splines. Here $\partial\Gamma_1$ denotes the boundary of Γ_1 relative to Γ, i.e. it is the union of all edges in $\mathcal{T}_h$ for which one adjacent triangle lies in Γ_1 and the other in $\Gamma \setminus \overline{\Gamma}_1$.

The definition of the spline spaces on subsets of Γ insures that $S_h^0(\Gamma_D) \times S_h^1(\Gamma_N)$ is a linear subspace of $\widetilde{H}^{-1/2}(\Gamma_D) \times \widetilde{H}^{1/2}(\Gamma_N)$ if Γ_D and Γ_N conform to the panel decomposition, i.e. they are unions of the panels $(\tau_j)_{j=1}^p$. Since the elements of $S_h^0(\Gamma_D)$ are piecewise constant on $\mathcal{T}_h|\Gamma_D$, their supports lie in $\overline{\Gamma}_1$, so that

$$S_h^0(\Gamma_D) \subseteq \widetilde{H}^{-s}(\Gamma_D)$$

for all $s \in [0,1]$. For $\varphi_h \in S_h^1(\Gamma_N)$, we note that $\varphi_h|_T$ continuously differentiable for every $T \in \mathcal{T}_h|\Gamma_N$. Together with the continuity across the elements of $\mathcal{T}_h|\Gamma_N$ this means that φ_h admits a weak gradient, so $\varphi_h \in H^1(\Gamma_N)$. Due to $\varphi_h|_{\partial\Gamma_N} = 0$, $\operatorname{supp}\varphi_h \subseteq \overline{\Gamma}_N$ and thus

$$\varphi_h \in \widetilde{H}^s(\Gamma_N)$$

for all $s \in [0,1]$.

Let $(T_i)_{i=1}^n$, $(x_j)_{j=1}^m$ be enumerations of the triangles in $\mathcal{T}_h|\Gamma_1$ and vertices in $\mathcal{T}_h|\Gamma_1$ without those on $\partial\Gamma_1$, respectively. Then $(\varphi_i^0)_{i=1}^n$ defines a basis of $S_h^0(\Gamma)$, where

$$\varphi_i^0(\boldsymbol{x}) = \begin{cases} 1, & \boldsymbol{x} \in T_i \\ 0, & \text{otherwise} \end{cases}, \quad \boldsymbol{x} \in \Gamma,\ i = 1,\dots,n.$$

Furthermore, the functions $(\psi_j^1)_{j=1}^m \subseteq S_h^1(\Gamma)$ uniquely determined by

$$\psi_j^1(\boldsymbol{x}_i) = \delta_{ij}, \quad i,j = 1,\dots,n.$$

form a basis of $S_h^1(\Gamma)$.

In the following, we assume that Γ_D and Γ_N conform to the panel decomposition of Γ and fix a conforming, regular triangulation $(\mathcal{T}_h)_h$ with $(n_h)_h$ triangles and $(m_h)_h$ vertices. The abstract approximation spaces $(H_h)_h$ from the beginning of the section are now

$$H_h = S_h^0(\Gamma_D) \times S_h^1(\Gamma_N).$$

With the traces sought in the form

$$\gamma_1 u \approx \sum_{l=1}^{n_h} \alpha_l \varphi_l^0, \quad \gamma_0 u \approx \sum_{j=1}^{m_h} \beta_j \psi_j^1,$$

for $\boldsymbol{\alpha} \in \mathbb{R}^{n_h}$, $\boldsymbol{\beta} \in \mathbb{R}^{m_h}$, the variational formulation (3.14) is equivalent to the linear system

$$\begin{aligned} &\begin{pmatrix} V_h^{DD} & -K_h^{DN} \\ (K_h^{DN})^\top & W_h^{NN} \end{pmatrix} \begin{pmatrix} \boldsymbol{\alpha}^D \\ \boldsymbol{\beta}^N \end{pmatrix} \\ &= \begin{pmatrix} \frac{1}{2}M_h^{DD} + K_h^{DD} & -V_h^{DN} \\ -W_h^{ND} & \frac{1}{2}(M_h^{NN})^\top - (K_h^{NN})^\top \end{pmatrix} \begin{pmatrix} \boldsymbol{\beta}^D \\ \boldsymbol{\alpha}^N \end{pmatrix} - \begin{pmatrix} \boldsymbol{N}_0^D \\ \boldsymbol{N}_1^N \end{pmatrix}, \end{aligned} \tag{3.15}$$

where

$$\begin{aligned} V_h[k,l] &= \frac{1}{4\pi} \int_{T_l} \int_{T_k} \frac{1}{|\boldsymbol{x}-\boldsymbol{y}|} \,\mathrm{d}S_{\boldsymbol{y}} \,\mathrm{d}S_{\boldsymbol{x}}, \\ W_h[i,j] &= \frac{1}{4\pi} \int_{\Gamma} \int_{\Gamma} \frac{\mathbf{curl}_\Gamma\, \psi_i^1(\boldsymbol{x}) \cdot \mathbf{curl}_\Gamma\, \psi_j^1(\boldsymbol{y})}{|\boldsymbol{x}-\boldsymbol{y}|} \,\mathrm{d}S_{\boldsymbol{y}} \,\mathrm{d}S_{\boldsymbol{x}}, \\ K_h[k,j] &= \frac{1}{4\pi} \int_{T_k} \int_{\Gamma} \frac{\boldsymbol{n}(\boldsymbol{y}) \cdot (\boldsymbol{x}-\boldsymbol{y})}{|\boldsymbol{x}-\boldsymbol{y}|^3} \psi_j^1(\boldsymbol{y}) \,\mathrm{d}S_{\boldsymbol{y}} \,\mathrm{d}S_{\boldsymbol{x}}, \\ M_h[k,j] &= \int_{T_k} \psi_j^1(\boldsymbol{y}) \,\mathrm{d}S_{\boldsymbol{y}}, \end{aligned} \tag{3.16}$$

for $k, l = 1, \dots, n_h$ and $i, j = 1, \dots, m_h$. The superscripts of the matrix blocks in (3.15) indicate that they are submatrices,

$$V_h = \begin{pmatrix} V_h^{DD} & V_h^{DN} \\ V_h^{ND} & V_h^{NN} \end{pmatrix}, \quad W_h = \begin{pmatrix} W_h^{NN} & W_h^{ND} \\ W_h^{DN} & W_H^{DD} \end{pmatrix},$$
$$K_h = \begin{pmatrix} K_h^{DN} & K_h^{DD} \\ K_h^{NN} & K_h^{ND} \end{pmatrix}, \quad M_h = \begin{pmatrix} M_h^{DN} & M_h^{DD} \\ M_h^{NN} & M_h^{ND} \end{pmatrix}.$$

The triangles and vertices are enumerated such that the first n_h^D, respectively, m_h^N lie in Γ_D, respectively, Γ_N and the rest in the respective complement. Similarly, the superscripts at the vectors mean that we only refer to the subvector that corresponds to triangles or vertices on the given part of the boundary. Lastly, the vectors $\boldsymbol{N}_0$, $\boldsymbol{N}_1$ are given by

$$\boldsymbol{N}_0[l] = \int_{T_l} \mathsf{N}_0 f(\boldsymbol{y}) \, \mathrm{d}S_{\boldsymbol{y}}, \quad \boldsymbol{N}_1[j] = \int_{\Gamma} \mathsf{N}_1 f(\boldsymbol{y}) \psi_j^1(\boldsymbol{y}) \, \mathrm{d}S_{\boldsymbol{y}},$$

for $l = 1, \dots, n_h$, $j = 1, \dots, m_h$ and N_0, N_1 are defined in (3.9). The coefficients $\left(\boldsymbol{\alpha}^N, \boldsymbol{\beta}^D\right)$ appearing on the right hand side are found by L_2 projection of the boundary data (g_N, g_D) onto the corresponding spline spaces, see the discussion before Corollary 3.88.

In view of Céa's Lemma 3.77, the next step would be to investigate the approximation error of

$$\Pi_h^E : H \to H_h, \ (\varphi, \psi) \mapsto \operatorname*{argmin}_{(\varphi_h, \psi_h) \in H_h} \|(\varphi, \psi) - (\varphi_h, \psi_h)\|,$$

which, since H is a Hilbert space, is equivalent to

$$\Pi_h^E(\varphi, \psi) = (\varphi_h^*, \psi_h^*),$$

where $(\varphi_h^*, \psi_h^*) \in H_h$ is the orthogonal projection of (φ, ψ) onto H_h,

$$\forall (\xi_h, \zeta_h) \in H_h : \big((\varphi_h^*, \psi_h^*), (\xi_h, \zeta_h)\big)_H = \big((\varphi, \psi), (\xi_h, \zeta_h)\big)_H.$$

However, this approach is computationally infeasible. The inner product on H involves the nonlocal inner product on $H^{1/2}(\Gamma)$ with a singular kernel (cf. Definition 3.56),

$$(u, v)_{1/2,\Gamma} = \int_{\Gamma} uv \, \mathrm{d}S_{\boldsymbol{x}} + \int_{\Gamma} \int_{\Gamma} \frac{\big(u(\boldsymbol{x}) - u(\boldsymbol{y})\big)\big(v(\boldsymbol{x}) - v(\boldsymbol{y})\big)}{|\boldsymbol{x} - \boldsymbol{y}|^3} \, \mathrm{d}S_{\boldsymbol{y}} \, \mathrm{d}S_{\boldsymbol{x}},$$

with $u, v \in H^{1/2}(\Gamma)$, and the inner product on $H^{-1/2}(\Gamma)$ is induced by the operator norm. Thus, we study projections with respect to the computationally accessible L_2 norm:

3.83 Definition (L_2 projection onto spline spaces) *Suppose $\Gamma_1 \subseteq \Gamma$ is open and conforms to the panel decomposition of Γ. We define the projection operators*

$$\Pi_{\Gamma_1,h}^k : L_2(\Gamma_1) \to S_h^k(\Gamma_1), \ u \mapsto \operatorname*{argmin}_{v_h \in S_h^k(\Gamma_1)} \|u - v_h\|_{0,\Gamma_1}, \quad k \in \{0, 1\}.$$

In the following, we shall review error estimates for the L_2 projection. In order to get optimal convergence rates for $h \to 0$, we have to require higher regularity of the projected function than (square-) integrability. Since the basis functions of the spline space are nonzero only on a small part of the boundary, higher regularity is only needed locally, i.e. on individual patches. This gives rise to piecewise Sobolev spaces. In a preparatory step, we define Sobolev spaces $H^s(\tau)$ for $s > 1$ on flat panels $\tau \subseteq \Gamma$.

3.84 Definition (Higher order Sobolev spaces on panels) *Let $\tau \subseteq \Gamma$ be an open and flat panel. Furthermore, let F be the plane that contains τ. For $s > 0$, the Sobolev space $H^s(\tau)$ is defined as the restriction of $H^s(F)$ on τ.*

For $s \in [0, 1]$ we have to show that this definition coincides with our previous definition of $H^s(\tau)$ as restriction of $H^s(\Gamma)$ on τ. To that end, we consider the diagram

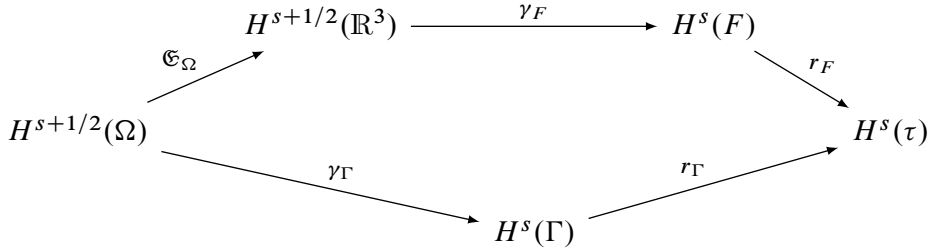

Here, $\mathfrak{E}_\Omega$ denotes the continuous extension operator on Ω from Lemma 3.53, γ_Γ and γ_F are the trace operators on Γ and F, respectively, and r_Γ, r_F the restriction operators on τ from Γ and F. The lower path in the diagram represents our previous definition of $H^s(\tau)$, the upper one Definition 3.84. Let $\varphi \in \mathcal{D}(\bar{\Omega})$. By construction of the extension and trace operators, we have

$$(r_F \gamma_F \mathfrak{E}_\Omega)\varphi = \varphi|_\tau,$$

which is also what we obtain when we restrict the trace $\gamma_\Gamma \varphi = \varphi|_\Gamma$ to τ. Thus,

$$r_F \circ \gamma_F \circ \mathfrak{E}_\Omega = r_\Gamma \circ \gamma_\Gamma \text{ on } \mathcal{D}(\bar{\Omega}).$$

Since $\mathcal{D}(\bar{\Omega})$ is dense in $H^{s+1/2}(\Omega)$ (Lemma 3.52) and all involved mapping are continuous, equality holds on $H^{s+1/2}(\Omega)$. This proves that both definitions give rise to the same space $H^s(\tau)$ for $s \in [0, 1]$.

3.85 Definition (piecewise Sobolev spaces) *Let $\Gamma_1 \subseteq \Gamma$ be the union of flat panels $(\tau_j)_{j \in \mathcal{P}}$ with $\mathcal{P} \subseteq \{1, \dots, p\}$. For $s \geq 0$, the piecewise Sobolev space of order s on Γ_1 is defined by*

$$H^s_{pw}(\Gamma_1) = \{u \in H^{s^*}(\Gamma_1) : \forall\, j \in \mathcal{P} : u|_{\tau_j} \in H^s(\tau_j)\}.$$

Here, $s^* = 0$ for $s \in [0, 1]$ and equals 1 for $s > 1$. Furnished with the norm

$$H^s_{pw}(\Gamma_1) \to [0, \infty),\ u \mapsto \left(\|u\|^2_{s^*,\Gamma_1} + \sum_{j \in \mathcal{P}} \|u\|^2_{s,\tau_j} \right)^{1/2},$$

this space is a Hilbert space.

The error estimates for the L_2 projection operators now follow by locally applying standard estimates for polynomial approximation, see for instance [22, Chapter 4] and [54, Chapter 1], as well as [138, Section 4.3] and [148, Chapter 10] for a derivation in the context of Boundary Element Methods.

3.86 Lemma *Let $(\mathcal{T}_h)_h$ be a regular triangulation that conforms to the panel decomposition of Γ. For the error of L_2 projection onto the spline space $S_h^k(\Gamma_1)$ it holds*

$$\|u - \Pi^k_{\Gamma_1,h} u\|_{-\sigma,\Gamma_1} \leq C h^{s+k+\sigma} \|u\|_{pw,s+k,\Gamma_1}, \quad u \in H^{s+k}_{pw}(\Gamma_1),$$

where $\Gamma_1 \subseteq \Gamma$ open is a collection of panels, $k \in \{0,1\}$, $s \in [0,1]$ and $\sigma \in [0,s]$. The constant $C > 0$ only depends on Γ_1, the shape regularity of $(\mathcal{T}_h)_h$ and k, s and σ.

A combination of Céa's Lemma 3.77, the projection estimates from Lemma 3.86 and so-called inverse estimates, which bound Sobolev norms of spline functions by lower order norms (cf. [148, Section 10.2], [54, Section 1.7], [22, Section 4.5]), yields a convergence estimate for the Galerkin method:

3.87 Theorem *Assume that Γ_D and Γ_N conform to the panel decomposition of Γ. Let $(\mathcal{T}_h)_h$ be a regular triangulation of Γ that also conforms to the panels. If the solution $(\widetilde{t}, \widetilde{u})$ of the variational formulation* (3.12) *fulfils*

$$(\widetilde{t}, \widetilde{u}) \in H^1_{pw}(\Gamma_D) \times H^2_{pw}(\Gamma_N),$$

and we use

$$H_h = S_h^0(\Gamma_D) \times S_h^1(\Gamma_N), \quad h > 0,$$

as approximating spaces, then the following L_2 estimates for the difference of (t_h, u_h), the solution of (3.14)*, and $(\widetilde{t}, \widetilde{u})$ hold:*

$$\begin{aligned} \|\widetilde{t} - t_h\|_{0,\Gamma_D} &\leq C h \|\widetilde{t}\|_{pw,1,\Gamma_D}, \\ \|\widetilde{u} - u_h\|_{0,\Gamma_N} &\leq C h^2 \|\widetilde{u}\|_{pw,2,\Gamma_N}. \end{aligned}$$

Here, the constant $C > 0$ only depends on Γ_D, Γ_N and the shape regularity of $(\mathcal{T}_h)_h$.

So far our analysis focused on the bilinear form a in the variational formulation and thereby ignoring the right hand side ℓ for which we have to compute (b_1, b_2) from (3.11),

$$b_1 = \left(\frac{1}{2} + \mathsf{K}\right) \overline{g}_D - \mathsf{V} \overline{g}_N - \mathsf{N}_0 f, \quad b_2 = \left(\frac{1}{2} - \mathsf{K}'\right) \overline{g}_N - \mathsf{W} \overline{g}_D - \mathsf{N}_1 f.$$

In most applications, it is difficult to find analytical expressions for the extensions $(\overline{g}_N, \overline{g}_D)$ of the boundary data. Therefore, we numerically construct $(\overline{g}_N, \overline{g}_D)$ by projecting the extensions by zero of (g_N, g_D) onto the spline space $S_h^0(\Gamma) \times S_h^1(\Gamma)$. In this way, we introduce an additional error in our formulation (3.14) which, by Lemma 3.86, is in the same order as the Galerkin error. By the use of the triangle inequality and the continuity of the solution with respect to the right hand side, we immediately obtain

3.88 Corollary *Under the assumptions of Theorem 3.87 with $(\overline{g}_N, \overline{g}_D)$ replaced by the L_2 projection of (g_N, g_D), the following error estimates hold:*

$$\begin{aligned} \|\widetilde{t} - t_h\|_{0,\Gamma_D} &\leq C h \Big(\|\widetilde{t}\|_{pw,1,\Gamma_D} + \|g_N\|_{pw,1,\Gamma_N} \Big), \\ \|\widetilde{u} - u_h\|_{0,\Gamma_N} &\leq C h^2 \Big(\|\widetilde{u}\|_{pw,2,\Gamma_N} + \|g_D\|_{pw,2,\Gamma_D} \Big). \end{aligned}$$

The method to derive estimates in weaker norms is known as Aubin–Nitsche lemma [54, Lemma 2.31] and requires a priori estimates for the solution of the variational formulation in higher order Sobolev norms. For Boundary Element Methods, these estimates rely on a result by Verchota [161, Theorem 3.3]:

3.89 Lemma *The single-layer operator*

$$V : L_2(\Gamma) \to H^1(\Gamma)$$

is continuous with a continuous inverse. By duality, this also holds for

$$V : H^{-1}(\Gamma) \to L_2(\Gamma).$$

With this lemma Steinbach [148, Theorem 12.3] concludes

3.90 Lemma *In the situation of Corollary 3.88 we have*

$$\|\widetilde{t} - t_h\|_{-1,\Gamma} \leq Ch^2\Big(\|\widetilde{t}\|_{pw,1,\Gamma_D} + \|g_N\|_{pw,1,\Gamma_N}\Big),$$

where $C > 0$ only depends on Γ_N, Γ_D and the shape regularity of $(\mathcal{T}_h)_h$.

With Corollary 3.88 and Lemma 3.90 we now discuss the error for the representation formula,

$$u = \mathcal{V}\big(\widetilde{t} + \overline{g}_N\big) - \mathcal{W}\big(\widetilde{u} + \overline{g}_D\big) + \mathcal{N} f,$$

where $(\overline{g}_N, \overline{g}_D)$ and $\big(\widetilde{t}, \widetilde{u}\big)$ are replaced by their Galerkin approximations. For $\boldsymbol{x} \in \Omega$, the functions $\gamma_0 U(\boldsymbol{x} - \cdot)$ and $\gamma_1 U(\boldsymbol{x} - \cdot) = -\boldsymbol{n} \cdot \nabla U(\boldsymbol{x} - \cdot)$ are smooth functions on Γ, i.e. they lie in $\mathcal{D}(\Gamma)$.

3.91 Lemma *Let Γ_D, Γ_N and $(\mathcal{T}_h)_h$ fulfil the assumptions of Theorem 3.87 and let $(\overline{g}_N, \overline{g}_D)$ constructed by L_2 projection. With $\overline{u}_h$, we denote the function obtained by inserting the Galerkin approximations of the traces into the representation formula. For $\boldsymbol{x} \in \Omega$, there exists $C > 0$ such that*

$$|u(\boldsymbol{x}) - \overline{u}_h(\boldsymbol{x})| \leq Ch^2\Big(\|\widetilde{t}\|_{pw,1,\Gamma_D} + \|g_N\|_{pw,1,\Gamma_N} + \|\widetilde{u}\|_{pw,2,\Gamma_N} + \|g_D\|_{pw,2,\Gamma_D}\Big),$$
$$|\nabla u(\boldsymbol{x}) - \nabla \overline{u}_h(\boldsymbol{x})| \leq Ch^2\Big(\|\widetilde{t}\|_{pw,1,\Gamma_D} + \|g_N\|_{pw,1,\Gamma_N} + \|\widetilde{u}\|_{pw,2,\Gamma_N} + \|g_D\|_{pw,2,\Gamma_D}\Big).$$

Proof. Let $\boldsymbol{x} \in \Omega$. With the panel decomposition

$$\Gamma = \bigcup_{k=1}^{p} \overline{\tau}_k,$$

the error in the representation formula is written as

$$\begin{aligned}
|u(\boldsymbol{x}) - \overline{u}_h(\boldsymbol{x})| &= \Bigg| \sum_{k=1}^{p} \int_{\tau_k} U(\boldsymbol{x} - \boldsymbol{y})\big[\gamma_1 u - t_h - \overline{g}_N\big](\boldsymbol{y}) \,\mathrm{d}S_{\boldsymbol{y}} \\
&\qquad + \int_{\tau_k} \boldsymbol{n}_k \cdot \nabla U(\boldsymbol{x} - \boldsymbol{y})\big[\gamma_0 u - u_h - \overline{g}_N\big](\boldsymbol{y}) \,\mathrm{d}S_{\boldsymbol{y}} \Bigg| \\
&\leq \sum_{k=1}^{p} \big|\langle U(\boldsymbol{x} - \cdot), \gamma_1 u - t_h - \overline{g}_N \rangle_{\tau_k}\big| \\
&\qquad + \big|\langle \boldsymbol{n}_k \cdot \nabla U(\boldsymbol{x} - \cdot), \gamma_0 u - u_h - \overline{g}_N \rangle_{\tau_k}\big| \\
&\leq \sum_{k=1}^{p} \|U(\boldsymbol{x} - \cdot)\|_{1,\tau_k} \|\gamma_1 u - t_h - \overline{g}_N\|_{-1,\Gamma} \\
&\qquad + \|\boldsymbol{n}_k \cdot \nabla U(\boldsymbol{x} - \cdot)\|_{0,\Gamma} \|\gamma_0 u - u_h - \overline{g}_N\|_{0,\tau_k}.
\end{aligned}$$

Here $\boldsymbol{n}_k = \boldsymbol{n}|_{\tau_k}$ denotes the constant outward normal vector on the flat panel τ_k, $k = 1, \dots, p$. We have $\gamma_0 u|_{\Gamma_D} = g_D$ and $\gamma_0 u|_{\Gamma_N} = \widetilde{u}$, so for panels in Γ_D the L_2 error is bounded by the projection estimate in Lemma 3.86. For the terms on Γ_N, we use the Galerkin estimates from Corollary 3.88. With Lemma 3.90 and again Lemma 3.86, we estimate the negative Sobolev norm of the Neumann traces. This proves that the error scales as h^2 for $h \to 0$. The same argument with U replaced by ∇U yields the error estimate for the gradient of the representation formula. ■

We conclude this section with two numerical examples that demonstrate the studied convergence rates. For a sequence of meshes with number of triangles $n_1, n_2, \dots$ we assume that the error follows

$$\mathrm{err}_k = c {n_k}^{\alpha}, \quad k \in \mathbb{N}, \tag{3.17}$$

for a constant $c > 0$ and the convergence rate $\alpha \in \mathbb{R}$. Based on this assumption, we compute the estimated order of convergence (eoc),

$$\mathrm{eoc}_k = \frac{\log \frac{\mathrm{err}_{k+1}}{\mathrm{err}_k}}{\log \frac{n_{k+1}}{n_k}}, \quad k \in \mathbb{N},$$

which, for errors of the form (3.17), evaluates to α.

3.92 Example We choose Ω as the unit ball in $\mathbb{R}^3$,

$$\Omega = B_1(\mathbf{0}), \quad \Gamma = S^2,$$

and

$$\Gamma_D = \{\boldsymbol{x} \in S^2 : x_3 > 0\}, \quad \Gamma_N = \Gamma \setminus \overline{\Gamma}_D.$$

The data (f, g_D, g_N) are chosen such that the harmonic polynomial

$$u : \Omega \to \mathbb{R}, \ \boldsymbol{x} \mapsto x_1^2 + x_2^2 - 2x_3^2$$

is the exact solution of the boundary value problem (3.7). Table 3.1 shows the approximation

Table 3.1.: Relative errors of the Cauchy datum, estimated order of convergence and number of pcg iterations for homogeneous boundary value problem in Example 3.92.

n_h	$\|\gamma_1 u - t_h\|_{0,\Gamma} / \|\gamma_1 u\|_{0,\Gamma}$	eoc	$\|\gamma_0 u - u_h\|_{0,\Gamma} / \|\gamma_0 u\|_{0,\Gamma}$	eoc	cg_V	cg_S
320	7.80×10^{-2}	—	1.51×10^{-2}	—	19	13
1280	3.84×10^{-2}	−0.51	3.67×10^{-3}	−1.02	23	13
5120	1.91×10^{-2}	−0.50	9.13×10^{-4}	−1.00	25	14
20 480	9.69×10^{-3}	−0.49	2.19×10^{-4}	−1.03	26	16
81 920	4.75×10^{-3}	−0.51	5.73×10^{-5}	−0.97	26	18

error of the Cauchy datum $(\gamma_1 u, \gamma_0 u)$ for a sequence of triangular meshes with n_h elements together with the estimated order of convergence with respect to n_h. Since n_h scales as h^{-2} for a regular triangulation, our results are in accordance with the convergence rates reported in Corollary 3.88. We use the preconditioned conjugated gradient method (pcg) to solve the linear system (3.15). For the inversion of V_{DD} we use the preconditioner developed by Stevenson and Venetië [151]. It is based on the hypersingular operator multiplied from the left and right with

two sparse matrices that depend on the connectivity of the triangular mesh and can be assembled in linear complexity with respect to the number of triangles.

Because its mapping properties are similar to that of the hypersingular operator W, the Schur complement S is preconditioned with a technique proposed by Stevenson and Venetië [150] for W that relies on V multiplied with two sparse matrices. These matrices can be again assembled in linear complexity. In contrast to the preconditioner in [148, p. 305], which uses a sparse mass matrix whose inverse is fully populated, the preconditioner in [150] involves an inversion of a diagonal matrix thus mitigating this issue.

Since the preconditioner is not directly designed for S, the number of pcg iterations is not bounded with increasing n_h but depends logarithmically on n_h [148, p. 326], as shown in the last column of Table 3.1.

3.93 Example We compute the electric field $\boldsymbol{E}$ of a particle $\boldsymbol{c}$ inside a grounded sphere. The electric potential ϕ satisfies

$$\begin{cases} -\Delta\phi = \delta_{\boldsymbol{c}}^{\sigma} & \text{in } B_1(\mathbf{0}), \\ \gamma_0\phi = 0 & \text{on } S^2, \end{cases} \tag{3.18}$$

with $\delta_{\boldsymbol{c}}^{\sigma} = |B_\sigma(\boldsymbol{c})|^{-1}\mathbb{1}_{B_\sigma(\boldsymbol{c})}$ and $\sigma > 0$ such that $\bar{B}_\sigma(\boldsymbol{c}) \subseteq B_1(\mathbf{0})$. The Green function for the unit ball with Dirichlet boundary conditions is constructed by the method of image charges [129, Section 3-5],

$$G(\boldsymbol{x},\boldsymbol{y}) = \frac{1}{4\pi}\frac{1}{|\boldsymbol{x}-\boldsymbol{y}|} - \frac{1}{4\pi}\frac{1}{|\boldsymbol{y}||\boldsymbol{x}-\boldsymbol{y}^*|}, \quad \boldsymbol{x},\boldsymbol{y} \in B_1(\mathbf{0}),$$

where $\boldsymbol{y}^*$ is the Kelvin transform of $\boldsymbol{y}$,

$$\boldsymbol{y}^* = \frac{\boldsymbol{y}}{|\boldsymbol{y}|^2}.$$

Written in terms of the Green function, the electric potential ϕ has the form

$$\phi(\boldsymbol{x}) = \int_{B_1(\mathbf{0})} G(\boldsymbol{x},\boldsymbol{y})\delta_{\boldsymbol{c}}^{\sigma}(\boldsymbol{y})\,\mathrm{d}\boldsymbol{y} = \frac{1}{|B_\sigma(\boldsymbol{c})|}\int_{B_\sigma(\boldsymbol{c})} G(\boldsymbol{x},\boldsymbol{y})\,\mathrm{d}\boldsymbol{y}, \quad \boldsymbol{x} \in B_1(\mathbf{0}).$$

For $\boldsymbol{x} \in B_1(\mathbf{0}) \setminus \bar{B}_\sigma(\boldsymbol{c})$, the integrand $G(\boldsymbol{x},\cdot)$ is harmonic in an open neighbourhood of $B_\sigma(\boldsymbol{c})$. Thus the integral simplifies to

$$\phi(\boldsymbol{x}) = G(\boldsymbol{x},\boldsymbol{c}), \quad \boldsymbol{x} \in B_1(\mathbf{0}) \setminus \bar{B}_\sigma(\boldsymbol{c}),$$

by means of the mean value property. In Fig. 3.1, we compare the relative pointwise errors of two different numerical methods for the solution of (3.18) at three points along the line

$$r \mapsto r\boldsymbol{e}(\pi/3, -\pi/5), \tag{3.19}$$

where

$$\boldsymbol{e}(\vartheta,\varphi) = \begin{pmatrix} \sin\vartheta\cos\varphi \\ \sin\vartheta\sin\varphi \\ \cos\vartheta \end{pmatrix}, \quad \vartheta \in [0,\pi],\ \varphi \in [-\pi,\pi].$$

The particle is put at $\boldsymbol{c} = (1/2, 0, 0)$ with $\sigma = 1 \times 10^{-3}$. The BEM solution is obtained by solving (3.15). In accordance with the theoretical results of Lemma 3.91 the error decays linearly with respect to the number of surface triangles, in particular close to the boundary.

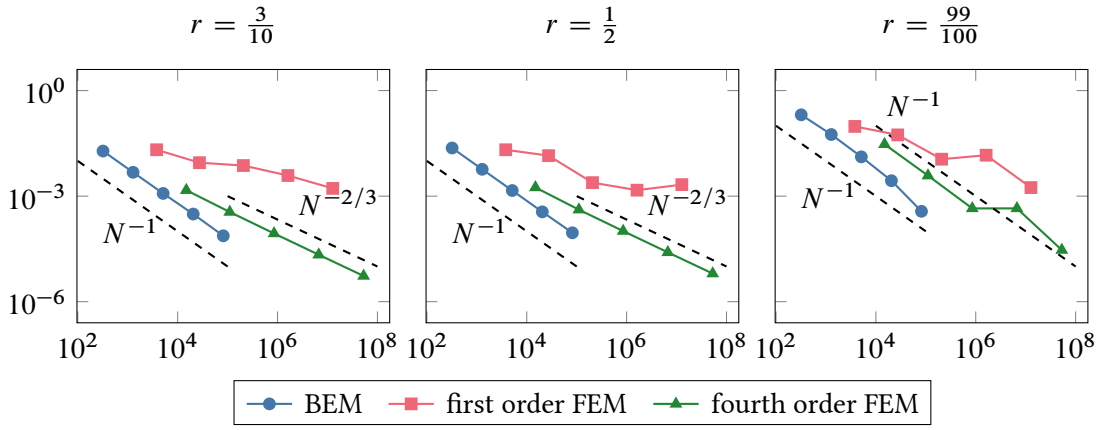

Figure 3.1.: Relative pointwise error of the gradient against degrees of freedom for the solution of (3.18) at three points along the line (3.19).

A direct application of the Finite Element Method (FEM) to (3.18) yields suboptimal convergence rates due to the low regularity of the right hand side, $\delta_{\boldsymbol{c}}^{\sigma} \in \widetilde{H}^{1/2-\varepsilon}(\Omega)$, $\varepsilon > 0$, cf. Lemma 3.43. Therefore, why we approximate the solution of the auxiliary boundary value problem

$$\begin{cases} -\Delta\phi_0 = 0 & \text{in } B_1(\mathbf{0}), \\ \gamma_0\phi_0 = -U(\cdot - \boldsymbol{c}) & \text{on } S^2, \end{cases}$$

instead. Here, we have used that $\overline{B}_{\sigma}(\boldsymbol{c}) \subseteq B_1(\mathbf{0})$ and, by Lemma 3.43, $\mathcal{N}\delta_{\boldsymbol{c}}^{\sigma} = U(\cdot - \boldsymbol{c})$ outside $B_{\sigma}(\boldsymbol{c})$. The results for linear and fourth order splines are calculated with the open source library `NGSolve`.[2] Standard convergence results on pointwise errors for FEM such as [22, Corollary 8.1.12] convey that the fourth order FEM should converge superlinearly and sublinearly if using first-order splines. This is reflected in our numerical study: In the centre of the ball, $r = 3/10$, the error decays very slowly. At $r = 1/2$, the error even increases in between. The good performance of the FEM error near the boundary is an artefact of the auxiliary formulation. Because the exact solution is imposed as Dirichlet condition, the evaluation of the gradient near the boundary essentially uses the projected exact solution rather than the FEM solution.

3.5. Application to Plasma Dynamics

After we have discussed Boundary Element Methods for the Poisson equation, we now return to our starting point, namely the computation of the electric field generated by a plasma. As we already know from Sections 2.3 and 2.4, the (nondimensional) electric field $\boldsymbol{E}$ of n_p particles with charges $q_1, \dots, q_{n_p}$ and positions $\boldsymbol{x}_1, \dots, \boldsymbol{x}_{n_p}$ in a bounded Lipschitz polyhedron $\Omega \subseteq \mathbb{R}^3$ equals $-\nabla\phi$, where ϕ is the solution of the boundary value problem

$$\begin{cases} -\Delta\phi = \dfrac{L_0^2}{\lambda_D^2} \displaystyle\sum_{j=1}^{n} q_j \delta_{\boldsymbol{x}_j}^{\sigma} & \text{in } \Omega, \\ \gamma_0\phi = g_D & \text{on } \Gamma_D, \\ \gamma_1\phi = g_N & \text{on } \Gamma_N, \end{cases}$$

[2] `https://ngsolve.org/`

with given data (g_N, g_D) and the regularised Dirac distribution $\delta_{\boldsymbol{x}}^{\sigma}$ discussed in Lemma 3.43. We now employ Boundary Elements Methods to find approximations of the exact Cauchy datum. To that end, let $(\xi_h, \zeta_h) \in S_h^0(\Gamma) \times S_h^1(\Gamma)$ denote the discretisations of $(\gamma_1\phi, \gamma_0\phi)$,

$$\xi_h = \sum_{l=1}^{n_h} \alpha_l \varphi_l^0, \quad \zeta_h = \sum_{k=1}^{m_h} \beta_k \psi_k^1,$$

where we have used the notation of Section 3.4. The coefficient vectors $\boldsymbol{\alpha}, \boldsymbol{\beta}$ are the solution of (3.15), reprinted here for reference,

$$\begin{pmatrix} V_h^{DD} & -K_h^{DN} \\ \left(K_h^{DN}\right)^\top & W_h^{NN} \end{pmatrix} \begin{pmatrix} \boldsymbol{\alpha}^D \\ \boldsymbol{\beta}^N \end{pmatrix} = \\ \begin{pmatrix} \frac{1}{2}M_h^{DD} + K_h^{DD} & -V_h^{DN} \\ -W_h^{ND} & \frac{1}{2}\left(M_h^{NN}\right)^\top - \left(K_h^{NN}\right)^\top \end{pmatrix} \begin{pmatrix} \boldsymbol{\beta}^D \\ \boldsymbol{\alpha}^N \end{pmatrix} - \begin{pmatrix} \boldsymbol{N}_0^D \\ \boldsymbol{N}_1^N \end{pmatrix}.$$

The matrix-vector product on the right hand side only depends on the surface mesh and the boundary conditions (g_N, g_D) and may be computed in advance. Only the vectors of the Newton potential depend on the particle positions, with $\boldsymbol{N}_0$ given by

$$\boldsymbol{N}_0[l] = \frac{L_0^2}{\lambda_D^2} \sum_{j=1}^{n_p} q_j \int_{T_l} U_\sigma(\boldsymbol{y} - \boldsymbol{x}_j) \, \mathrm{d}S_{\boldsymbol{y}}, \quad l = 1, \dots, n_h,$$

where $U_\sigma = \mathcal{N}\delta_{\boldsymbol{0}}^{\sigma}$, c.f. (2.13) and Lemma 3.43. Afterwards, we compute $\boldsymbol{N}_1$ by means of the discrete form of Lemma 3.74,

$$\boldsymbol{N}_1 = \left(-\frac{1}{2}M_h^\top + K_h^\top\right) V_h^{-1} \boldsymbol{N}_0,$$

thus avoiding an integration of ∇U_σ over Γ. Here, the application of the inverse V_h^{-1} is computed efficiently with the cg method. Because we use the preconditioner [151], c.f. Example 3.92, we only need a constant number of iterations to reach a given error tolerance, independent of the number of triangles. Afterwards, we solve (3.15) as described in Example 3.92 with a combination of the preconditioners [150, 151] for the Schur complement and for the single-layer operator, respectively.

The approximate solution then reads

$$\phi_h = \mathcal{V}\xi_h - \mathcal{W}\zeta_h + \frac{L_0^2}{\lambda_D^2} \sum_{j=1}^{n_p} q_j U_\sigma(\cdot - \boldsymbol{x}_j).$$

Note that ϕ_h is differentiable and by the harmonicity of the single- and double-layer potentials it additionally holds

$$-\Delta\phi_h = \frac{L_0^2}{\lambda_D^2} \sum_{j=1}^{n_p} q_j \delta_{\boldsymbol{x}_j}^{\sigma},$$

so ϕ_h is an exact solution of the Poisson equation and thus incorporates the physically relevant long-range behaviour together with a nearfield smoothing consistent with the mean field limit. Fully written out, the approximation of the electric field $\boldsymbol{E}_h$ at the position of the i-th particle is

$$\begin{aligned}\boldsymbol{E}_h(\boldsymbol{x}_i) =& \frac{L_0^2}{\lambda_D^2} \sum_{j=1}^{n_p} \frac{q_j}{4\pi} \begin{cases} \dfrac{\boldsymbol{x}_i - \boldsymbol{x}_j}{\sigma^3}, & |\boldsymbol{x}_i - \boldsymbol{x}_j| \leq \sigma, \\ \dfrac{\boldsymbol{x}_i - \boldsymbol{x}_j}{|\boldsymbol{x}_i - \boldsymbol{x}_j|^3}, & |\boldsymbol{x}_i - \boldsymbol{x}_j| > \sigma, \end{cases} \\ &+ \sum_{l=1}^{n_h} \frac{\alpha_l}{4\pi} \int_{T_l} \frac{\boldsymbol{x}_i - \boldsymbol{y}}{|\boldsymbol{x}_i - \boldsymbol{y}|^3} \,\mathrm{d}S_{\boldsymbol{y}} \\ &- \sum_{k=1}^{m_h} \frac{\beta_k}{4\pi} \int_{\operatorname{supp} \psi_k^1} \left(3 \frac{\boldsymbol{n}(\boldsymbol{y}) \cdot (\boldsymbol{x}_i - \boldsymbol{y})(\boldsymbol{x}_i - \boldsymbol{y})}{|\boldsymbol{x}_i - \boldsymbol{y}|^5} - \frac{\boldsymbol{n}(\boldsymbol{y})}{|\boldsymbol{x}_i - \boldsymbol{y}|^3} \right) \psi_k^1(\boldsymbol{y}) \,\mathrm{d}S_{\boldsymbol{y}} \end{aligned} \tag{3.20}$$

for $i = 1, \ldots, n_p$. Here, the surface integrals can be computed analytically and a reliable evaluation of $\boldsymbol{E}_h$ is ensured in all parts of the domain, in particular near the boundary [77]. In this form, however, the computational time for the evaluation of the electric field at all particle positions scales quadratically with their number n_p. Moreover, since the matrices in (3.15) are fully populated, the complexity of solving for $\boldsymbol{\alpha}$ and $\boldsymbol{\beta}$ depends quadratically on n_h. Consequently, a direct computation of $\boldsymbol{E}_h$ is prohibitively expensive even for a moderate numbers of particles and triangles. By the use of hierarchical approximations we review next, the computational complexity is reduced from $\mathcal{O}(n_p^2 + n_h^2)$ to $\mathcal{O}\big(r(n_p + n_h)\big)$ with a parameter $r \ll n_p, n_h$.

4. Hierarchical Approximation

Bäume wachsen nicht in den Himmel.[1]

(German adage)

Hierarchical matrices ($\mathcal{H}$-matrices) unify the treatment of tree-based approximation methods such as the Barnes–Hut algorithm [5], the Fast Multipole Method [70, 72], or the panel cluster method [79]. In this section, we focus on a specific subsets of $\mathcal{H}$-matrices, called $\mathcal{H}^2$-matrices. For their presentation, we follow [15], see also [78] and [7]. The monograph [134] is devoted to applications of hierarchical methods in Boundary Element Methods.

The computation of the electric field of the particle system (3.20) involves the assembly of fully populated matrices (3.16),

$$A[i,j] = \int_\Gamma \int_\Gamma \psi_i(\boldsymbol{x}) \mathfrak{K}(\boldsymbol{x},\boldsymbol{y}) \varphi_j(\boldsymbol{y}) \,\mathrm{d}S_{\boldsymbol{y}} \,\mathrm{d}S_{\boldsymbol{x}}, \quad i \in \mathcal{I}, j \in \mathcal{J}, \tag{4.1}$$

for a singular kernel $\mathfrak{K}$, index sets $\mathcal{I}, \mathcal{J}$, test functions $(\psi_i)_{i\in\mathcal{I}}$ and trial functions $(\varphi_j)_{j\in\mathcal{J}}$. For the evaluation of the Newton potential, matrix-vector products with matrices of the form

$$A[i,j] = \mathfrak{K}(\boldsymbol{x}_i, \boldsymbol{y}_j), \quad i \in \mathcal{I}, j \in \mathcal{J} \tag{4.2}$$

have be to performed. Here, $(\boldsymbol{x}_i)_{i\in\mathcal{I}}$ and $(\boldsymbol{y}_j)_{j\in\mathcal{J}}$ may represent particle positions or quadrature points on the boundary Γ. The treatment of these matrices is greatly simplified if the kernel has a special structure:

4.1 Definition (Degenerated expansion) *A kernel $\mathfrak{K} : X \times Y \to \mathbb{R}$, $X, Y \subseteq \mathbb{R}^3$, admits a degenerated expansion if there exist $r \in \mathbb{N}$ and functions $\mathfrak{g}_k : X \to \mathbb{R}$, $\mathfrak{h}_k : Y \to \mathbb{R}$ for $k = 1, \ldots, r$ such that*

$$\mathfrak{K}(\boldsymbol{x},\boldsymbol{y}) = \sum_{k=1}^{r} \mathfrak{g}_k(\boldsymbol{x}) \mathfrak{h}_k(\boldsymbol{y}), \quad (\boldsymbol{x},\boldsymbol{y}) \in X \times Y.$$

In this case, r is called the rank of the expansion.

4.2 Lemma *If the kernel $\mathfrak{K}$ in* (4.1) *or* (4.2) *has a degenerated expansion $\left(\mathfrak{g}_k, \mathfrak{h}_k\right)_{k=1}^r$, $r \in \mathbb{N}$, then $A \in \mathbb{R}^{|\mathcal{I}|\times|\mathcal{J}|}$ can be written as*

$$A = \mathfrak{G}\mathfrak{H}^\top$$

with $\mathfrak{G} \in \mathbb{R}^{|\mathcal{I}|\times r}$ and $\mathfrak{H} \in \mathbb{R}^{|\mathcal{J}|\times r}$. If $r \ll \min\{|\mathcal{I}|, |\mathcal{J}|\}$, we say that A admits a low-rank factorisation.

The storage complexity for A is reduced from $\mathcal{O}(|\mathcal{I}| \cdot |\mathcal{J}|)$ to $\mathcal{O}\big(r(|\mathcal{I}| + |\mathcal{J}|)\big)$. In particular, a matrix-vector multiplication is performed with $\mathcal{O}\big(r(|\mathcal{I}| + |\mathcal{J}|)\big)$ operations.

[1] "Trees do not grow to the sky."

Proof. We only give the proof for (4.1),

$$A[i,j] = \int_\Gamma \int_\Gamma \psi_i(\boldsymbol{x}) \mathcal{K}(\boldsymbol{x},\boldsymbol{y}) \varphi_j(\boldsymbol{y}) \,\mathrm{d}S_{\boldsymbol{y}} \,\mathrm{d}S_{\boldsymbol{x}}, \quad i \in \mathcal{I},\ j \in \mathcal{J},$$

the case of (4.2) being proved in complete analogy. For $i \in \mathcal{I}$, $j \in \mathcal{J}$ we obtain after inserting the degenerated expansion of $\mathcal{K}$,

$$\begin{aligned} A[i,j] &= \sum_{k=1}^{r} \left(\int_\Gamma \psi_i(\boldsymbol{x}) \mathfrak{g}_k(\boldsymbol{x}) \,\mathrm{d}S_{\boldsymbol{x}} \right) \left(\int_\Gamma \mathfrak{h}_k(\boldsymbol{y}) \varphi_j(\boldsymbol{y}) \,\mathrm{d}S_{\boldsymbol{y}} \right) \\ &= \sum_{k=1}^{r} \mathfrak{G}[i,k] \mathfrak{H}^\top[k,j], \end{aligned}$$

where

$$\mathfrak{G}[i,k] = \int_\Gamma \psi_i(\boldsymbol{x}) \mathfrak{g}_k(\boldsymbol{x}) \,\mathrm{d}S_{\boldsymbol{x}}, \quad \mathfrak{H}[j,k] = \int_\Gamma \varphi_j(\boldsymbol{y}) \mathfrak{h}_k(\boldsymbol{y}) \,\mathrm{d}S_{\boldsymbol{y}}, \quad k = 1,\dots,r.$$

The storage complexity for the matrices $\mathfrak{G}$ and $\mathfrak{H}$ is $\mathcal{O}(r|\mathcal{I}|)$ and $\mathcal{O}(r|\mathcal{J}|)$, respectively, so A needs $\mathcal{O}\big(r(|\mathcal{I}| + |\mathcal{J}|)\big)$ words of memory. Since every element of A is touched once during the matrix-vector multiplication, its complexity is $\mathcal{O}\big(r(|\mathcal{I}| + |\mathcal{J}|)\big)$. ∎

The kernels in our application do not degenerate but belong to a set of functions that allow for a degenerated expansion up to an error term that locally decays exponentially with increasing rank.

4.3 Definition (Asymptotically smooth functions) *The kernel $\mathcal{K}$ is asymptotically smooth if it is smooth outside the diagonal $\{(\boldsymbol{x},\boldsymbol{x}) : \boldsymbol{x} \in \mathbb{R}^3\}$ and there exists $c > 0$, $\nu > 0$ such that for all $\boldsymbol{\alpha}, \boldsymbol{\beta} \in \mathbb{N}^3$*

$$|D_{\boldsymbol{x}}^{\boldsymbol{\alpha}} D_{\boldsymbol{y}}^{\boldsymbol{\beta}} \mathcal{K}(\boldsymbol{x},\boldsymbol{y})| \leq c(\boldsymbol{\alpha}+\boldsymbol{\beta})! \nu^{|\boldsymbol{\alpha}|+|\boldsymbol{\beta}|} \frac{|\mathcal{K}(\boldsymbol{x},\boldsymbol{y})|}{|\boldsymbol{x}-\boldsymbol{y}|^{|\boldsymbol{\alpha}|+|\boldsymbol{\beta}|}}, \quad \boldsymbol{x} \neq \boldsymbol{y} \in \mathbb{R}^3.$$

4.4 Example The fundamental solution

$$\mathcal{K}(\boldsymbol{x},\boldsymbol{y}) = \frac{1}{4\pi} \frac{1}{|\boldsymbol{x}-\boldsymbol{y}|}, \quad \boldsymbol{x} \neq \boldsymbol{y} \in \mathbb{R}^3,$$

is asymptotically smooth with $\nu = 1$.

Before we construct exponentially converging degenerated expansions for asymptotically smooth kernels by the use of a truncated Taylor expansion, we first introduce some notation. For $B_1, B_2 \subseteq \mathbb{R}^3$, the diameter of B_1 is given by

$$\operatorname{diam}(B_1) = \sup_{(\boldsymbol{x},\boldsymbol{y}) \in B_1 \times B_1} |\boldsymbol{x}-\boldsymbol{y}|.$$

With

$$\operatorname{dist}(B_1,B_2) = \inf_{(\boldsymbol{x},\boldsymbol{y}) \in B_1 \times B_2} |\boldsymbol{x}-\boldsymbol{y}|$$

we denote the distance between B_1 and B_2. For a bounded function $\mathfrak{F} : B_1 \times B_2 \to \mathbb{R}$,

$$\|\mathfrak{F}\|_{B_1 \times B_2} = \sup_{(x,y) \in B_1 \times B_2} |\mathfrak{F}(x,y)|$$

is its least upper bound.

4.5 Lemma *Let $\mathfrak{K}$ be asymptotically smooth with constants (c, ν) . For two open, bounded, convex and disjoint sets $B_1, B_2 \subseteq \mathbb{R}^3$ such that*

$$\eta = \frac{\operatorname{diam}(B_1)}{\operatorname{dist}(B_1, B_2)} < \frac{1}{\nu}, \tag{4.3}$$

the Taylor series with respect to x converges exponentially, that is, the remainder of the Taylor expansion

$$\mathfrak{K}(x,y) = \sum_{|\alpha| \leq r} \frac{1}{\alpha!} D_x^\alpha \mathfrak{K}(x_0, y)(x - x_0)^\alpha + \mathfrak{R}_{x_0,r}(x,y) \tag{4.4}$$

fulfils

$$\|\mathfrak{R}_{x_0,r}\|_{B_1 \times B_2} \leq \frac{c}{2} \|\mathfrak{K}\|_{B_1 \times B_2} (r+3)(r+2)\big(\eta\nu\big)^{r+1}$$

for all $x_0 \in B_1$ and $r \in \mathbb{N}$.

Proof. Let $x_0 \in B_1$. The remainder of the Taylor expansion of order $r \in \mathbb{N}$ around x_0 has the form [98, p. 65]

$$\mathfrak{R}_{x_0,r}(x,y) = \sum_{|\alpha|=r+1} \frac{1}{\alpha!} D_x^\alpha \mathfrak{K}(\xi, y)(x - x_0)^\alpha, \quad (x,y) \in B_1 \times B_2,$$

for ξ on the line between x_0 and x. With the estimate on the derivatives of $\mathfrak{K}$ in Definition 4.3, we conclude

$$\begin{aligned}
|\mathfrak{R}_{x_0,r}(x,y)| &\leq c \sum_{|\alpha|=r+1} \nu^{|\alpha|} \frac{|\mathfrak{K}(\xi,y)|}{|\xi - y|^{|\alpha|}} |x - x_0|^{|\alpha|} \\
&= c\nu^{r+1} \left(\frac{|x - x_0|}{|\xi - y|} \right)^{r+1} |\mathfrak{K}(\xi,y)| \sum_{|\alpha|=r+1} 1 \\
&\leq c\nu^{r+1} \left(\frac{\operatorname{diam}(B_1)}{\operatorname{dist}(B_1, B_2)} \right)^{r+1} |\mathfrak{K}(x,y)| \sum_{|\alpha|=r+1} 1 \\
&= \frac{c}{2}(r+3)(r+2)\big(\nu\eta\big)^{r+1} |\mathfrak{K}(\xi,y)|.
\end{aligned}$$

Taking the supremum over all points in $B_1 \times B_2$ yields the desired estimate. For the computation of the sum over all multiindices $\alpha \in N_0^3$ with $|\alpha| = r+1$, we use the following combinatorial argument [154, pp. 15 f.]. Suppose we have $k \in \mathbb{N}$ balls placed along a line,

We now divide them into d groups by inserting $d - 1$ sticks between them, where we also allow empty groups,

Every multiindex of order k corresponds to exactly one of the possible configurations. To count their total number, we note there are $k + d - 1$ positions where we can place the sticks to separate the balls. Because the sticks are indistinguishable, there are

$$\binom{k+d-1}{d-1} = \frac{(k+d-1)!}{k!(d-1)!}$$

different configurations. Applying this to our situation with $\widetilde{d} = 3$ and $\widetilde{k} = r + 1$ yields

$$\sum_{|\boldsymbol{\alpha}|=r+1} 1 = \binom{r+3}{2} = \frac{1}{2}(r+3)(r+2),$$

thus proving the upper bound for the remainder. ■

Apart from the asymptotical smoothness of the kernel function, an essential ingredient for the exponential convergence of the remainder is condition (4.3) which means that B_1 and B_2 are well separated and thus admissible for a rapidly converging degenerate expansion. Since we later focus on symmetric expansions, we slightly sharpen (4.3):

4.6 Definition (Admissibility condition) *Two sets $B_1, B_2 \subseteq \mathbb{R}^3$ are called η-admissible for $\eta > 0$ if*

$$\max\{\operatorname{diam}(B_1), \operatorname{diam}(B_2)\} \leq \eta \operatorname{dist}(B_1, B_2).$$

4.7 Lemma *Let $\mathcal{K}$ be asymptotically smooth. For $B_1, B_2 \subseteq \mathbb{R}^3$ open, bounded and η-admissible with sufficiently small $\eta > 0$, and given error tolerance $\varepsilon > 0$, there exist $r \in \mathbb{N}$ with $r = \mathcal{O}(\log \varepsilon)$ and functions $\big((\mathfrak{g}_k, \mathfrak{h}_k) : B_1 \times B_2 \to \mathbb{R}\big)_{k=1}^{r}$ such that the least upper bound for the error*

$$B_1 \times B_2 \to \mathbb{R},\ (\boldsymbol{x}, \boldsymbol{y}) \mapsto \mathcal{K}(\boldsymbol{x}, \boldsymbol{y}) - \sum_{k=1}^{r} \mathfrak{g}_k(\boldsymbol{x})\mathfrak{h}_k(\boldsymbol{y})$$

is smaller than ε.

Proof. This is a direct consequence of Lemma 4.5. Note that in (4.4), the variables are separated. We thus set

$$\mathfrak{g}_{\boldsymbol{\alpha}}(\boldsymbol{x}) = \frac{1}{\boldsymbol{\alpha}!}(\boldsymbol{x} - \boldsymbol{x}_0)^{\boldsymbol{\alpha}}, \quad \mathfrak{h}_{\boldsymbol{\alpha}}(\boldsymbol{y}) = D_{\boldsymbol{x}}^{\boldsymbol{\alpha}}\mathcal{K}(\boldsymbol{x}_0, \boldsymbol{y}), \quad (\boldsymbol{x}, \boldsymbol{y}) \in B_1 \times B_2,$$

for a fixed point $\boldsymbol{x}_0 \in B_1$, up to multiindices $\boldsymbol{\alpha} \in \mathbb{N}^3$ that guarantee an error not larger than ε. Since the remainder decays exponentially with growing $|\boldsymbol{\alpha}|$, the maximum order of the derivatives only grows logarithmically with the error threshold. ■

Several schemes have been proposed to generate approximate degenerated expansions, for instance the Fast Multipole Method [29, 32, 70, 72, 71], applied to Boundary Element Methods in [125, 126], Adaptive Cross Approximation [6, 7, 8, 134], Lagrange interpolation [19, 20], Hybrid Cross Approximation [18], or the Green hybrid method [17]. In the following, we elaborate on Lagrange interpolation.

4.8 Definition (Chebyshev nodes) *The Chebyshev nodes of order $m \in \mathbb{N}$ on $[-1,1]$ are given by*

$$\cos\left(\frac{2k-1}{2m}\pi\right), \quad k = 1, \dots, m.$$

4.9 Definition (Lagrange polynomial) *Let $\boldsymbol{a}, \boldsymbol{b} \in \mathbb{R}^3$ with $a_i < b_i$ for $i = 1,2,3$, and let $B = [a_1, b_1] \times [a_2, b_2] \times [a_3, b_3]$. For $m \in \mathbb{N}$ and Chebyshev nodes $(z_k)_{k=1}^m$ we define the $\boldsymbol{k}$th Lagrange polynomial,*

$$L_{\boldsymbol{k}}^{(B)}(\boldsymbol{x}) = \prod_{i=1}^{3} \widetilde{L}_{k_i}\left(\frac{x_i - (b_i + a_i)/2}{(b_i - a_i)/2}\right),$$

with $\boldsymbol{k} = (k_1, k_2, k_3) \in \mathbb{N}^3$ and $k_i \leq m$, $i = 1,2,3$, where $\widetilde{L}_\ell$ denotes the ℓth Lagrange basis polynomial with respect to the Chebyshev nodes $(z_k)_{k=1}^m$,

$$\widetilde{L}_\ell(z) = \prod_{\substack{k=1 \\ k \neq \ell}}^{m} \frac{z - z_k}{z_\ell - z_k}, \quad z \in \mathbb{R}.$$

Similar to approximation by Taylor expansion, the error for Lagrange interpolation decays exponentially, but in this case, without restriction on the parameter η:

4.10 Lemma ([15, Theorem 4.22]) *Let $\mathcal{K}$ be asymptotically smooth with parameters (c, ν). For two η-admissible boxes $B_1, B_2 \subseteq \mathbb{R}^3$, the error of the m-th order Lagrange interpolation,*

$$\mathcal{R} : B_1 \times B_2 \to \mathbb{R}, (\boldsymbol{x}, \boldsymbol{y}) \mapsto \mathcal{K}(\boldsymbol{x}, \boldsymbol{y}) - \sum_{|\boldsymbol{k}|_\infty \leq m} \sum_{|\boldsymbol{\ell}|_\infty \leq m} L_{\boldsymbol{k}}^{(B_1)}(\boldsymbol{x}) \mathcal{K}\left(\boldsymbol{z}_{\boldsymbol{k}}^{(B_1)}, \boldsymbol{z}_{\boldsymbol{\ell}}^{(B_2)}\right) L_{\boldsymbol{\ell}}^{(B_2)}(\boldsymbol{y}),$$

decays exponentially,

$$\|\mathcal{R}\|_{B_1 \times B_2} \leq 36c \left(\frac{2}{\pi}\log(m+1) + 2\right)^6 (1 + 2\nu\eta)\left(\frac{\nu\eta}{1+\nu\eta}\right)^m \|\mathcal{K}\|_{B_1 \times B_2}.$$

Here, $|\boldsymbol{k}|_\infty = \max\{k_1, k_2, k_3\}$ and for a box B with lower left corner $\boldsymbol{a} \in \mathbb{R}^3$ and upper right corner $\boldsymbol{b} \in \mathbb{R}^3$

$$\boldsymbol{z}_{\boldsymbol{k}}^{(B)} = \frac{1}{2}(\boldsymbol{b} + \boldsymbol{a}) + \frac{1}{2}(\boldsymbol{b} - \boldsymbol{a}) \odot \begin{pmatrix} z_{k_1} \\ z_{k_2} \\ z_{k_3} \end{pmatrix},$$

where $\odot$ denotes the componentwise product and $(z_k)_{k=1}^m$ are the Chebyshev nodes of order m.

With X and Y we denote the geometry associated to $\mathcal{I}$ and $\mathcal{J}$, respectively. For BEM matrices (4.1),

$$X = \{\operatorname{supp}\psi_i : i \in \mathcal{I}\}, \quad Y = \{\operatorname{supp}\varphi_j : j \in \mathcal{J}\}.$$

In view of the employed regularisation of the Dirac distribution, cf. Lemma 3.43, a suitable choice for matrices of the kind (4.2) is

$$X = \{B_\sigma(\boldsymbol{x}_i) : i \in \mathcal{I}\}, \quad Y = \{B_\sigma(\boldsymbol{y}_j) : j \in \mathcal{J}\},$$

with $\sigma > 0$. By X_t (Y_s), we denote the subset of X (Y) whose elements correspond to indices $t \subseteq \mathcal{I}$ ($s \subseteq \mathcal{J}$). We say that the two index sets t and s are admissible if the geometries X_t and Y_s are admissible according to Definition 4.6. Since the Lagrange interpolation in Lemma 4.10

relies on axis-parallel boxes, we furthermore associate a box B_t to X_t with $X_t \subseteq B_t$. In practical computations, we replace X_t and Y_s with their bounding boxes, that is X_t and Y_s are η-admissible if

$$\max\{\operatorname{diam}(B_t), \operatorname{diam}(B_s)\} \leq \eta \operatorname{dist}(B_t, B_s).$$

Note that the bounding boxes are supersets of X_t and Y_s, so this condition implies the usual one but is much simpler to check. To minimise the computational cost for the fully populated matrices (4.1) and (4.2), we seek a partition $\mathcal{P}$ of $\mathcal{I} \times \mathcal{J}$ such that $A|_b$ admits a exponentially converging low-rank factorisation for a maximal number of $b \in \mathcal{P}$. However, the number of partitions increases super-exponentially[2] with $|\mathcal{I}|$ and $|\mathcal{J}|$, so searching for the optimal partition is computationally infeasible. Therefore, we construct partitions of $\mathcal{I} \times \mathcal{J}$ via partitions of $\mathcal{I}$ and $\mathcal{J}$. For further analysis and practical purposes, they are organised in a tree structure.

4.11 Definition (Cluster tree) *A tree $T(\mathcal{I})$ whose nodes are subsets of $\mathcal{I}$ is called cluster tree if*

- *$\mathcal{I}$ is its root node,*
- *for $t \in T(\mathcal{I})$ not a leaf node, t is the disjoint union of its sons,*
- *the number of sons of a non leaf node is larger than one.*

4.12 Remark

- In actual computations, we furthermore require that the number of elements in a node is bounded from below by $n_{\min} > 1$. As we shall see later, this limits the minimal block size in the matrix partition. Compared to an unrestricted cluster tree, a discretisation adopted $n_{\min}$ typically improves the performance of the scheme.
- A cluster tree $T(\mathcal{I})$ for the geometry X is constructed as follows: Starting from a bounding box that contains X, it is recursively subdivided into disjoint subboxes. There are several possibilities for this step. One may split along each coordinate axis, resulting in eight subboxes (octree), periodically cycle through the dimensions and split along the corresponding axis, subdivide the boxes such that each new box contains the same number of entities (cardinality splitting) or split the box orthogonal to the direction of largest extend (principal component analysis), see [7, Section 1.4] for more details.

4.13 Definition (Block cluster tree) *Let $T(\mathcal{I})$ and $T(\mathcal{J})$ be cluster trees and $\eta > 0$. The block cluster tree $T(\mathcal{I} \times \mathcal{J})$ is a cluster tree uniquely determined by its* sons *mapping,*

$$\operatorname{sons}(t \times s) = \begin{cases} \varnothing, & t \times s \text{ is admissible or } \operatorname{sons}(t) = \varnothing = \operatorname{sons}(s), \\ \operatorname{sons}(t) \times \{s\}, & \operatorname{sons}(t) \neq \varnothing, \operatorname{sons}(s) = \varnothing, \\ \{t\} \times \operatorname{sons}(s), & \operatorname{sons}(t) = \varnothing, \operatorname{sons}(s) \neq \varnothing, \\ \operatorname{sons}(t) \times \operatorname{sons}(s), & \text{else}, \end{cases}$$

[2] The number of partitions of a set with n elements is known as the nth Bell number B_n [154, p. 20]. It obeys the asymptotic expansion [24, p. 108]

$$\frac{\log B_n}{n} = \log n - \log\log n - 1 + \frac{\log\log n}{\log n} + \frac{1}{\log n} + \frac{1}{2}\left(\frac{\log\log n}{\log n}\right)^2 + \mathcal{O}\left(\frac{\log\log n}{(\log n)^2}\right), \quad n \to \infty,$$

from which we infer that for $n > 3$,

$$B_n > \left(\frac{n}{e \log n}\right)^n.$$

starting with $t \times s = \mathcal{I} \times \mathcal{J}$.

The following definition specifies the requirements for partitions of $\mathcal{I} \times \mathcal{J}$ we discussed before.

4.14 Definition (Admissible partition) *An admissible partition* $\mathcal{P}$ *of* $\mathcal{I} \times \mathcal{J}$ *with respect to a block cluster tree* $T(\mathcal{I} \times \mathcal{J})$ *is a subset of* $T(\mathcal{I} \times \mathcal{J})$ *such that its elements are mutually disjoint,*

$$b_1, b_2 \in \mathcal{P} \implies b_1 = b_2 \text{ or } b_1 \cap b_2 = \varnothing,$$

and it contains all elements of $\mathcal{I} \times \mathcal{J}$,

$$\bigcup_{b \in \mathcal{P}} b = \mathcal{I} \times \mathcal{J}.$$

Moreover, every $t \times s \in \mathcal{P}$ *is either admissible or*

$$\max\{|t|, |s|\} \leq n_{min}.$$

With

$$\mathcal{P}^+ = \{b \in \mathcal{P} : b \text{ is admissible}\}, \quad \mathcal{P}^- = \mathcal{P} \setminus \mathcal{P}^+,$$

we denote the near- and farfield of $\mathcal{P}$*, respectively.*

A direct consequence from the construction of the cluster trees and the resulting block cluster tree is

4.15 Lemma *The leafs of a block cluster tree form an admissible partition.*

By utilising interpolation of order $m \in \mathbb{N}$ for an admissible partition $\mathcal{P}$ of $\mathcal{I} \times \mathcal{J}$, the approximation of A reads

$$\widetilde{A} = \sum_{t \times s \in \mathcal{P}^-} A|_{t \times s} + \sum_{t \times s \in \mathcal{P}^+} \mathfrak{V}_t \mathfrak{S}_{t \times s} \mathfrak{W}_s^\top,$$

where $\mathfrak{S}_{t \times s}$ is the coupling matrix,

$$\mathfrak{S}_{t \times s}[\boldsymbol{k}, \boldsymbol{\ell}] = \mathcal{K}\left(z_{\boldsymbol{k}}^{(B_t)}, z_{\boldsymbol{\ell}}^{(B_s)}\right), \quad |\boldsymbol{k}|_\infty, |\boldsymbol{\ell}|_\infty \leq m,$$

and $\left(\mathfrak{V}_t\right)_{t \in T(\mathcal{I})}$, $\left(\mathfrak{W}_s\right)_{s \in T(\mathcal{J})}$ are called cluster basis for $T(\mathcal{I})$ and $T(\mathcal{J})$, respectively. For BEM matrices (4.1),

$$\mathfrak{V}_t[i, \boldsymbol{k}] = \int_\Gamma \psi_i(\boldsymbol{y}) L_{\boldsymbol{k}}^{(B_t)}(\boldsymbol{y}) \, \mathrm{d}S_{\boldsymbol{y}}, \quad i \in t, \ |\boldsymbol{k}|_\infty \leq m,$$

and point evaluations for (4.2),

$$\mathfrak{V}_t[i, \boldsymbol{k}] = L_{\boldsymbol{k}}^{(B_t)}(\boldsymbol{x}_i), \quad i \in t, \ |\boldsymbol{k}|_\infty \leq m.$$

It is not necessary to compute the cluster basis for all nodes of the tree. Let $t \in T(\mathcal{I})$ with son t'. Both Lagrange bases $\left(L_{\boldsymbol{k}}^{(B_{(t)})}\right)_{|\boldsymbol{k}|_\infty \leq m}$ and $\left(L_{\boldsymbol{k}}^{(B_{t'})}\right)_{|\boldsymbol{k}|_\infty \leq m}$ span the same polynomial space. Therefore,

$$L_{\boldsymbol{k}}^{(B_t)}(\boldsymbol{x}) = \sum_{|\boldsymbol{\ell}|_\infty \leq m} L_{\boldsymbol{k}}^{(B_t)}\left(z_{\boldsymbol{\ell}}^{(B_{t'})}\right) L_{\boldsymbol{\ell}}^{(B_{t'})}(\boldsymbol{x}), \quad \boldsymbol{x} \in B_{t'},$$

and hence

$$\mathfrak{V}_t[i,\boldsymbol{k}] = \sum_{|\boldsymbol{\ell}|_\infty \le m} \mathfrak{V}_{t'}[i,\boldsymbol{\ell}]\mathfrak{T}_{t',t}[\boldsymbol{\ell},\boldsymbol{k}], \quad i \in t',\ |\boldsymbol{k}|_\infty \le m,$$

where $\mathfrak{T}_{t',t}$ is the transfer matrix between t' and t,

$$\mathfrak{T}_{t',t}[\boldsymbol{\ell},\boldsymbol{k}] = L_{\boldsymbol{k}}^{(B_t)}\left(z_{\boldsymbol{\ell}}^{(B_{t'})}\right), \quad |\boldsymbol{k}|_\infty, |\boldsymbol{\ell}|_\infty \le m.$$

Since the sons of t are a disjoint partition of t, we can use the transfer matrices to express $\mathfrak{V}_t$ by its sons,

$$\mathfrak{V}_t = \begin{pmatrix} \mathfrak{V}_{t_1}\mathfrak{T}_{t_1,t} \\ \vdots \\ \mathfrak{V}_{t_p}\mathfrak{T}_{t_p,t} \end{pmatrix}, \quad \operatorname{sons}(t) = \{t_1,\dots,t_p\},\ p \in \mathbb{N}.$$

This motivates our next definition:

4.16 Definition (Nested cluster basis) *For a given rank $r \in \mathbb{N}$ and cluster tree $T(\mathcal{I})$, the set of matrices*

$$\mathfrak{V}_t \in \mathbb{R}^{|t|\times r}, \quad t \in T(\mathcal{I}),$$

is called nested cluster basis if for each non-leaf node $t \in T(\mathcal{I})$ there are transfer matrices

$$\mathfrak{T}_{t',t} \in \mathbb{R}^{r\times r}, \quad t' \in \operatorname{sons}(t)$$

such that

$$\mathfrak{V}_t = \begin{pmatrix} \mathfrak{V}_{t_1}\mathfrak{T}_{t_1,t} \\ \vdots \\ \mathfrak{V}_{t_p}\mathfrak{T}_{t_p,t} \end{pmatrix}, \quad \operatorname{sons}(t) = \{t_1,\dots,t_p\},\ p \in \mathbb{N}.$$

4.17 Definition ($\mathcal{H}^2$-matrix) *A matrix $A \in \mathbb{R}^{|\mathcal{I}|\times|\mathcal{J}|}$ is called $\mathcal{H}^2$-matrix of rank $r \in \mathbb{N}$ with respect to an admissible partition $\mathcal{P}$ of $\mathcal{I}\times\mathcal{J}$ if there exist nested cluster bases $\left(\mathfrak{V}_t\right)_{t\in T(\mathcal{I})}$, $(\mathfrak{W}_s)_{s\in T(\mathcal{J})}$ such that for all $b = t\times s \in \mathcal{P}^+$*

$$A|_b = \mathfrak{V}_t \mathfrak{S}_b \mathfrak{W}_s^\top$$

with a matrix $\mathfrak{S}_b \in \mathbb{R}^{r\times r}$.

For $\mathcal{H}^2$-matrices the required storage and therefore the complexity for typical matrix operations like a matrix-vector multiplication are drastically reduced by exploiting its organisation in a tree structure. Section 3.7 in [15] gives the algorithmic details for the efficient computation of the $\mathcal{H}^2$-matrix-vector product.

4.18 Theorem ([15, Corollary 3.49]) *If there exists a constant $C_{sp} > 0$ such that*

$$|\{s \in T(\mathcal{J}) : t\times s \in T(\mathcal{I}\times\mathcal{J})\}|, |\{t \in T(\mathcal{I}) : t\times s \in T(\mathcal{I}\times\mathcal{J})\}| \le C_{sp} \tag{4.5}$$

for all $t \in T(\mathcal{I})$ and $s \in T(\mathcal{J})$ independent of the discretisation parameter of the underlying problem, then a $\mathcal{H}^2$-matrix of rank $r \in \mathbb{N}$ needs

$$\mathcal{O}\big(r\cdot(|\mathcal{I}| + |\mathcal{J}|)\big)$$

units of storage. Moreover, the matrix-vector multiplication can be performed in as many operations.

4.19 Remark Condition (4.5) can be interpreted as a sparsity condition, similar to the number of nonzero entries of a sparse matrix. The influence of the geometry and the triangulation on the constant C_{sp} is discussed in [78, Section 6.4].

5. Plasma Oscillations

> Die folgenden Erörterungen werden uns nichts Neues über die Prinzipien der Mechanik lehren. Die große Bedeutung der Schwingungsvorgänge für Physik und Technik fordert aber zu ihrer gesonderten systematischen Behandlung auf.[1]
>
> *(Arnold Sommerfeld [142])*

In equilibrium, the components of a two-component plasma consisting of electrons and positively charged ions distribute such that the total charge density is locally zero. If the electrons are uniformly displaced from equilibrium (the much heavier ions are assumed to be immobile), a negative charge forms at one end of the plasma that gives rise to a positive net charge on the opposite site. The generated electrical field then accelerates the electrons into the opposite direction of their displacement. Once they reach the opposite end, the electric field forces the electrons to move back to their equilibrium position, causing them to oscillate.

This phenomenon is called plasma oscillation and was first experimentally observed by Tonks and Langmuir [156] in 1929. In their work, they also derive the frequency of the electron oscillation in an infinite slab, known as plasma frequency,[2]

$$\omega_p = \sqrt{\frac{n_e e^2}{\varepsilon_0 m_e}}, \tag{5.1}$$

where n_e is the number density of the electrons, e is the elementary charge and m_e is the electron mass. Bohm and Gross [12, 13] extended this theory to account for nonzero temperature, collisions or nonuniform electron densities. By a famous result of Landau [104], plasma oscillations are exponentially damped with a rate that can be computed from the dispersion relation. This analytically available information makes plasma oscillations and their exponential damping one of the most used test cases for numerical methods, see the literature cited in Chapter 1. Plasma oscillations can be also used to construct measuring instruments. The plasma absorption probe [97, 109] exploits that the plasma is excited in resonance by an external electromagnetic field close to a multiple of the plasma frequency. Since the only nonconstant quantity in the definition of ω_p is the number density n_e, this method allows to measure n_e.

In this chapter, we utilise the single-layer potential and Boundary Element Methods to investigate oscillations of bounded plasmas with arbitrary shape. We show how to numerically compute the frequencies and provide analytical expressions for the frequencies of a plasma of ellipsoidal shape. This generalises the results of Dubin [48] for a spheroid (an ellipsoid with two equal semiaxes) obtained from the linearisation of a fluid model for a one-component plasma with uniform background charge. Numerical examples are presented in Section 6.1.

[1] "The following discussions will not teach us anything new about the principles of mechanics. However, the great importance of oscillatory processes for physics and engineering calls for their separate systematic treatment."

[2] The authors use the CGS system, so to convert the quantities to SI units, $1/4\pi$ has to be replaced by ε_0 in their formulas.

5.1. Theoretical Results

In the following, let $\Omega \subseteq \mathbb{R}^3$ be open and bounded with Lipschitz boundary Γ. We assume that the ions are uniformly distributed inside Ω, so that the number density is $n_e \mathbb{1}_\Omega$. The Vlasov equation for the electron distribution function f reads

$$\partial_t f + \boldsymbol{v} \cdot \nabla_{\boldsymbol{x}} f + \frac{e}{m_e} \nabla_{\boldsymbol{x}} \phi \cdot \nabla_{\boldsymbol{v}} f = 0,$$

where the solution of the Poisson equation with charge density

$$e n_e \mathbb{1}_\Omega - e \int_{\mathbb{R}^3} f(\cdot, \boldsymbol{v}, \cdot) \, \mathrm{d}\boldsymbol{v}$$

in all $\mathbb{R}^3$ is given by the Newton potential,

$$\phi(\boldsymbol{x}) = \frac{1}{4\pi\varepsilon_0} \int_{\mathbb{R}^3} \frac{1}{|\boldsymbol{x} - \boldsymbol{y}|} \left(e n_e \mathbb{1}_\Omega(\boldsymbol{y}) - e \int_{\mathbb{R}^3} f(\cdot, \boldsymbol{v}, \boldsymbol{y}) \, \mathrm{d}\boldsymbol{v} \right) \mathrm{d}\boldsymbol{y}, \quad \boldsymbol{x} \in \mathbb{R}^3.$$

We now assume that the positions of the electrons are uniformly shifted by $\boldsymbol{d}(t) \in \mathbb{R}^3$,

$$\int_{\mathbb{R}^3} f(t, \boldsymbol{x}, \boldsymbol{v}) \, \mathrm{d}\boldsymbol{v} = n_e \mathbb{1}_\Omega\big(\boldsymbol{x} - \boldsymbol{d}(t)\big).$$

5.1 Lemma *The linearisation of*

$$\phi(\boldsymbol{x}) = \frac{e n_e}{4\pi\varepsilon_0} \int_{\mathbb{R}^3} \frac{1}{|\boldsymbol{x} - \boldsymbol{y}|} \left[\mathbb{1}_\Omega(\boldsymbol{y}) - \mathbb{1}_\Omega(\boldsymbol{y} - \boldsymbol{d}) \right] \, d\boldsymbol{y}, \quad \boldsymbol{x} \in \mathbb{R}^3,$$

in $\boldsymbol{d}$ around $\mathbf{0}$ is given by

$$\phi_0(\boldsymbol{x}) = -\frac{e n_e}{\varepsilon_0} (\mathcal{V}\boldsymbol{n})(\boldsymbol{x}) \cdot \boldsymbol{d}, \quad \boldsymbol{x} \in \mathbb{R}^3,$$

where $\mathcal{V}$ is the single-layer potential and $\boldsymbol{n}$ denotes the outward normal vector field of Ω.

Proof. The calculation is most conveniently carried out in Fourier space. With Lemma 3.27 we get

$$\begin{aligned} \widehat{\phi}(\boldsymbol{\xi}) &= \frac{e n_e}{\varepsilon_0} \widehat{U}(\boldsymbol{\xi}) \left[1 - \exp(\mathrm{i}\, \boldsymbol{d} \cdot \boldsymbol{\xi}) \right] \widehat{\mathbb{1}}_\Omega(\boldsymbol{\xi}) \\ &= \frac{e n_e}{\varepsilon_0} \widehat{U}(\boldsymbol{\xi}) (-\mathrm{i}\, \boldsymbol{d} \cdot \boldsymbol{\xi}) \widehat{\mathbb{1}}_\Omega(\boldsymbol{\xi}) + \mathcal{O}(|\boldsymbol{d}|^2) \\ &= \frac{e n_e}{\varepsilon_0} \mathcal{F}\big[U * \operatorname{div}(\boldsymbol{d}\, \mathbb{1}_\Omega) \big](\boldsymbol{\xi}) + \mathcal{O}(|\boldsymbol{d}|^2), \end{aligned}$$

where $\operatorname{div}(\boldsymbol{d}\, \mathbb{1}_\Omega)$ is the distributional divergence,

$$\operatorname{div}(\boldsymbol{d}\, \mathbb{1}_\Omega)\psi = -\int_{\mathbb{R}^3} \mathbb{1}_\Omega \boldsymbol{d} \cdot \nabla\psi \, \mathrm{d}\boldsymbol{x} = -\int_\Omega \operatorname{div}(\boldsymbol{d}\, \psi) \, \mathrm{d}\boldsymbol{x} = -\int_\Gamma \boldsymbol{d} \cdot \boldsymbol{n}\, \psi \, \mathrm{d}S$$

for $\psi \in \mathcal{D}(\mathbb{R}^3)$. Therefore, in first order of $|\boldsymbol{d}|$ the potential is

$$\phi_0 = \frac{e n_e}{\varepsilon_0} U * \operatorname{div}(\boldsymbol{d}\mathbb{1}_\Omega).$$

To compute the convolution, we use Definition 3.21,

$$\begin{aligned}(U * \operatorname{div}(\boldsymbol{d}\mathbb{1}_\Omega))\psi &= -\int_{\mathbb{R}^3}\int_\Gamma U(\boldsymbol{x})\boldsymbol{d}\cdot\boldsymbol{n}(\boldsymbol{y})\psi(\boldsymbol{x}+\boldsymbol{y})\,\mathrm{d}S_{\boldsymbol{y}}\,\mathrm{d}\boldsymbol{x}\\ &= -\int_{\mathbb{R}^3}\left(\int_\Gamma U(\boldsymbol{x}-\boldsymbol{y})\boldsymbol{d}\cdot\boldsymbol{n}(\boldsymbol{y})\,\mathrm{d}S_{\boldsymbol{y}}\right)\psi(\boldsymbol{x})\,\mathrm{d}\boldsymbol{x}, \quad \psi \in \mathcal{D}(\mathbb{R}^3),\end{aligned}$$

where we identify the term in brackets as the single-layer potential for Γ, evaluated at $\boldsymbol{d}\cdot\boldsymbol{n}$. ■

The linearisation of $\boldsymbol{E}$ is now

$$\boldsymbol{E}_0(\boldsymbol{x}) = -\nabla\phi_0(\boldsymbol{x}) = \frac{e n_e}{\varepsilon_0}\nabla(\mathcal{V}\boldsymbol{n})(\boldsymbol{x})\boldsymbol{d}, \quad \boldsymbol{x}\in\mathbb{R}^3, \tag{5.2}$$

where $\nabla(\mathcal{V}\boldsymbol{n})$ is the transposed Jacobi matrix of $\mathcal{V}\boldsymbol{n}$,

$$(\nabla(\mathcal{V}\boldsymbol{n}))_{i,j} = \frac{\partial \mathcal{V}n_j}{\partial x_i}, \quad i,j\in\{1,2,3\}.$$

5.2 Lemma *For $\boldsymbol{x}\in\Omega$, the matrix $\nabla(\mathcal{V}\boldsymbol{n})(\boldsymbol{x})$ is symmetric with trace equal to one.*

Proof. Let $\boldsymbol{x}\in\Omega$ and $\varepsilon>0$ such that $\overline{B}_\varepsilon(\boldsymbol{x})\subseteq\Omega$. For $i,j\in\{1,2,3\}$, we compute

$$\begin{aligned}\frac{\partial \mathcal{V}n_j}{\partial x_i}(\boldsymbol{x}) &= -\int_\Gamma \frac{\partial}{\partial y_i}U(\boldsymbol{x}-\boldsymbol{y})n_j(\boldsymbol{y})\,\mathrm{d}S_{\boldsymbol{y}}\\ &= -\int_\Gamma \frac{\partial}{\partial y_i}U(\boldsymbol{x}-\boldsymbol{y})n_j(\boldsymbol{y})\,\mathrm{d}S_{\boldsymbol{y}} + \int_{\partial B_\varepsilon(\boldsymbol{x})}\frac{\partial}{\partial y_i}U(\boldsymbol{x}-\boldsymbol{y})\frac{y_j-x_j}{\varepsilon}\,\mathrm{d}S_{\boldsymbol{y}}\\ &\qquad - \int_{\partial B_\varepsilon(\boldsymbol{x})}\frac{\partial}{\partial y_i}U(\boldsymbol{x}-\boldsymbol{y})\frac{y_j-x_j}{\varepsilon}\,\mathrm{d}S_{\boldsymbol{y}}\\ &= -\int_{\Omega\setminus\overline{B}_\varepsilon(\boldsymbol{x})}\frac{\partial^2}{\partial y_j\partial y_i}U(\boldsymbol{x}-\boldsymbol{y})\,\mathrm{d}\boldsymbol{y} - \int_{\partial B_\varepsilon(\boldsymbol{x})}\frac{\partial}{\partial y_i}U(\boldsymbol{x}-\boldsymbol{y})\frac{y_j-x_j}{\varepsilon}\,\mathrm{d}S_{\boldsymbol{y}},\end{aligned}$$

where the last equality follows from Gauß' theorem for $\Omega\setminus\overline{B}_\varepsilon(\boldsymbol{x})$. We now turn to the second term,

$$\begin{aligned}-\int_{\partial B_\varepsilon(\boldsymbol{x})}\frac{\partial}{\partial y_i}U(\boldsymbol{x}-\boldsymbol{y})\frac{y_j-x_j}{\varepsilon}\,\mathrm{d}S_{\boldsymbol{y}} &= -\frac{1}{4\pi}\int_{\partial B_\varepsilon(\boldsymbol{x})}\frac{x_i-y_i}{|\boldsymbol{x}-\boldsymbol{y}|^3}\frac{y_j-x_j}{\varepsilon}\,\mathrm{d}S_{\boldsymbol{y}}\\ &= \frac{1}{4\pi\varepsilon^4}\int_{\partial B_\varepsilon(\boldsymbol{x})}(y_j-x_j)(y_i-x_i)\,\mathrm{d}S_{\boldsymbol{y}}\\ &= \frac{1}{4\pi}\int_{S^2} y_j\,y_i\,\mathrm{d}S_{\boldsymbol{y}} = \frac{1}{3}\delta_{ji}.\end{aligned}$$

To summarise, we have shown that

$$\nabla(\mathcal{V}\boldsymbol{n})(\boldsymbol{x}) = \frac{1}{3}I_3 - \int\limits_{\Omega\setminus\overline{B}_\varepsilon(\boldsymbol{x})} D_{\boldsymbol{y}}^2 U(\boldsymbol{x}-\boldsymbol{y})\,\mathrm{d}\boldsymbol{y}.$$

Since the right hand side is a symmetric matrix, so is $\nabla(\mathcal{V}\boldsymbol{n})(\boldsymbol{x})$. Furthermore,

$$\operatorname{Tr}\nabla(\mathcal{V}\boldsymbol{n})(\boldsymbol{x}) = 1 - \int\limits_{\Omega\setminus\overline{B}_\varepsilon(\boldsymbol{x})} \Delta_{\boldsymbol{y}} U(\boldsymbol{x}-\boldsymbol{y})\,\mathrm{d}\boldsymbol{y} = 1,$$

as the fundamental solution U is harmonic on $\mathbb{R}^3\setminus\{\boldsymbol{0}\}$. ■

5.3 Lemma *The eigenvalues of $\nabla(\mathcal{V}\boldsymbol{n})$ are invariant under rigid motions of Ω. If Ω is convex, they are also invariant under scaling of Ω.*

Proof. Let $R(\boldsymbol{y}) = Q\boldsymbol{y} + \boldsymbol{b}$ be a rigid motion with a vector $\boldsymbol{b}\in\mathbb{R}^3$ and an orthogonal matrix $Q\in\mathbb{R}^{3\times 3}$. Writing $\widetilde{\Omega} = R(\Omega)$ for the image after rotation and translation, we have

$$\boldsymbol{n}_{\widetilde{\Omega}}(\widetilde{\boldsymbol{y}}) = Q\boldsymbol{n}_\Omega(R^{-1}\widetilde{\boldsymbol{y}})$$

and $\widetilde{\Gamma} = \partial\widetilde{\Omega} = R(\Gamma)$. Therefore,

$$\begin{aligned}\nabla(\mathcal{V}_{\widetilde{\Omega}}\boldsymbol{n}_{\widetilde{\Omega}})(\widetilde{\boldsymbol{x}}) &= -\frac{1}{4\pi}\int\limits_{\widetilde{\Gamma}} \frac{\widetilde{\boldsymbol{x}}-\boldsymbol{y}}{|R\boldsymbol{x}-\boldsymbol{y}|^3}\,\boldsymbol{n}_{\widetilde{\Omega}}(\widetilde{\boldsymbol{y}})^\top\,\mathrm{d}S_{\widetilde{\boldsymbol{y}}}\\ &= -\frac{1}{4\pi}\int\limits_{\Gamma} R\frac{R^{-1}\widetilde{\boldsymbol{x}}-\boldsymbol{y}}{|R^{-1}\widetilde{\boldsymbol{x}}-\boldsymbol{y}|^3}\,(Q\boldsymbol{n}_\Omega(\boldsymbol{y}))^\top\,\mathrm{d}S_{\boldsymbol{y}}.\end{aligned}$$

Inserting the definition of R into the last integral yields

$$\nabla(\mathcal{V}_{\widetilde{\Omega}}\boldsymbol{n}_{\widetilde{\Omega}})(\widetilde{\boldsymbol{x}}) = -\frac{1}{4\pi}\int\limits_{\Gamma} Q\frac{R^{-1}\widetilde{\boldsymbol{x}}-\boldsymbol{y}}{|R^{-1}\widetilde{\boldsymbol{x}}-\boldsymbol{y}|^3}\,\boldsymbol{n}_\Omega(\boldsymbol{y})^\top Q^\top\,\mathrm{d}S_{\boldsymbol{y}} - \frac{1}{4\pi}\int\limits_{\Gamma}\boldsymbol{b}\boldsymbol{n}_\Omega(\boldsymbol{y})^\top Q^\top\,\mathrm{d}S_{\boldsymbol{y}}.$$

The first term equals $Q\nabla(\mathcal{V}_\Omega\boldsymbol{n}_\Omega)(R^{-1}\widetilde{\boldsymbol{x}})$. The second integral vanishes since every component of the integrand is a linear polynomial in $\boldsymbol{n}_\Omega$ with constant coefficients and

$$\int\limits_{\Gamma} n_j(\boldsymbol{y})\,\mathrm{d}S_{\boldsymbol{y}} = \int\limits_{\Omega}\operatorname{div}(\boldsymbol{e}_j)\,\mathrm{d}\boldsymbol{y} = 0$$

by Gauß' theorem, where $\boldsymbol{e}_j$ denotes the jth standard basis vector. Thus, $(\nabla\mathcal{V}_{\widetilde{\Omega}}\boldsymbol{n}_{\widetilde{\Omega}})(\widetilde{\boldsymbol{x}})$ and $(\nabla V_\Omega\boldsymbol{n}_\Omega)(R^{-1}\widetilde{\boldsymbol{x}})$ are similar matrices and hence have the same eigenvalues.

Now let us assume that, in addition, Ω is convex. By the preceding discussion we may assume that, after a suitable rigid motion, $\boldsymbol{0}\in\Omega$ and $\boldsymbol{x} = \boldsymbol{0}$. For $\sigma > 0$ and a set $A\subseteq\mathbb{R}^3$, let

$$A_\sigma = \{\sigma\boldsymbol{x} : \boldsymbol{x}\in A\}.$$

With Ω and $\overline{\Omega}$ the sets Ω_σ and $\overline{\Omega}_\sigma = \overline{\Omega_\sigma}$ are convex too. For convex sets, its interior and the interior of its closure coincide [64, Korollar 2.10]. Therefore,

$$\partial\Omega_\sigma = \overline{\Omega_\sigma}\setminus\operatorname{int}(\overline{\Omega_\sigma}) = \overline{\Omega}_\sigma\setminus\Omega_\sigma = \Gamma_\sigma,$$

so the boundary of the rescaled set Ω_σ is the rescaled boundary Γ_σ. The outward normal to Ω_σ is given by

$$\boldsymbol{n}_{\Omega_\sigma}(\boldsymbol{y}) = \boldsymbol{n}_\Omega(\boldsymbol{y}/\sigma), \quad \boldsymbol{y} \in \Omega_\sigma.$$

Hence,

$$4\pi\nabla(\mathcal{V}_{\Omega_\sigma}\boldsymbol{n}_{\Omega_\sigma})(\boldsymbol{0}) = \int_{\Gamma_\sigma} \frac{\boldsymbol{y}}{|\boldsymbol{y}|^3}\boldsymbol{n}_\Omega(\boldsymbol{y}/\sigma)^\top \,\mathrm{d}S_{\boldsymbol{y}} = \int_\Gamma \frac{1}{\sigma^2}\frac{\boldsymbol{y}}{|\boldsymbol{y}|^3}\boldsymbol{n}_\Omega(\boldsymbol{y})\sigma^2 \,\mathrm{d}S_{\boldsymbol{y}} = 4\pi\nabla(\mathcal{V}_\Omega\boldsymbol{n}_\Omega)(\boldsymbol{0}),$$

which proves the scaling invariance of the eigenvalues. ■

Having derived the linearisation of $\boldsymbol{E}$ in (5.2), we use it to linearise the system of characteristic curves,

$$\begin{aligned}\dot{\boldsymbol{X}}(t) &= \boldsymbol{V}(t),\\ \dot{\boldsymbol{V}}(t) &= -\frac{e}{m_e}\boldsymbol{E}(\boldsymbol{X}(t)),\end{aligned}$$

for $t > 0$ and the initial conditions $\boldsymbol{X}(0) = \boldsymbol{x}_0$, $\boldsymbol{V}(0) = \boldsymbol{0}$.

5.4 Theorem *The linearisation of above system is*

$$\ddot{\boldsymbol{d}}(t) = -\frac{e^2 n_e}{\varepsilon_0 m_e}\nabla(\mathcal{V}\boldsymbol{n})(\boldsymbol{x}_0)\,\boldsymbol{d}(t) = -\omega_p^2\,\nabla(\mathcal{V}\boldsymbol{n})(\boldsymbol{x}_0)\,\boldsymbol{d}(t),$$

with the initial displacement $\boldsymbol{d}(0) = \boldsymbol{d}_0 \in \mathbb{R}^3$ from the equilibrium position $\boldsymbol{x}_0 \in \Omega$ and velocity $\dot{\boldsymbol{d}}(0) = \boldsymbol{0}$. If the eigenvalues $\lambda_1, \lambda_2, \lambda_3$ of $\nabla(\mathcal{V}\boldsymbol{n})(\boldsymbol{x}_0)$ are positive, the plasma locally oscillates along three orthonormal directions with frequencies

$$\omega_i = \sqrt{\lambda_i}\omega_p, \quad i = 1, 2, 3.$$

Proof. We write

$$\boldsymbol{X}(t) = \boldsymbol{x}_0 + \boldsymbol{d}(t), \quad \boldsymbol{V}(t) = \dot{\boldsymbol{d}}(t),$$

and use the linearisation of the electric field $\boldsymbol{E}$ from (5.2),

$$\ddot{\boldsymbol{d}}(t) = \dot{\boldsymbol{V}}(t) = -\frac{e^2 n_e}{\varepsilon_0 m_e}\nabla(\mathcal{V}\boldsymbol{n})(\boldsymbol{x}_0)\,\boldsymbol{d}(t) = -\omega_p^2\,\nabla(\mathcal{V}\boldsymbol{n})(\boldsymbol{x}_0)\,\boldsymbol{d}(t). \tag{5.3}$$

From Lemma 5.2, we know that $\nabla(\mathcal{V}\boldsymbol{n})(\boldsymbol{x}_0)$ is symmetric. Therefore, there exists an orthonormal basis of eigenvectors $(\boldsymbol{b}_1, \boldsymbol{b}_2, \boldsymbol{b}_3)$ with corresponding eigenvalues $(\lambda_1, \lambda_2, \lambda_3)$, which are positive by assumption. In the eigenbasis, (5.3) is readily integrated,

$$\boldsymbol{d}(t) = \sum_{i=1}^{3} \boldsymbol{d}_0 \cdot \boldsymbol{b}_i \cos\left(\sqrt{\lambda_i}\omega_p\, t\right)\boldsymbol{b}_i, \quad t \geq 0,$$

which proves the last part of the theorem. ■

It is an open problem to characterise the sets Ω for which $\nabla(\mathcal{V}\boldsymbol{n})$ is positive definite in all points of the domain. By the following lemma, see e.g. [67, Lemma 4.2], this problem is equivalent to the concavity of the Newton potential.

5.5 Lemma *Let $\Omega \subseteq \mathbb{R}^3$ be open and bounded with Lipschitz boundary. Then the Newton potential*

$$w(\boldsymbol{x}) = (\mathcal{N}\mathbb{1}_\Omega)(\boldsymbol{x}) = \int_\Omega U(\boldsymbol{x}-\boldsymbol{y})\,d\boldsymbol{y}, \quad \boldsymbol{x} \in \Omega,$$

is twice continuously differentiable with Hessian

$$D^2 w(\boldsymbol{x}) = -\nabla(\mathcal{V}\boldsymbol{n})(\boldsymbol{x}), \quad \boldsymbol{x} \in \Omega.$$

The proof of Lemma 5.2 provides a second alternative expression for $\nabla(\mathcal{V}\boldsymbol{n})$.

5.6 Lemma *Let $\Omega \subseteq \mathbb{R}^3$ be open and bounded with Lipschitz boundary. For $\boldsymbol{x} \in \Omega$ and $\varepsilon > 0$ with $\overline{B}_\varepsilon(\boldsymbol{x}) \subseteq \Omega$,*

$$\nabla(\mathcal{V}\boldsymbol{n})(\boldsymbol{x}) = \frac{1}{3} I_3 - \int_{\Omega \setminus \overline{B}_\varepsilon(\boldsymbol{x})} D_{\boldsymbol{y}}^2 U(\boldsymbol{x}-\boldsymbol{y})\,d\boldsymbol{y}.$$

Little is known about the concavity of the Newton potential, i.e. under which conditions $\nabla(\mathcal{V}\boldsymbol{n})$ is positive (semi-) definite. If, however, Ω is close to a ball, we are able to prove local positive definiteness.

5.7 Lemma *Let $\Omega \subseteq \mathbb{R}^3$ be open and bounded with Lipschitz boundary. Suppose for a point $\boldsymbol{x} \in \Omega$ there holds*

$$\frac{|\Omega \setminus B_R(\boldsymbol{x})|}{|B_R(\boldsymbol{x})|} < \frac{1}{2},$$

where $R = \operatorname{dist}(\boldsymbol{x}, \partial\Omega)$ denotes the distance of $\boldsymbol{x}$ to the boundary. Then, $\nabla(\mathcal{V}\boldsymbol{n})$ is positive definite in a neighbourhood of $\boldsymbol{x}$.

5.8 Remark Visualised in two dimensions, the condition in Lemma 5.7 states that the shaded area in Fig. 5.1 must be smaller than half of the area of $B_R(\boldsymbol{x})$. It is related to the Fraenkel

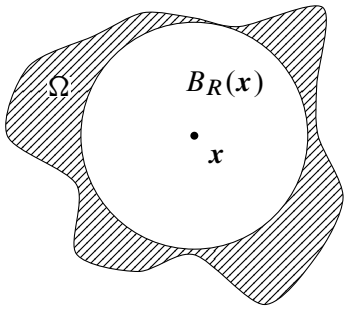

Figure 5.1.: Visualisation of the condition in Lemma 5.7.

asymmetry $\alpha(\Omega)$ of Ω [81, p. 99], frequently employed in potential theory [82] and for variants of the isoperimetric inequality [59],

$$\alpha(\Omega) = \inf_{\boldsymbol{y} \in \mathbb{R}^3} \frac{|\Omega \setminus B_\varrho(\boldsymbol{y})|}{|B_\varrho(\boldsymbol{y})|},$$

where $\varrho > 0$ is chosen such that $|\Omega| = |B_\varrho(\boldsymbol{0})|$. In general, $R < \varrho$, so our condition is more restrictive than the requirement $\alpha(\Omega) < 1/2$.

Proof of Lemma 5.7. The function $h(r) = |\Omega \setminus B_r(\boldsymbol{x})|/|B_r(\boldsymbol{x})|$, $r \in (0, R]$, is continuous and decreasing. By assumption, $h(R) < 1/2$, so by continuity there exits $r < R$ with $h(r) < 1/2$ and furthermore $\bar{B}_r(\boldsymbol{x}) \subseteq \Omega$ by the choice of R. Since $\nabla(\mathcal{V}\boldsymbol{n})(\boldsymbol{x})$ is symmetric by Lemma 5.2 its smallest eigenvalue equals

$$\inf_{\boldsymbol{e}\in S^2} \boldsymbol{e}^\top \nabla(\mathcal{V}\boldsymbol{n})(\boldsymbol{x})\boldsymbol{e}.$$

With Lemma 5.6 we have for all $\boldsymbol{e} \in S^2$,

$$\begin{aligned}
\boldsymbol{e}^\top \nabla(\mathcal{V}\boldsymbol{n})(\boldsymbol{x})\boldsymbol{e} &= \frac{1}{3} - \int_{\Omega\setminus\bar{B}_r(\boldsymbol{x})} \boldsymbol{e}^\top D_{\boldsymbol{y}}^2 U(\boldsymbol{x}-\boldsymbol{y})\boldsymbol{e}\,\mathrm{d}\boldsymbol{y} \\
&= \frac{1}{3} - \frac{1}{4\pi} \int_{\Omega\setminus\bar{B}_r(\boldsymbol{x})} \frac{1}{|\boldsymbol{x}-\boldsymbol{y}|^3} \left(3\left(\frac{\boldsymbol{x}-\boldsymbol{y}}{|\boldsymbol{x}-\boldsymbol{y}|}\cdot\boldsymbol{e}\right)^2 - 1\right) \mathrm{d}\boldsymbol{y} \\
&\geq \frac{1}{3} - \frac{2}{4\pi} \int_{\Omega\setminus\bar{B}_r(\boldsymbol{x})} \frac{1}{|\boldsymbol{x}-\boldsymbol{y}|^3}\,\mathrm{d}\boldsymbol{y},
\end{aligned}$$

where we have bounded the spherical polynomial $3(\boldsymbol{e}'\cdot\boldsymbol{e})^2 - 1$ for two unit vectors $\boldsymbol{e}', \boldsymbol{e}$ by its maximal value 2, attained for $\boldsymbol{e}' = \pm\boldsymbol{e}$. Owing to $\boldsymbol{y} \in \Omega \setminus \bar{B}_r(\boldsymbol{x})$ the integrand in the ultimate inequality is bounded by $1/r^3$, yielding

$$\boldsymbol{e}^\top \nabla(\mathcal{V}\boldsymbol{n})(\boldsymbol{x})\boldsymbol{e} \geq \frac{1}{3} - \frac{2}{3}\frac{3}{4\pi r^3}|\Omega \setminus \bar{B}_r(\boldsymbol{x})| = \frac{1}{3}\left(1 - 2\frac{|\Omega \setminus \bar{B}_r(\boldsymbol{x})|}{|\bar{B}_r(\boldsymbol{x})|}\right) > 0.$$

Since S^2 is compact,

$$\inf_{\boldsymbol{e}\in S^2} \boldsymbol{e}^\top \nabla(\mathcal{V}\boldsymbol{n})(\boldsymbol{x})\boldsymbol{e} > 0,$$

showing the the smallest eigenvalue is strictly positive. Because $\nabla(\mathcal{V}\boldsymbol{n})$ is continuous, the inequality remains strict in a neighbourhood of $\boldsymbol{x}$. ■

The example of a torus shows that the smallest eigenvalue may be negative in large parts of Ω. Figure 5.2 depicts the three eigenvalues in a section of a torus,

$$\{\boldsymbol{x} \in \mathbb{R}^3 : x_2 = 0, (x_1 - R)^2 + {x_3}^2 < r^2\},$$

with major radius $R = 1$ and minor radius $r = 1/5$. Since the torus is rotationally invariant around the x_3-axis, the three-dimensional distribution of the eigenvalues in the torus is given by rotating the two-dimensional distributions in Fig. 5.2 around the x_3-axis. We see that for $x_1 < 1$, the smallest eigenvalue is negative. In particular near $(4/5, 0)$, one eigenvalue is negative while the remaining two are positive, so the Newton potential is neither convex nor concave in a neighbourhood of this point.

More is known about the concavity of the related torsion function u, the unique solution of

$$\begin{cases} -\Delta u = 1 & \text{in } \Omega, \\ u = 0 & \text{on } \Gamma. \end{cases}$$

If Ω is convex, then $\sqrt{u}$ is concave [92]. Clearly, the concavity of u^α for $\alpha \geq 0$ implies that u^β is concave for all $\beta \leq \alpha$. If we set

$$\alpha^*(\Omega) = \sup\{\alpha \geq 0 : u^\alpha \text{ is concave}\},$$

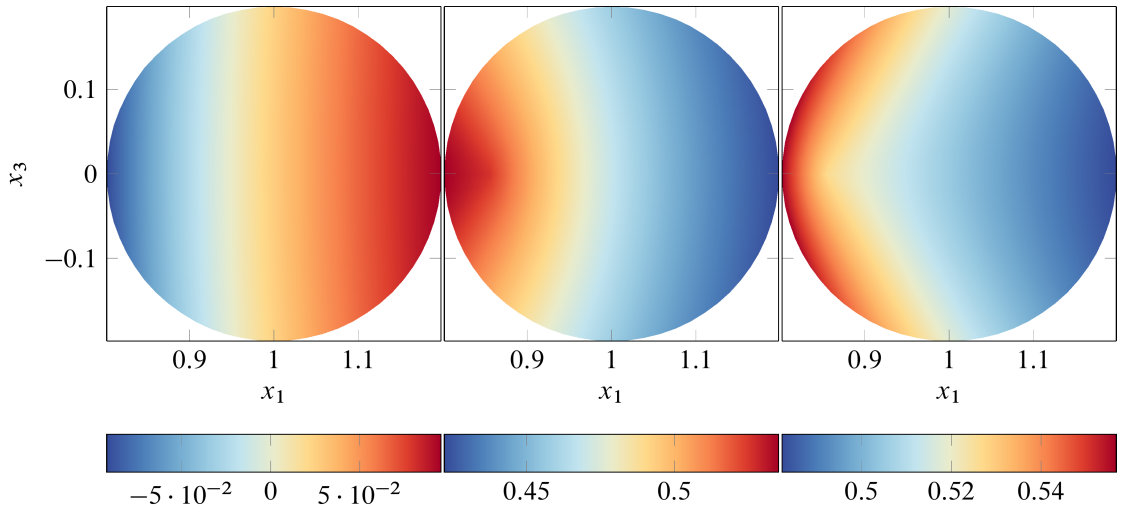

Figure 5.2.: Eigenvalues of $\nabla(\mathcal{V}\boldsymbol{n})$ in a section of the torus in ascending order from left to right.

then $1/2 \leq \alpha^*(\Omega) \leq 1$, where the lower bound cannot be improved and the upper bound is attained for ellipsoids [85]. Recently, Steinerberger [149] showed that u is concave, assuming the curvature of the boundary of the convex set Ω in two dimensions is sufficiently small. His proof, however, does not generalise to higher dimensions.

5.2. Analytical Results on Plasma Oscillation Eigenfrequencies

Usually, the frequency of the oscillation depends on the initial position and the direction of the initial displacement. But for a special set of geometries, $\nabla(\mathcal{V}\boldsymbol{n})$ is either constant or becomes constant in a limit case.

5.9 Example For a ball of radius $r_0 > 0$,

$$\Omega = \{\boldsymbol{x} \in \mathbb{R}^3 : |\boldsymbol{x}| < r_0\},$$

the matrix $\nabla(\mathcal{V}\boldsymbol{n})$ is constant and diagonal,

$$\nabla(\mathcal{V}\boldsymbol{n}) = \frac{1}{3} I_3.$$

To see this, we calculate for $\boldsymbol{x} \in \Omega$,

$$\begin{aligned}\mathcal{V}\boldsymbol{n}(\boldsymbol{x}) &= \frac{1}{4\pi} \int_{r_0 S^2} \frac{\boldsymbol{y}/r_0}{|\boldsymbol{x} - \boldsymbol{y}|} \,\mathrm{d}S_{\boldsymbol{y}} = \frac{r_0}{4\pi} \int_{S^2} \frac{\boldsymbol{y}}{|\boldsymbol{x}/r_0 - \boldsymbol{y}|} \,\mathrm{d}S_{\boldsymbol{y}} \\ &= \frac{r_0}{2} \int_{-1}^{1} \frac{\zeta \boldsymbol{x}/|\boldsymbol{x}|}{\sqrt{|\boldsymbol{x}|^2/r_0^2 + 1 - 2|\boldsymbol{x}|/r_0 \zeta}} \,\mathrm{d}\zeta = \frac{r_0}{2} \frac{2|\boldsymbol{x}|}{3r_0} \frac{\boldsymbol{x}}{|\boldsymbol{x}|} = \frac{1}{3}\boldsymbol{x}.\end{aligned}$$

A ball of radius r_0 therefore oscillates with a frequency of $\omega_p/\sqrt{3}$, see [48, Eq. (3.8)].

For most geometries, analytically computing $\nabla(\mathcal{V}\boldsymbol{n})$ is not possible. But with the tools we have at our disposal from Boundary Element Methods, we can numerically compute $\nabla(\mathcal{V}\boldsymbol{n})$

and thus the frequencies once we have discretised the boundary. To that end, we interpret the evaluation of $\nabla(\mathcal{V}\boldsymbol{n})$ as the gradient of the representation formula (3.13) with specific densities,

$$\boldsymbol{u} = \mathcal{V}\boldsymbol{n} = \mathcal{V}\boldsymbol{n} - \mathcal{W}\boldsymbol{0}.$$

If Γ is a Lipschitz polyhedron, then $\boldsymbol{n} \in S_h^0(\Gamma)$ and $\boldsymbol{0} \in S_h^1(\Gamma)$ for every triangulation $(\mathcal{T}_h)_h$ since the normal vector is constant on every triangle of a given mesh. Hence,

$$\nabla(\mathcal{V}\boldsymbol{n})(\boldsymbol{x}) = \sum_{T\in\mathcal{T}_h} \int_T \nabla_{\boldsymbol{x}} U(\boldsymbol{x}-\boldsymbol{y})\boldsymbol{n}_T^\top \,\mathrm{d}S_{\boldsymbol{y}}$$

for $\boldsymbol{x} \in \Omega$. The integrals over the individual triangles can be calculated in closed form by means of double-layer potential and one-dimensional integrals over the edges of the triangles [77].

5.10 Example We place a cylinder of height 10 and diameter 1 parallel to the x_3-axis and discretise its surface with 76 000 triangles. The matrix $\nabla(\mathcal{V}\boldsymbol{n})$ is then evaluated at equidistant points in the plane

$$\{\boldsymbol{x} \in \mathbb{R}^3 : x_2 = 0\}.$$

Figure 5.3 shows the eigenvalues as a function of x_1 and x_3. In the homogeneous part in the middle of the cylinder two eigenvalues close to $1/2$, while the third one is about two magnitudes smaller. Near the corners the smallest eigenvalue is negative as depicted in Fig. 5.4.

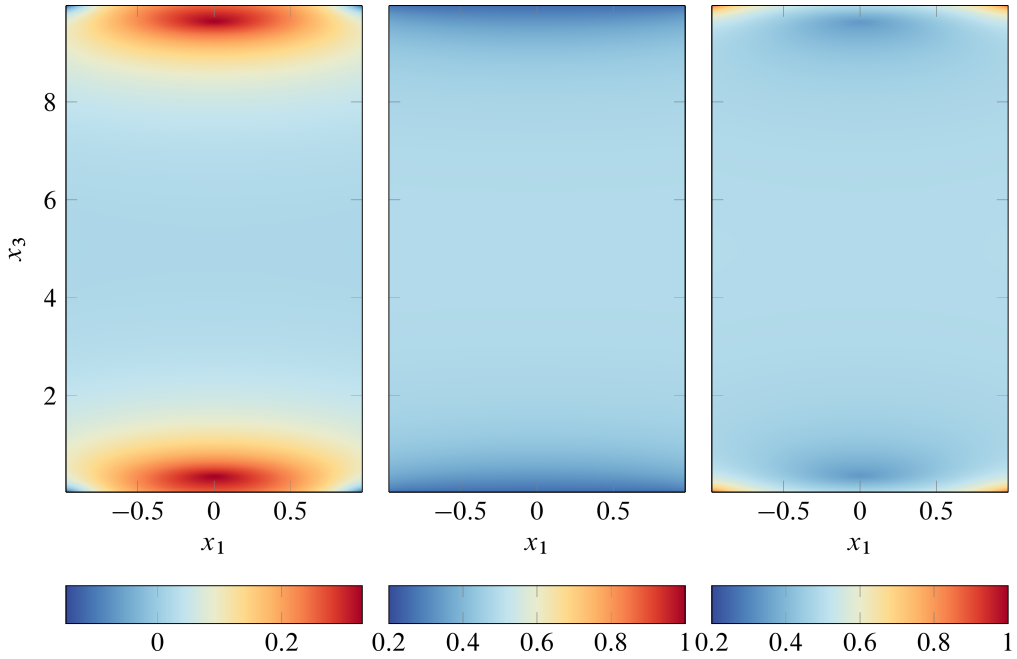

Figure 5.3.: Eigenvalues of $\nabla(\mathcal{V}\boldsymbol{n})$ in a section of a cylinder parallel to the x_3-axis in ascending order from left to right.

For our last example, we calculate the frequencies of an oscillating ellipsoid. The results for the previously examined geometries are recovered in certain limits.

5.11 Example Let

$$\Omega = \left\{\boldsymbol{x} \in \mathbb{R}^3 : \frac{x_1^2}{a^2} + \frac{x_2^2}{b^2} + \frac{x_3^2}{c^2} < 1\right\}$$

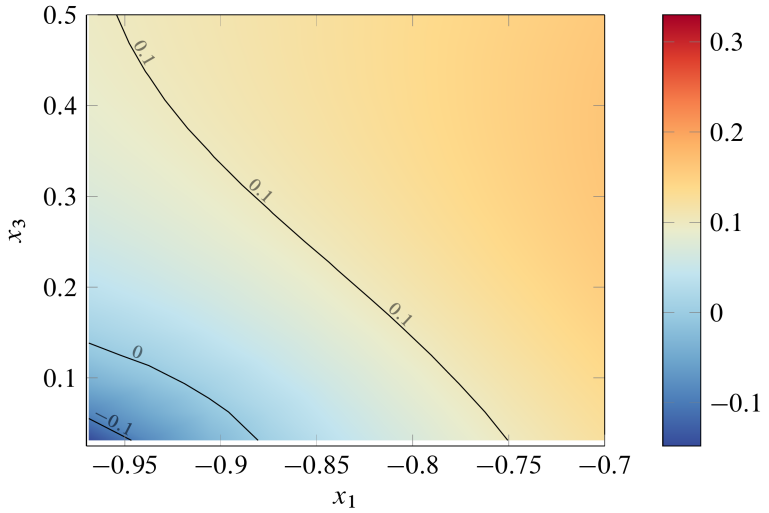

Figure 5.4.: Smallest eigenvalue of $\nabla(\mathcal{V}\boldsymbol{n})$ near the corner of a cylinder.

be an ellipsoid with semiaxes $0 < a \leq b \leq c$. As first observed by Dirichlet, see [46] for a modern exposition his argument and Bucerius [25] for a rigorous justification of his method, the potential inside Ω is given by

$$w(\boldsymbol{x}) = \frac{1}{4}abc \int_0^\infty \left(1 - \frac{x_1^2}{a^2+s} - \frac{x_2^2}{b^2+s} - \frac{x_3^2}{c^2+s}\right) \frac{1}{\sqrt{(a^2+s)(b^2+s)(c^2+s)}}\,\mathrm{d}s,$$

where $\boldsymbol{x} \in \Omega$. In view of Lemma 5.5, we see that $\nabla(\mathcal{V}\boldsymbol{n})$ is a constant diagonal matrix with entries

$$\lambda_\ell = \frac{1}{2}abc \int_0^\infty \frac{1}{\ell^2+s} \frac{1}{\sqrt{(a^2+s)(b^2+s)(c^2+s)}}\,\mathrm{d}s, \quad \ell \in \{a,b,c\}.$$

The integrals are evaluated in detail in Appendix A. In the following, we summarise the results. The triaxial case $0 < a < b < c$ gives

$$\lambda_a = \frac{1}{b^2-a^2}\left(b^2 - \frac{abc}{\sqrt{c^2-a^2}}\mathrm{E}(\vartheta,\nu)\right),$$

$$\lambda_b = \frac{1}{b^2-a^2}\left(\frac{abc}{\sqrt{c^2-a^2}}\left\{\frac{c^2-a^2}{c^2-b^2}\mathrm{E}(\vartheta,\nu) - \frac{b^2-a^2}{c^2-b^2}\mathrm{F}(\vartheta,\nu)\right\} - a^2\right),$$

$$\lambda_c = \frac{1}{b^2-a^2}\frac{b^2-a^2}{c^2-b^2}\frac{abc}{\sqrt{c^2-a^2}}\Big(\mathrm{F}(\vartheta,\nu) - \mathrm{E}(\vartheta,\nu)\Big),$$

where

$$\vartheta = \arcsin\frac{\sqrt{c^2-a^2}}{c}, \quad \nu = \sqrt{\frac{c^2-b^2}{c^2-a^2}},$$

and F and E denote the elliptic integrals of first and second kind, respectively,

$$\mathrm{F}(\varphi, k) = \int_0^\varphi \frac{1}{\sqrt{1 - k^2 \sin^2 \alpha}} \,\mathrm{d}\alpha,$$
$$\mathrm{E}(\varphi, k) = \int_0^\varphi \sqrt{1 - k^2 \sin^2 \alpha} \,\mathrm{d}\alpha.$$

The formulas for the eigenvalues simplify if two semiaxes have equal length. For an oblate ellipsoid of revolution, $a < b = c$,

$$\lambda_a = \frac{1}{1 - a^2/c^2} \left(1 - \frac{a/c}{\sqrt{1 - a^2/c^2}} \operatorname{arccot} \frac{a/c}{\sqrt{1 - a^2/c^2}} \right),$$
$$\lambda_c = \frac{1}{2(1 - a^2/c^2)} \left(\frac{a/c}{\sqrt{1 - a^2/c^2}} \operatorname{arccot} \frac{a/c}{\sqrt{1 - a^2/c^2}} - \frac{a^2}{c^2} \right).$$

The eigenvalues are depicted in Fig. 5.5 as a function of a/c. With above eigenvalues, we can

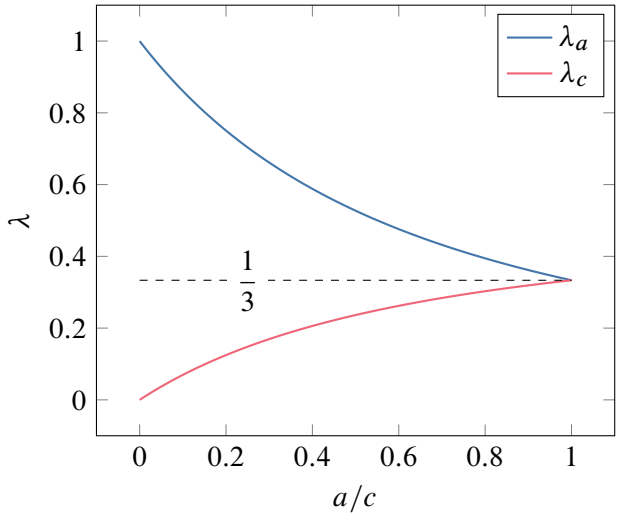

Figure 5.5.: Eigenvalues of $\nabla(\mathcal{V}\boldsymbol{n})$ for an oblate ellipsoid of revolution with semidiameters $a < c$ as a function of a/c.

rigorously derive the classical result of Tonks and Langmuir [156] from the beginning of this chapter. Suppose that we prepare a plasma in a spherical shape with radius $r_0 > 0$. By squeezing the plasma in one direction, for instance by an electromagnetic field, its shape changes to an oblate ellipsoid of revolution with semiaxes $a < c$. Since the volume of the plasma is constant in this transformation, we have $a = \sigma r_0$, $c = \sigma^{-1/2} r_0$ with $\sigma \in (0, 1)$. This means that $a/c = \sigma^{3/2}$ tends to 0 for $\sigma \to 0$. In the limit $\sigma \to 0$ the plasma fills a plane in $\mathbb{R}^3$. Thus, we can treat the plasma as one-dimensional system since it is translation invariant on the two-dimensional plane. Computing the eigenvalues in the limit $\sigma \to 0$, we see

$$\lim_{\sigma \to 0} (\lambda_a, \lambda_c, \lambda_c) = (1, 0, 0),$$

so by Theorem 5.4, the plasma oscillates with angular frequency ω_p.

In case of a prolate ellipsoid of revolution, $a = b < c$, we obtain

$$\begin{aligned} \lambda_a &= \frac{1}{2(1-a^2/c^2)} \left(1 - \frac{a^2/c^2}{\sqrt{1-a^2/c^2}} \operatorname{acoth} \frac{1}{\sqrt{1-a^2/c^2}} \right), \\ \lambda_c &= \frac{1}{1-a^2/c^2} \left(\frac{a^2/c^2}{\sqrt{1-a^2/c^2}} \operatorname{acoth} \frac{1}{\sqrt{1-a^2/c^2}} - \frac{a^2}{c^2} \right), \end{aligned} \tag{5.4}$$

see Fig. 5.6 for the eigenvalues as a function of a/c. Similar to the discussion on the oblate

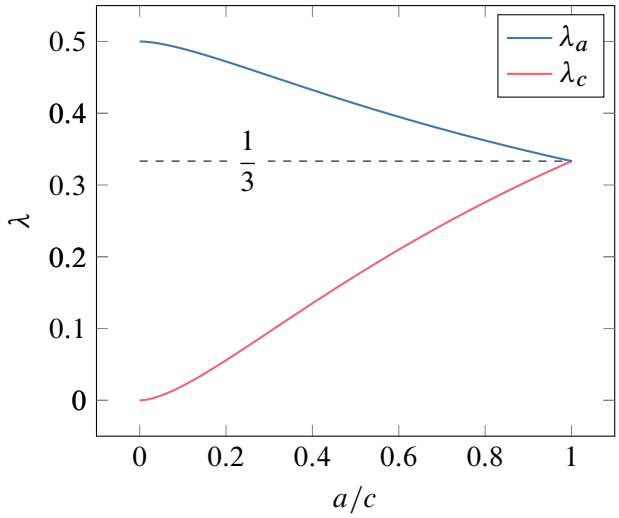

Figure 5.6.: Eigenvalues of $\nabla(\mathcal{V}\boldsymbol{n})$ for a prolate ellipsoid of revolution with semidiameters $a < c$ as a function of a/c.

ellipsoid of revolution, we use this result for the explanation of a previous example. Again, we consider a ball plasma with radius r_0. When we stretch it in one direction, the ball becomes a prolate ellipsoid of revolution with semidiameters $a < c$. With the same argument as before, we have $a = \sigma^{1/2} r_0$ and $c = \sigma^{-1} r_0$ and thus $a/c = \sigma^{3/2}$ tends to 0 when $\sigma \to 0$. Eventually, the ball degenerates to a line in $\mathbb{R}^3$. We have reduced the degrees of freedom of the plasma by one. Furthermore,

$$\lim_{\sigma \to 0} (\lambda_a, \lambda_a, \lambda_c) = \left(\frac{1}{2}, \frac{1}{2}, 0 \right),$$

explaining our observation in Example 5.10, where we numerically computed the eigenvalues for a long cylinder and saw that they approach $(1/2, 1/2, 0)$ in the centre. By Theorem 5.4 the thin wire (or equivalently the infinite cylinder) oscillates with angular frequency $\omega_p/\sqrt{2}$ perpendicular to its symmetry axis. Baldwin and Ignat [4] obtained the same result in their study of resonances in an idealised plasma column of infinite height.

6. Numerical Examples

> Mein Zahlengedächtnis, sonst erträglich fix, behält die Zahl der Biergläser stets schlecht.[1]
>
> *(Ludwig Boltzmann [14])*

In Section 3.5 we have seen how to compute the self-consistent electric field of a plasma by discretisation of the boundary only. The approximation error of the electric field is $\mathcal{O}(h^2)$, in particular close to the boundary. The computational complexity, however, scales quadratically with the number of triangles and the number of particles. It can be drastically reduced by using hierarchical approximations. Albeit they introduce a further approximation error, this error is known to decay exponentially with the interpolation order, see Lemma 4.10. Thus, it usually does not interfere with the BEM error for small- to mid-sized problems and with a mild (logarithmic) increase of the interpolation order for larger degrees of freedom we are able to retain the optimal convergence order. For the practical realisation of $\mathcal{H}^2$-matrices we use the software library `H2Lib`.[2]

In the following, we validate the theoretical predictions for plasma oscillations from Chapter 5. Since we consider a plasma in free space, the BEM discretisation reduces to the computation of the Newton potential. This allows us analyse the influence of the hierarchical approximation on the inter-particle forces. As the following results show, we obtain excellent agreement with the analytically computed frequencies in Section 5.2.

The assembly of and operations on $\mathcal{H}^2$-matrices such as the matrix-vector product require to traverse the associated block cluster tree. This can be parallelised by threads in combination with an enumeration of the block cluster tree on a shared memory system [102] or by the Message-Passing Interface [75, 74] on distributed memory systems [90]. Börm and Bendoraityte [16] propose an algorithm for the efficient computation of the $\mathcal{H}^2$-matrix-vector product on distributed memory systems and prove its optimal scaling with the number of threads. For our implementation on shared memory system we use `OpenMP`'s `task` directive, specifically designed for nonstructured parallelism [130, Chapter 3]. In contrast to approaches cited above where the execution order is determined at compile time, the use of `OpenMP task` leaves the execution order to the `OpenMP` runtime. This allows for a greater flexibility (and only minimal changes in the source code of a serial implementation) but may result in less performant code compared to a finely grained, hand-written load balancing.

With the approximation of the electric field $\boldsymbol{E}_h$, the ith macroparticle evolves (in the absence of boundaries) according to

$$\begin{aligned} \dot{\boldsymbol{x}}_i &= \boldsymbol{v}_i, \\ \dot{\boldsymbol{v}}_i &= \frac{q_i}{m_i} \boldsymbol{E}_h[\boldsymbol{x}_1, \dots, \boldsymbol{x}_{n_p}](\boldsymbol{x}_i), \end{aligned}$$

[1] "My memory for numbers, otherwise reliable, always retains the number of beer glasses poorly."
[2] `http://h2lib.org/`

where the notation $\boldsymbol{E}_h[\dots]$ emphasises that the electric field also depends on the position of all macroparticles at a given time. Above system of ordinary differential equations is numerically integrated by so-called symplectic methods [80]. They discretely conserve linear first integrals[3] such as the total momentum but in general do not conserve quadratic first integrals. Rather, the numerical value oscillates around the initial value with an amplitude that decays algebraically with the time step size on exponentially large time intervals [80, Theorem 8.1, Chapter IX.8]. Additionally, a discrete version of Liouville's theorem for volume-preserving flows [3, Section 16] holds. For symplectic Runge–Kutta methods with at most two stages the associated numerical flow is volume-preserving [80, Theorem 9.4, Chapter VI.9]. The Störmer–Verlet method that we use for our computations is a one-stage Runge–Kutta method. For a discretisation of the time interval with step size Δt the state $(\boldsymbol{x}_i{}^k, \boldsymbol{v}_i{}^k)$ of the ith macroparticle at step $k \in \mathbb{N}$ is updated according to

$$\boldsymbol{v}_i{}^{k+1/2} \leftarrow \boldsymbol{v}_i{}^k + \frac{\Delta t}{2}\frac{q_i}{m_i}\boldsymbol{E}_h\big[\boldsymbol{x}_1{}^k, \dots, \boldsymbol{x}_{n_p}{}^k\big](\boldsymbol{x}_i{}^k), \tag{6.1a}$$

$$\boldsymbol{x}_i{}^{k+1} \leftarrow \boldsymbol{x}_i{}^k + \Delta t\, \boldsymbol{v}_i{}^{k+1/2}, \tag{6.1b}$$

$$\boldsymbol{v}_i{}^{k+1} \leftarrow \boldsymbol{v}_i{}^{k+1/2} + \frac{\Delta t}{2}\frac{q_i}{m_i}\boldsymbol{E}_h\big[\boldsymbol{x}_1{}^{k+1}, \dots, \boldsymbol{x}_{n_p}{}^{k+1}\big](\boldsymbol{x}_i{}^{k+1}). \tag{6.1c}$$

Like the continuous equations the discrete system is time-reversible: Running the simulation for k time steps with step size Δt and then again k steps with $-\Delta t$ yields (assuming exact arithmetic) the initial condition. Therefore, odd orders of Δt in the analysis of the truncation error cancel and we obtain a second-order accurate method. In total, the discretisation error is $\mathcal{O}\big((\Delta t)^2 + h^2\big)$.

Even though the electric field appears twice in the formulation of the Störmer–Verlet method it needs to be computed only once per time step. The field at the positions at end of step k in (6.1c) is equal to the field in (6.1a) for the next step $\widetilde{k} = k + 1$. It is only in the first time step that we also have to compute the electric field twice. As pointed out by Feynman in his famous "lost lecture", the idea of Störmer–Verlet method was already used by Newton in his geometric proof of Kepler's second law [68, pp. 84 ff.].

In the presence of boundaries (6.1b) has to be modified. First, we check if the ray starting at $\boldsymbol{x}_i{}^k$ with direction $\boldsymbol{v}_i{}^{k+1/2}$ intersects the boundary in the parameter interval $[0, \Delta t]$. This is a classic problem in computational geometry, see [124, Chapter 7]. If the particle does not reach the boundary within the time Δt, we update its position according to (6.1b). Otherwise, we move the particle until the first time of intersection with the boundary and apply the boundary condition. The remaining time reduces to a fractional of Δt. We then iterate above algorithm until the remaining time is zero. The ray-boundary intersection can be computed in sublinear time by exploiting the cluster tree of the boundary triangles we build for the hierarchical approximation of the BEM matrices. Here, we first check if the ray intersects the hierarchical structured boundary boxes [165]. Only at the leafs of the tree we actually compute the interaction with a small number of triangles [118]. Thus, the computational cost is reduced from $\mathcal{O}(n_h)$ to $\mathcal{O}(r \operatorname{depth} T_h)$, where n_h denotes the number of surfaces triangles and T_h is their cluster tree with at most r triangles in each leaf. For a regular triangulation of the boundary, the depth of the cluster tree depends logarithmically on n_h [7, pp. 36 ff.], so we obtain a complexity of $\mathcal{O}(r \log n_h)$.

[3] A first integral is a conserved quantity that only involves the positions and velocities but not their derivatives [144, p. 93].

6.1. Plasma Oscillations in Free Space

To be able to observe oscillations we need two components in our plasma with opposite charges. In the following simulations, one half of the n_p particles represent electrons, the other half ions. Since we assume the ions to be immobile on our typical time scale, we choose $q_i = 1$ and $m_i = 10^{10}$ for the charge and mass of ions relative to the electron charge and mass, respectively. The first challenge we have to tackle is the preparation of an admissible initial state before we are able to observe oscillations. In contrast to the continuum model, where the resulting electric field equals zero if the number densities of the electrons and the ions coincide, the finite samples of the initial condition generate a nonvanishing electric field. Therefore, the initial configuration is not in equilibrium, so that our results for the linearisation of the forces do not apply. Displacing the electrons will not result in a stable oscillation. By the rapid change of acceleration in the first time step, electrons close to the boundary gain large momentum and escape the attractive potential of the ions. To mitigate this issue, we prepare an admissible initial state similar to the treatment of a real plasma in a laboratory.

At first, we add an external field with potential

$$\phi_{\text{trap}}(t, \boldsymbol{x}) = -\frac{1}{2}\Xi_{\text{trap}}(t)|\boldsymbol{x}|^2, \quad t > 0,\ \boldsymbol{x} \in \mathbb{R}^3,$$

called trap potential with amplitude Ξ_{trap}. Depending on its strength, the trap confines the electrons in a sphere not larger than the unit sphere. Since the additional potential adds energy to our system, we have to add a cooling mechanism. In a laboratory, this is usually done via laser cooling, see the recent publications [2, 107] and the reviews [28, 49]. A simple model is a quadratic friction force,

$$\boldsymbol{F}_{\text{fric}}(t, \boldsymbol{v}) = -\kappa(t)|\boldsymbol{v}|\boldsymbol{v}, \quad t > 0,\ \boldsymbol{v} \in \mathbb{R}^3.$$

Here, κ is a nonnegative function describing the strength of the cooling. In total, the modified equations of motion for the particles in nondimensional form read

$$\begin{aligned}
\dot{\boldsymbol{x}}_i(t) &= \boldsymbol{v}_i(t),\\
\dot{\boldsymbol{v}}_i(t) &= -\frac{L_0^2}{\lambda_D^2}\frac{1}{n/2}\sum_{\substack{j=1\\ j\neq i}}^{n_p}\frac{q_i q_j}{m_i}\nabla_{\boldsymbol{x}_i} U_\sigma(\boldsymbol{x}_i(t) - \boldsymbol{x}_j(t))\\
&\qquad - \frac{q_i}{m_i}\nabla_{\boldsymbol{x}}\phi_{\text{trap}}(t, \boldsymbol{x}_i(t)) + \frac{1}{m_i}\boldsymbol{F}_{\text{fric}}(t, \boldsymbol{v}_i(t)),
\end{aligned}$$

for $t > 0$ and $i = 1, \ldots, n_p$. The regularisation parameter σ is chosen equal to ${n_p}^{-1/3}$ and U_σ is given by (2.13),

$$U_\sigma(\boldsymbol{x}) = \frac{1}{4\pi}\begin{cases}\dfrac{3}{2\sigma} - \dfrac{|\boldsymbol{x}|^2}{2\sigma^3}, & |\boldsymbol{x}| \le \sigma,\\[2ex] \dfrac{1}{|\boldsymbol{x}|}, & \text{else,}\end{cases} \qquad \boldsymbol{x} \in \mathbb{R}^3.$$

In actual computations, the sum over the regularised fundamental solution is replaced by the hierarchical approximation reviewed in Chapter 4 which permits a rapid evaluation in linear rather than quadratic complexity.

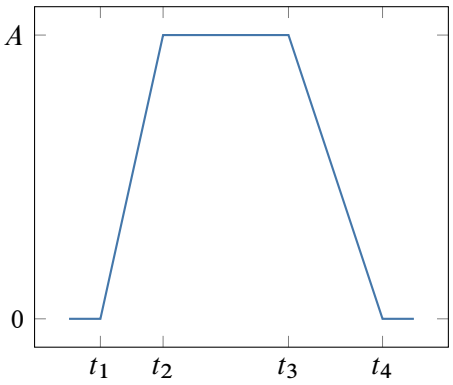

	Ξ_{trap}	κ	Ξ_{exc}
A	5	1	−25
$t_1/\Delta t$	0	0	450
$t_2/\Delta t$	0	0	452
$t_3/\Delta t$	300	300	453
$t_4/\Delta t$	400	400	455

Figure 6.1.: Continuous piecewise linear ramp profile. The table on the right shows the parameters used for the simulation.

After a given time, we remove the trap and the cooling. The charges are then separated by a shortly applied homogeneous external electric field $\boldsymbol{E}_{\text{exc}}$,

$$\boldsymbol{E}_{\text{exc}}(t, \boldsymbol{x}) = \Xi_{\text{exc}}(t) \begin{pmatrix} 1 \\ 0 \\ 0 \end{pmatrix}, \quad t > 0,\ \boldsymbol{x} \in \mathbb{R}^3.$$

The amplitude of the oscillation decreases exponentially due to Landau damping [31, Section 7.4] and was also observed by Dubin [47] in his numerical study of plasma oscillations.

In our simulation, Ξ_{trap}, κ and Ξ_{exc} follow a simple ramp profile, see Fig. 6.1 for the sketch of a sample graph and the parameters used for the subsequent computations. Furthermore, we fix

$$L_0 = 0.1\,\text{m}, \quad m_0 = m_e, \quad q_0 = e,$$

and vary the characteristic number density n_0 and temperature T_0. We recall that the characteristic time scale t_0 depends on T_0,

$$t_0 = \frac{L_0}{V_0} = L_0 \sqrt{\frac{m_0}{k_B T_0}}. \tag{6.2}$$

For the discretisation parameters, we choose

$$n_p = 1 \times 10^5, \quad \Delta t = 1 \times 10^{-2}$$

and compute 1×10^3 time steps. Figure 6.2 shows the course of the electrons' centre of mass $\boldsymbol{C}$ for $n_0 = 2 \times 10^{14}\,\text{m}^{-3}$, $k_B T_0 = 30\,\text{eV}$. and the energy spectrum of the first component, i.e. the squared modulus of the coefficients of the discrete Fourier transform. To avoid a linear growth of $\boldsymbol{C}$ due to single electrons escaping the potential barrier of ϕ_{trap} at the beginning, we only consider electrons inside a ball of radius 2 for the calculation of the centre of mass. The dominant frequency is found by fitting the function

$$\nu \mapsto a\big(\text{Vp}(\delta, \varepsilon; \nu - \mu) + \text{Vp}(\delta, \varepsilon; \nu + \mu)\big) \tag{6.3}$$

on the energy spectrum with respect to the amplitude a, the width parameters δ and ε and the position of the peak μ. Here, Vp denotes the Voigt profile, first derived by Voigt in 1912 for the

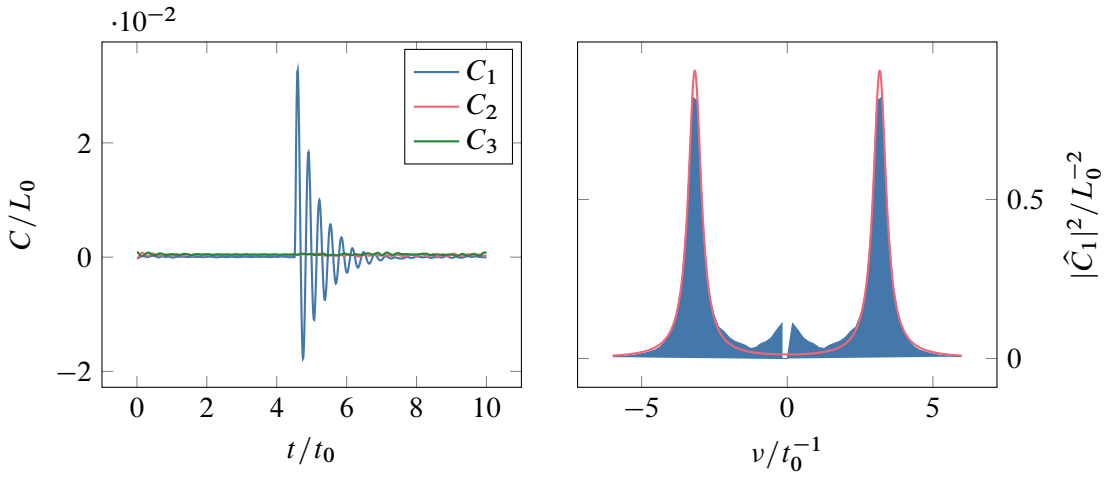

Figure 6.2.: Time evolution of the electrons' centre of mass $\boldsymbol{C}$ (left panel) and energy spectrum of C_1 (right panel) with fit (6.3) for $k_B T_0 = 30\,\mathrm{eV}$ and $n_0 = 2 \times 10^{14}\,\mathrm{m}^{-3}$. The parameters are $a = 0.763$, $\delta = 0.269$, $\varepsilon = 0.0001$ and $\mu = 3.174$. In the energy spectrum, the coefficient of the constant mode is set to zero.

intensity distribution of line spectra in gases [162]. For parameters $\delta, \varepsilon > 0$, $\mathrm{Vp}(\delta, \varepsilon; \cdot)$ is the convolution of a Cauchy–Lorentz distribution with parameter δ,

$$\nu \mapsto \frac{1}{\pi\delta} \frac{1}{1 + (\nu/\delta)^2}$$

and a normal distribution with zero mean and standard deviation ε.

Results on Temperature Dependency

According to our theoretical results in Section 5.1, the oscillation frequency should only depend on n_0 but not on T_0. To investigate the temperature dependency, we fix a number density of $n_0 = 2 \times 10^{14}\,\mathrm{m}^{-3}$ and vary $k_B T_0$ in a range from 2.5 eV to 40 eV. The resulting frequencies, together with the theoretical prediction, are depicted in Fig. 6.3. For our particular choice of parameters, the numerical value of plasma frequency is

$$\omega_p = \sqrt{\frac{n_0 q_0^2}{\varepsilon_0 m_0}} = 7.978 \times 10^8\,\mathrm{Hz}.$$

The characteristic time scale for $k_B T_0 = 1\,\mathrm{eV}$ evaluates to

$$t_0 = 2.384 \times 10^{-7}\,\mathrm{s},$$

so that for the nondimensional frequency[4] of the unit ball,

$$\frac{1}{2\pi} t_0 \frac{\omega_p}{\sqrt{3}} = 17.481.$$

[4]The plasma frequency is the *angular* frequency of the oscillation, so we have to divide by 2π in order to obtain the frequency, i.e. the inverse of a period.

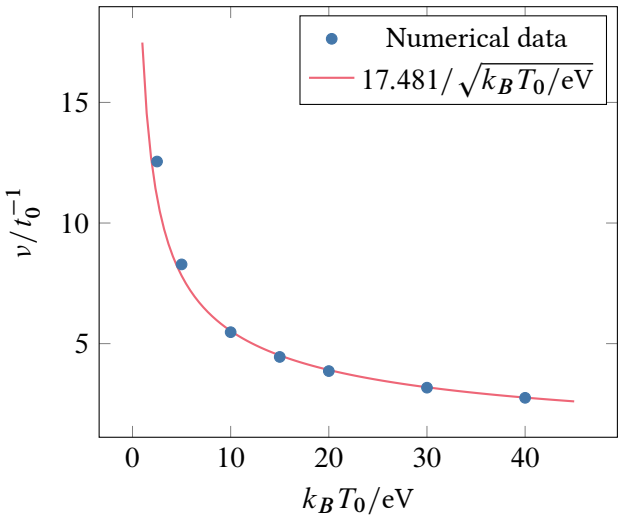

Figure 6.3.: Dominating frequency in the energy spectrum of the electrons' centre of mass for fixed number density $n_0 = 2 \times 10^{14}\,\mathrm{m}^{-3}$ and varying temperature T_0. The relative error in the first data point is 11 % and 6 % for the second. For the remainig frequencies, the relative error is below 1 %.

Since t_0 scales as $T_0^{-1/2}$, cf. (6.2), we have

$$\frac{1}{2\pi} t_0 \frac{\omega_p}{\sqrt{3}} = 17.481 \Big/ \sqrt{\frac{k_B T_0}{\mathrm{eV}}} \tag{6.4}$$

for a general characteristic temperature T_0. Therefore, the nondimensional plasma frequency depends on T_0, which is reflected in the numerical values for the frequencies in Fig. 6.3. Except for the first two frequencies where the temporal resolution dominates the error, our results are in very good agreement with the theoretical result (6.4).

Results on Number Density Dependency

Lastly, we fix $k_B T_0 = 20\,\mathrm{eV}$ and vary the number density n_0. From the definition of the plasma frequency (5.1), it follows

$$\frac{1}{2\pi} t_0 \frac{\omega_p}{\sqrt{3}} = 0.276 \sqrt{\frac{n_0}{1 \times 10^{12}\,\mathrm{m}^{-3}}}.$$

As before, the dominating frequency of the oscillation is extracted from the power spectrum of the electrons' centre of mass by fitting the Voigt profile (6.3). The results are displayed in Fig. 6.4 together with the theoretical prediction. With relative errors below 1 %, the numerically obtained frequencies match very well with theory.

Extension to General Domains

The procedure for exciting plasma oscillations does not change in principle when we treat nonspherical geometries Ω; we still add a trap potential, cool the particles and apply a short electric pulse to separate the different charges. The trap potential is adjusted according to

$$\phi_{\mathrm{trap}}(t, \boldsymbol{x}) = -\frac{1}{2} \Xi_{\mathrm{trap}}(t) \sum_{i=1}^{3} \frac{x_i^2}{\zeta_i^2}, \quad t > 0,\ \boldsymbol{x} \in \mathbb{R}^3,$$

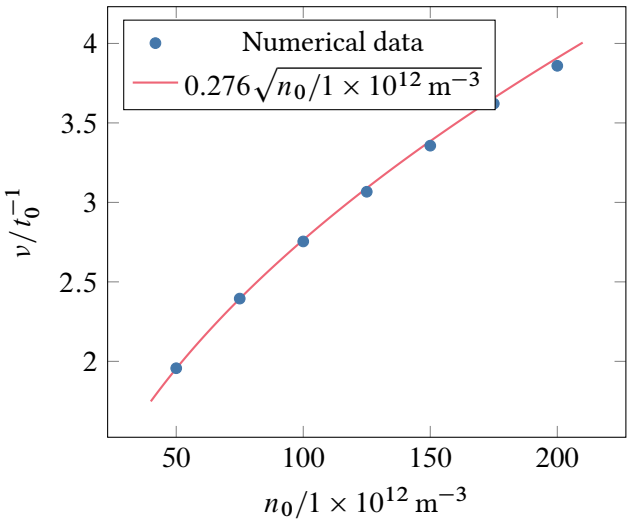

Figure 6.4.: Dominating frequency in the power spectrum of the electrons' centre of mass for fixed temperature $k_B T_0 = 20\,\mathrm{eV}$ and varying number density n_0. The relative error increases with n_0 and is 0.1 % for the left and 1.1 % for the right data point.

where $\boldsymbol{\zeta} = (\zeta_1, \zeta_2, \zeta_3)^\top \in \mathbb{R}^3$ measures the extent of Ω along the coordinate axes. For an axis-aligned ellipsoid, a possible choice for $\boldsymbol{\zeta}$ are its semidiameters. As an example, we analyse the frequencies of an ellipsoid with semidiameters $(2, 1, 1)$,

$$\Omega = \left\{ \boldsymbol{x} \in \mathbb{R}^3 : (x_1/2)^2 + x_2^2 + x_3^2 < 1 \right\}.$$

From Example 5.11 we know that the main axes of the oscillation are the coordinate axes with eigenvalues that depend nonlinearly on the quotient of the semidiameters. In our case, the two smaller semidiameters are equal. Therefore, the spectrum consists of two distinct eigenvalues, see (5.4),

$$\lambda_1 = \frac{1}{1-r^2}\left(\frac{r^2}{\sqrt{1-r^2}}\operatorname{acoth}\frac{1}{\sqrt{1-r^2}} - r^2\right) \approx 0.174,$$
$$\lambda_2 = \frac{1}{2(1-r^2)}\left(1 - \frac{r^2}{\sqrt{1-r^2}}\operatorname{acoth}\frac{1}{\sqrt{1-r^2}}\right) \approx 0.413,$$

where λ_1, λ_2 correspond to an oscillation along larger, respectively, smaller axis of the ellipsoid, and $r = 1/2$ is the quotient of the semidiameters. With Theorem 5.4, we conclude that the angular frequencies of the oscillation are

$$\omega_1 = \sqrt{\lambda_1}\omega_p, \quad \omega_2 = \sqrt{\lambda_2}\omega_p.$$

Expressed in nondimensional units for $n_0 = 1 \times 10^{14}\,\mathrm{m}^{-3}$, $k_B T_0 = 20\,\mathrm{eV}$,

$$\frac{1}{2\pi} t_0 \omega_1 \approx 1.994, \quad \frac{1}{2\pi} t_0 \omega_2 \approx 3.077.$$

From the simulation data depicted in Fig. 6.5, we obtain by fitting the Voigt profile (6.3) on the power spectrum,

$$\nu_1 = 1.996, \quad \nu_2 = 3.088,$$

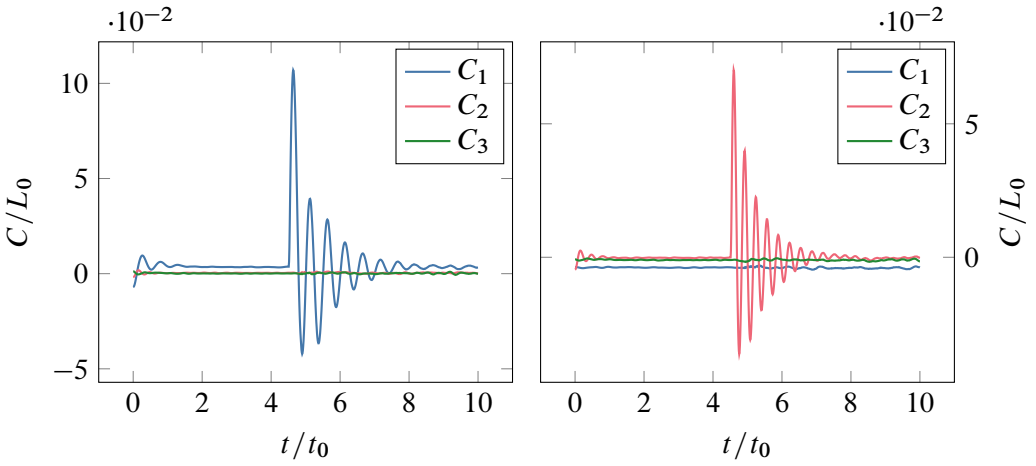

Figure 6.5.: Time evolution of the electrons' centre of mass for an axis-parallel ellipsoidal with semidiameters $(2, 1, 1)$ after an excitation along the major axis (left panel) and a minor axis (right panel). Relevant characteristic quantities are $k_B T_0 = 20\,\mathrm{eV}$ and $n_0 = 1 \times 10^{14}\,\mathrm{m}^{-3}$.

as numerical frequencies. The relative error is 6.0×10^{-4} for the first and 3.3×10^{-3} for the second frequency. Choosing a larger regularisation parameter, for instance $\sigma = 2{n_p}^{-1/3}$, hardly affects the obtained results. The 99.994 % confidence interval[5] for the frequency μ of the oscillation along the short axis, obtained by the nonlinear regression of Voigt profile for reads

$$[2.9713, 3.1253]$$

and almost agrees with that for the original choice $\sigma = {n_p}^{-1/3}$. For σ smaller than ${n_p}^{-1/3}$, individual particle interactions in the nearfield quickly dominate the dynamics after a few oscillations since the maximal force increases quadratically with smaller σ. Consequently, the frequency of the fitted profile is shifted to a higher value.

Discussion of the Numerical Error

As we have seen in the previous paragraphs, the relative error of the frequencies is well below 1×10^{-2}, usually in order of 1×10^{-3}. However, it is generally hard to reduce the error further, especially for higher frequencies. First of all, the Shannon sampling theorem [89, Section 7.3] limits the maximal frequency present in the discrete spectrum and thus the inter-frequency distance. This influences the approximation quality of the Voigt profile (6.3). Furthermore, the frequencies are derived for the continuous Vlasov–Poisson system, whereas the numerical frequencies are obtained form the dynamics of finitely many particles in the mean field scaling. Even though important properties of the plasma frequency, such as temperature independence and the square root dependency on the number density, hold, some phenomena are only present in the discrete formulation, with the most important being electrons escaping the ions' field. The remaining plasma in Ω is then positively charged, such that our assumption on the neutrality of the plasma does not hold. Furthermore, we compute the full forces on the particles. This means that, in addition to the linear terms that lead to the plasma frequency, the numerically obtained frequencies also include higher order corrections. All effects discussed so far become

[5] This corresponds to four standard deviations of a Gauß distribution.

more dominant for higher frequencies. This is a possible explanation for higher deviations from the prediction of the theory in the high frequency regime.

6.2. Formation of Plasma Sheaths And Mean Field Scaling

Consider a plasma of negatively charged electrons and positively charges ions confined in a finite volume with grounded conducting walls that absorb outflowing particles. The much lighter electrons of high velocity quickly reach the boundary of the volume are absorbed. Thus, a positive net charge near the boundary forms. Because we impose a constant potential on the boundary this gives rise to a negatively charged surface density that counters the positive potential of the ions. Consequently, slower electrons are repelled by the potential barrier established by the negative surface charges. A small area free of negative charge emerges near the boundary. This particular area is called plasma sheath, a term coined by Langmuir [108], and has a diameter of a few Debye lengths [133]. Sheaths were one of the first nonlinear plasma effects studied, see [1] for a historic review, but their measurement is difficult and predictions of simple theoretical models cannot be reproduced in experiments [86]. In case plasma parameters such as density are measured by Langmuir or emissive probes that are placed in direct contact with the plasma, the formation of sheaths needs to be taken into account both for their design and data analysis, see the introductory article [114] and the review articles [33, 139]. The articles [40, 136] discuss the probe design for fusion reactors.

In this section, we use the formation of sheaths as a validation of our discretisation in bounded domains. Since the sheath is only a thin layer near the boundary it is of great importance to accurately compute the electric field in this region. From our numerical study of plasma oscillations in Section 6.1 we know that the particle discretisation together with the hierarchical approximation of the Coulomb forces is able to accurately capture the theoretically predicted frequencies. Example 3.93 shows that the BEM discretisation approximates the electric field with the theoretical rate, in particular very close to the boundary. We thus expect that our method precisely resolves the plasma sheath, i.e. the sudden drop of the electron density near the boundary. Furthermore, we use this numerical example to verify the correct implementation of the mean field scaling in our particle discretisation. In the limit $n_p \to \infty$, the mean field scaling guarantees that the discrete system converges to the Vlasov–Poisson system. For the results of our simulation this means that the shape of the plasma sheath should approach the (unknown) shape described by the solution of the Vlasov–Poisson system when increasing n_p.

In this example, we confine the electron plasma inside the unit sphere with absorbing boundary and impose a zero Dirichlet condition for the potential ϕ. The positively charged ions are modelled by constant background charge density. In nondimensional units the Poisson equation reads

$$\begin{cases} -\Delta\phi = \dfrac{L_0^2}{\lambda_D^2}\left(1 - \dfrac{|B_1(\mathbf{0})|}{n_p}\displaystyle\sum_{j=1}^{n_p}\delta_{\boldsymbol{x}_j}^{\sigma}\right), & \text{in } B_1(\mathbf{0}), \\ \phi = 0 & \text{on } S^2 \end{cases}$$

for n_p electrons and the regularisation parameter σ chosen as a function of n_p,

$$\sigma = \frac{{n_p}^{-1/3}}{100}.$$

The constant charge density on the right hand side is eliminated by noting that

$$\phi_{\text{ion}}(\boldsymbol{x}) = -\frac{L_0^2}{\lambda_D^2}\left(\frac{|\boldsymbol{x}|^2}{6} - \frac{1}{6}\right), \quad \boldsymbol{x} \in \mathbb{R}^3,$$

is the unique solution of

$$\begin{cases} -\Delta\phi_{\text{ion}} = -\dfrac{L_0^2}{\lambda_D^2} & \text{in } B_1(\mathbf{0}), \\ \phi_{\text{ion}} = 0 & \text{on } S^2, \end{cases}$$

so we split ϕ into $\phi = \phi_{\text{ion}} + \phi_{\text{el}}$, where ϕ_{el} describes the electric potential generated by the electrons,

$$\begin{cases} -\Delta\phi_{\text{el}} = \dfrac{L_0^2}{\lambda_D^2}\dfrac{|B_1(\mathbf{0})|}{n_p}\displaystyle\sum_{j=1}^{n_p}\delta_{\boldsymbol{x}_j}^{\sigma}, & \text{in } B_1(\mathbf{0}), \\ \phi_{\text{el}} = 0 & \text{on } S^2. \end{cases} \tag{6.5}$$

For the numerical solution of (6.5) we discretise the unit sphere by a triangular mesh with 5120 elements. The cluster parameter η for the hierarchical approximation is equal to 2 for all particle numbers. The choice of the interpolation order for the different choices of n_p is summarised in Table 6.1. Initially, the particles are uniformly distributed inside the unit ball with velocities

Table 6.1.: Interpolation order of the $\mathcal{H}^2$-approximation for varying particle number in the plasma sheath example.

n_p	m
1×10^3	5
5×10^3	5
1×10^4	7
5×10^4	7
1×10^5	7
5×10^5	9

sampled from a centred Maxwellian with temperature equals one. As characteristic quantities we choose $L_0 = 0.1\,\text{m}$, $k_B T_0 = 1\,\text{eV}$ and $n_0 = 1 \times 10^{13}\,\text{m}^{-3}$. The time evolution of the system is computed with the Störmer–Verlet method using the time step size $\Delta t = 1 \times 10^{-3}$ and 1×10^3 time steps. Figure 6.6 depicts the radial distribution of the particles at the time $t = 1$. Here, the histograms are smoothed by convolution with a triangular kernel function of width $b > 0$,

$$W_b(s) = 1 - |s/b|$$

for $s \in [-b, b]$ and zero else. The bandwidth b depends on the input data and is calculated according to Silverman's rule [141, Chapter 3].

By inspecting the histograms for different number of particles we see that with the exception of $n_p = 1 \times 10^3$ the radial particle distribution follow closely the radial distribution of a uniform distribution on the ball with radius $R = 0.925$,

$$p_R(r) = \frac{3}{R^3}r^2, \quad r \in [0, R].$$

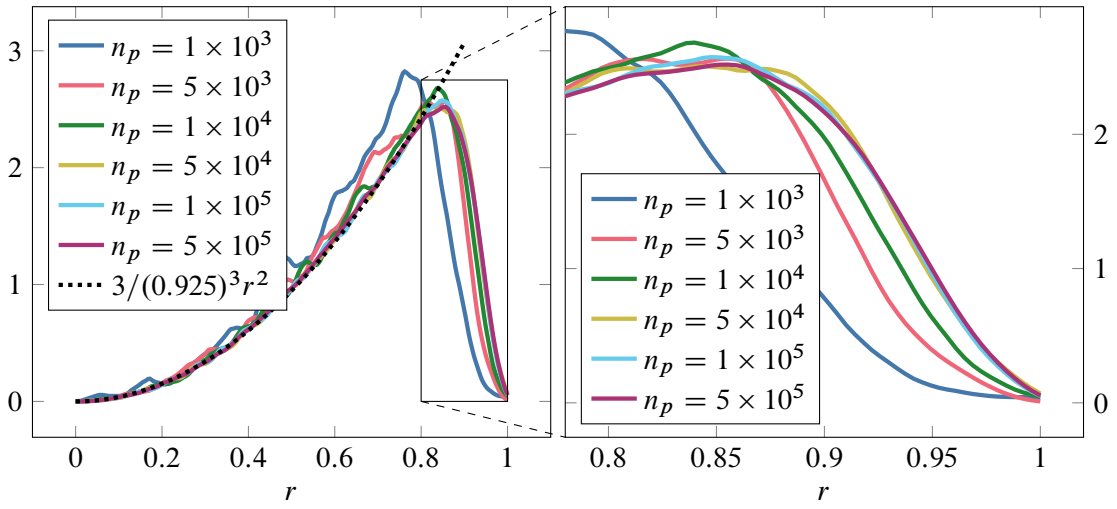

Figure 6.6.: Radial particle density in the unit ball at the time $t = 1$ for varying number of initial particles n_p on the left. The dotted curve is the radial density of the uniform distribution in a ball with radius 0.925. The right panel magnifies the area of the plasma sheath near the boundary.

This is in accordance with the physical theory which predicts that the formation of sheaths is a local phenomenon with little influence from the state of the plasma in the interior. Since we started with a uniform distribution in equilibrium, this state is maintained throughout the time evolution. Close to the boundary the radial density of the particle distribution strongly deviates from the uniform distribution and exhibits the characteristic rapid decay in the region of the sheath. For particle numbers larger than 1×10^4, the different curves are distinguishable only under magnification on the right panel of Fig. 6.6. Here, we observe that for n_p above 1×10^4 the distributions almost agree. This confirms the expected behaviour of the solution for larger n_p in which case we assumed that our results tend to the shape of the plasma sheath predicted by the equation of the mean field limit, the Vlasov–Poisson system.

6.3. Particle Accelerator

As a last numerical example we consider a particle accelerator with mixed boundary conditions for both the particle density function and the electric potential. The accelerator comprises different chambers depicted in Fig. 6.7. The particles enter the first chamber from the left and are mildly accelerated to reach the focal chamber. Here, the potential difference between the beginning and the end of the chamber, together with the homogeneous Neumann condition focuses the particle beam on the narrow accelerator chamber.

With the exception of the inflow part Γ_{in},

$$\Gamma_{\text{in}} = \left\{ \boldsymbol{x} \in \mathbb{R}^3 : x_1 = -1/2,\ {x_2}^2 + {x_3}^2 < 1/4 \right\},$$

the particles are absorbed at the boundary. The total mass of the inflowing particles over a time interval Δt is

$$M_{\text{in}} = |\Gamma_{\text{in}}| \Delta t \int_{\mathbb{R}^3_{\text{in}}} |\boldsymbol{v} \cdot \boldsymbol{n}| f_{\text{in}}(\boldsymbol{v}) \, \mathrm{d}\boldsymbol{v}.$$

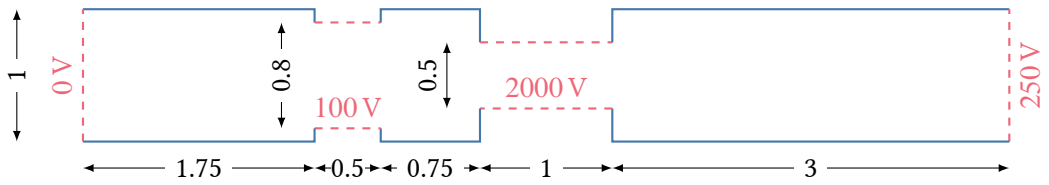

Figure 6.7.: Cross section of the radially symmetric accelerator profile. Dashed lines represent the Dirichlet boundary, solid ones the homogeneous Neumann part. Labels show the length of the corresponding segment, respectively the value of the electric potential on the Dirichlet boundary.

For a Maxwellian inflow condition,

$$f_{\text{in}}(\boldsymbol{v}) = \frac{\rho}{(2\pi T)^{3/2}} \exp\left(-\frac{|\boldsymbol{v}-\boldsymbol{V}|^2}{2T}\right), \quad \boldsymbol{v} \in \mathbb{R}^3_{\text{in}},$$

the integral simplifies to

$$M_{\text{in}} = \rho|\Gamma_{\text{in}}|\Delta t \sqrt{\frac{T}{2\pi}} \left\{\exp\left(-\frac{(\boldsymbol{V}\cdot\boldsymbol{n})^2}{2T}\right) - \sqrt{\pi}\frac{\boldsymbol{V}\cdot\boldsymbol{n}}{\sqrt{2T}} \operatorname{erfc}\left(\frac{\boldsymbol{V}\cdot\boldsymbol{n}}{\sqrt{2T}}\right)\right\},$$

where erfc denotes the complementary error function,

$$\operatorname{erfc}(z) = \frac{2}{\sqrt{\pi}} \int_z^\infty \exp(-\zeta^2)\,\mathrm{d}\zeta.$$

The total number of inflowing particles per time step is chosen to match the inflowing mass. For a given particle weight $w = |\Omega|/n_p$[6] the number of inflow particles n_{in} is the closest integer to the quotient M_{in}/w.[7] The positions and velocities of the n_{in} inflow particles are sampled according to f_{in}. Since f_{in} is independent of time and space, this amounts to generate the velocity according to a Maxwell distribution on $\mathbb{R}^3_{\text{in}}$ and the positions according to a uniform distribution on Γ_{in}. For the latter, we exploit that Γ_{in} is the union of triangles.

6.1 Lemma *Let $T_1, \dots, T_n$ be pairwise disjoint surface triangles that comprise Γ_{in}. For random variables $\boldsymbol{X}_1, \dots, \boldsymbol{X}_n$, where $\boldsymbol{X}_k$ is uniformly distributed on T_k, and a discrete random variable N with values in $\{1, \dots, n\}$ and density vector*

$$\left(\frac{|T_1|}{|\Gamma_{in}|}, \dots, \frac{|T_n|}{|\Gamma_{in}|}\right),$$

that is independent of $(\boldsymbol{X}_1, \dots, \boldsymbol{X}_n)$, the random variable $\boldsymbol{X}_N$ is uniformly distributed on Γ_{in}.

[6] Here, n_p does not refer to the actual number of particles but steers the granularity of the overall approximation. The actual number of particles is determined by the boundary conditions, in particular absorption. However, we can expect this number to have the same magnitude as n_p.

[7] A stochastic model of the inflow condition is a Markovian queue with an exponentially distributed waiting time $\Delta t/n_{\text{in}}$, so that the number of inflowing particles per time interval is Poisson distributed with parameter n_{in} [21, Chapter 14]. Since the Poisson distribution is infinitely divisible [140, pp. 342 f.], the cumulative distribution function is well approximated by that of normal distribution with mean n_{in} and standard deviation $\sqrt{n_{\text{in}}}$ for large n_{in}. The error is uniformly bounded by $\mathcal{O}\big(1/\sqrt{n_{\text{in}}}\big)$ owing to the Berry–Esseen theorem [140, p. 374]. Even for a moderate number of $n_{\text{in}} = 1 \times 10^4$, 99.85 % of the inflowing particles lie in the interval $\big[n_{\text{in}} - 3\sqrt{n_{\text{in}}}, n_{\text{in}} + 3\sqrt{n_{\text{in}}}\big] = [9700, 10\,300]$. Therefore, the deviation around the mean is too small to affect the qualitative results of this section.

Proof. Let P denote the probability measure on the joint probability space of $(\boldsymbol{X}_1, \dots, \boldsymbol{X}_n)$ and N. For a Borel subset $A \subseteq \Gamma_{\text{in}}$ we have, owing to the independence of N and $(\boldsymbol{X}_1, \dots, \boldsymbol{X}_n)$,

$$P[\boldsymbol{X}_N \in A] = \sum_{k=1}^{n} P[\boldsymbol{X}_k \in A \cap T_k, N = k] = \sum_{k=1}^{n} \frac{|A \cap T_k|}{|T_k|} \frac{|T_k|}{|\Gamma_{\text{in}}|} = \frac{|A|}{|\Gamma_{\text{in}}|},$$

showing that $\boldsymbol{X}_N$ is uniformly distributed on Γ_{in}. ∎

Thus, generating a sample of a uniformly distributed random variable on Γ_{in} reduces to the generation of a uniform sample on a single triangle. This can be done via rejection sampling: Starting with a uniform sampling on the unit square $[0, 1]^2$, we only accept points inside the lower triangle and then transform this point to the physical boundary Γ by the affine parametrisation. Finally, the positions are updated by the given velocity and a time step uniformly distributed on $(0, \Delta t)$ to reflect that we compute the total inflow over a time interval of length Δt during that particles may enter the domain at any time.

Fig. 6.8 shows the two-dimensional electron density at $t = 0.5$ for

$$n_p = 1 \times 10^6, \quad \Delta t = 1 \times 10^{-2},$$

and a surface mesh with 4496 triangles. In total, 788 822 particles are inside the accelerator. The values of the characteristic quantities are

$$L_0 = 0.1\,\text{m}, \quad n_0 = 1 \times 10^{12}\,\text{m}^{-3}, \quad k_B T_0 = 10\,\text{eV}.$$

Initially, we start in vacuum with particles entering the domain through Γ_{in} with temperature $T = 1$ and velocity $\boldsymbol{V} = (1, 0, 0)^\top$. The fully three-dimensional distribution at $t = 0.5$ is

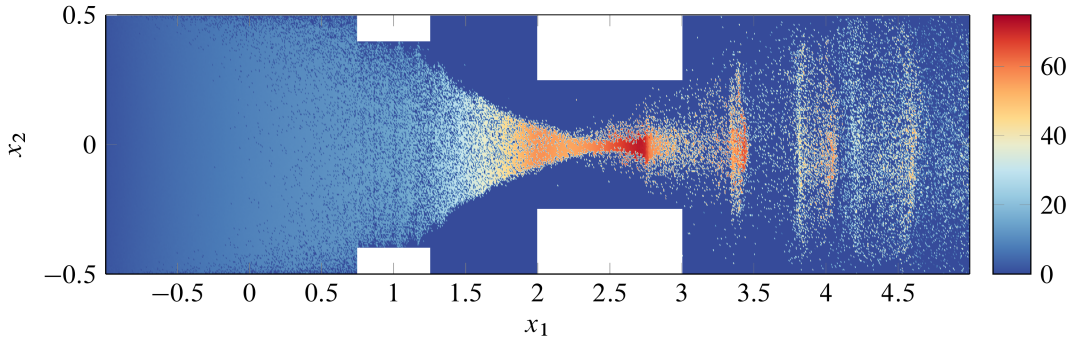

Figure 6.8.: Integrated particle distribution along the x_3-axis in the accelerator at $t = 0.5$. The colour indicates their speed.

depicted in Fig. 6.9. We see that the accelerator works as expected. The wide particle beam is focused on the centre of the accelerator at $x_1 = 2.5$ where the particles reach their maximal speed. Afterwards, the beam widens because of the repulsive Coulomb force between the electrons. They leave the accelerator to the right with a higher velocity than they entered it.

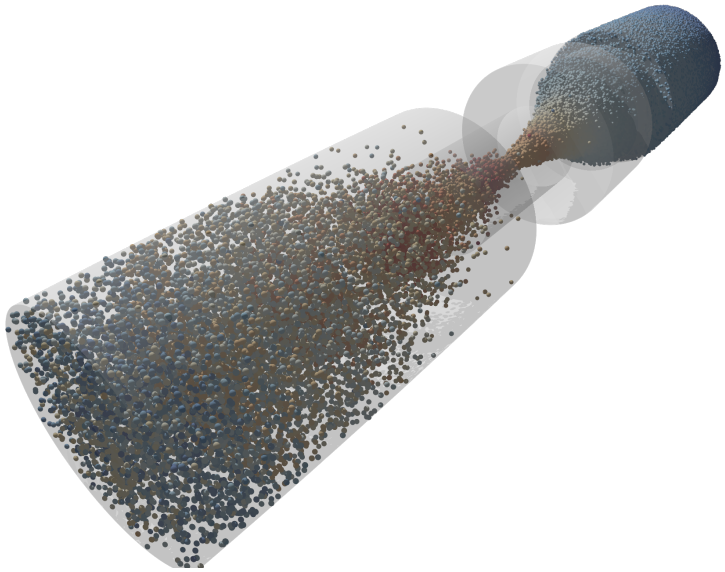

Figure 6.9.: Distribution of the particles inside the accelerator at $t = 0.5$. The colour mapping is the same as in Fig. 6.8.

7. Conclusion

> Wer das kapiert hat, den versteht bald keiner mehr.[1]
>
> *(Peter Rühmkopf [137])*

In this thesis, we have employed boundary integral equations to gain new theoretical results on the oscillation of plasmas and to construct a numerical method for the Vlasov–Poisson system that allows for the precise evaluation of the electric field generated by the particles. The approximate electric field is always an exact solution to Gauß' law of electrostatics. Hence, the long-range character of the Coulomb forces between the particles of the plasma is preserved on the discrete level. This is one reason for the very good performance of our method. The second one is the absence of a volume mesh and a discretisation of the boundary only. On the computational side, the number of unknowns is reduced by several orders of magnitude. This allows us to simulate a three-dimensional particle accelerator of complex geometry with relatively few unknowns. Moreover, the pointwise error of the electric field decays linearly with the number of mesh elements, a scaling that is not achieved by typical finite difference or finite element methods. With our discretisation we are furthermore able to analytically compute the electric field, thus we do not need to use quadrature for the evaluation of the surface integrals. This is particularly important in the vicinity of the boundary, where the contribution of the surface potentials is most relevant.

The analytic computation of the electric field is a key element in our study of plasma oscillations as it allows us to accurately compute the eigenfrequencies for arbitrarily shaped plasmas. Among others, our computations have shown the linear instability of the oscillations in case of a torus. This example is highly relevant in practice. In conjunction with an external magnetic field it may serve as a model for plasma in a fusion reactor. It would be interesting to study the influence of linear instability on the one hand and of the possible nonlinear stabilisation mechanism on the other hand. The example of the cylinder of finite height justifies the assumption of an oscillating plasma column of infinite height in the design of probes such as the plasma absorption probe. For most parts of the cylinder, the eigenfrequencies resemble that of an infinite cylinder. It is only in the corners of the cylinder that the eigenfrequencies significantly differ from the idealised values and where the smallest squared frequency becomes negative. This is also of mathematical interest as it tells us that the question of the concavity of the Newton potential is related to the smoothness and curvature of the boundary. Our result concerning the local concavity of the Newton potential is a first step into this direction. When using plasma oscillations as a test case for numerical methods, domains with constant frequencies are of great interest. We have proven that one important domain with constant frequency is the general ellipsoid, generalising previously known results. A more general classification classification of those domains with constant frequency remains an open research question.

The use of boundary integral equations is not limited to bounded domains. Since our method only relies on the traces of the electric potential on the boundary, a simple change of its orientation

[1] "Whoever understands this will soon no longer be understood by anyone."

suffice to solve the problem in unbounded domains. This applies to problems that are naturally posed in unbounded domains such as the modelling of a plasma propulsion engine or where the region of interest is much smaller than the surrounding walls, e.g. surface modification of thin layers or the formation of sheaths around probes.

Our strategy to express the electric field by boundary integral is also applicable to other models for plasma dynamics. As one important example we mention gyrokinetic models, where the three-dimensional Poisson equation degenerates in the presence of a strong external magnetic field $\boldsymbol{B}$ to two-dimensional Poisson equations along the magnetic field lines. In order to account for the rapid motion of the particles around the field lines, these models include an averaging over small circles perpendicular to $\boldsymbol{B}$. In our formulation, the numerical solution to the electric potential is represented by harmonic functions or function that are harmonic outside a small set, so these averages are equal to a simple point evaluation almost everywhere by the mean value property. Finally, it is tempting to generalise the use of BEM for the computation of the Lorentz force to Maxwell's equations. So far, most literature is concerned with Maxwell's equations in frequency domain and a treatment in time domain would be a welcome addition.

Appendix

A. Integrals for Example 5.11

For $0 < a \le b \le c$, we set

$$\lambda_\ell = \frac{1}{2}abc \int_0^\infty \frac{1}{\ell^2 + s} \frac{1}{\sqrt{(a^2+s)(b^2+s)(c^2+s)}}\,\mathrm{d}s, \quad \ell \in \{a, b, c\}.$$

To calculate these integrals we use *Table of Integrals, Series and Products* by Gradshteyn and Ryzhik [69]. First, we treat the case $a < b < c$. The integrals [69, 3.133 (6), (12), (18)] read

$$\int_{\widetilde{u}}^\infty \frac{1}{\sqrt{(x-\widetilde{a})^3(x-\widetilde{b})(x-\widetilde{c})}}\,\mathrm{d}x = \frac{2}{(\widetilde{b}-\widetilde{a})\sqrt{\widetilde{a}-\widetilde{c}}}\mathrm{E}(\widetilde{\nu},\widetilde{q}) + \frac{2}{\widetilde{a}-\widetilde{b}}\sqrt{\frac{\widetilde{u}-\widetilde{b}}{(\widetilde{u}-\widetilde{a})(\widetilde{u}-\widetilde{c})}}, \quad [\widetilde{u} > \widetilde{a} > \widetilde{b} > \widetilde{c}],$$

$$\int_{\widetilde{u}}^\infty \frac{1}{\sqrt{(x-\widetilde{a})(x-\widetilde{b})^3(x-\widetilde{c})}}\,\mathrm{d}x = \frac{2\sqrt{\widetilde{a}-\widetilde{c}}}{(\widetilde{a}-\widetilde{b})(\widetilde{b}-\widetilde{c})}\mathrm{E}(\widetilde{\nu},\widetilde{q}) - \frac{2}{(\widetilde{b}-\widetilde{c})\sqrt{\widetilde{a}-\widetilde{c}}}\mathrm{F}(\widetilde{\nu},\widetilde{q}) - \frac{2}{\widetilde{a}-\widetilde{b}}\sqrt{\frac{\widetilde{u}-\widetilde{a}}{(\widetilde{u}-\widetilde{b})(\widetilde{u}-\widetilde{c})}}, \quad [\widetilde{u} \ge \widetilde{a} > \widetilde{b} > \widetilde{c}],$$

$$\int_{\widetilde{u}}^\infty \frac{1}{\sqrt{(x-\widetilde{a})(x-\widetilde{b})(x-\widetilde{c})^3}}\,\mathrm{d}x = \frac{2}{(\widetilde{b}-\widetilde{c})\sqrt{\widetilde{a}-\widetilde{c}}}\Big(\mathrm{F}(\widetilde{\nu},\widetilde{q}) - \mathrm{E}(\widetilde{\nu},\widetilde{q})\Big), \quad [\widetilde{u} \ge \widetilde{a} > \widetilde{b} > \widetilde{c}],$$

where

$$\widetilde{\nu} = \arcsin\sqrt{\frac{\widetilde{a}-\widetilde{c}}{\widetilde{u}-\widetilde{c}}}, \quad \widetilde{q} = \sqrt{\frac{\widetilde{b}-\widetilde{c}}{\widetilde{a}-\widetilde{c}}}.$$

With the choice $\widetilde{a} = -a^2$, $\widetilde{b} = -b^2$, $\widetilde{c} = -c^2$ and $\widetilde{u} = 0$ we get

$$\begin{aligned}
\lambda_a &= \frac{1}{b^2-a^2}\left(b^2 - \frac{abc}{\sqrt{c^2-a^2}}\mathrm{E}(\vartheta,\nu)\right),\\
\lambda_b &= \frac{1}{b^2-a^2}\left(\frac{abc}{\sqrt{c^2-a^2}}\left\{\frac{c^2-a^2}{c^2-b^2}\mathrm{E}(\vartheta,\nu) - \frac{b^2-a^2}{c^2-b^2}\mathrm{F}(\vartheta,\nu)\right\} - a^2\right),\\
\lambda_c &= \frac{1}{b^2-a^2}\frac{b^2-a^2}{c^2-b^2}\frac{abc}{\sqrt{c^2-a^2}}\Big(\mathrm{F}(\vartheta,\nu) - \mathrm{E}(\vartheta,\nu)\Big),
\end{aligned}$$

where

$$\vartheta = \arcsin\frac{\sqrt{c^2-a^2}}{c}, \quad \nu = \sqrt{\frac{c^2-b^2}{c^2-a^2}}.$$

For an oblate ellipsoid of revolution, $a < b = c$,

$$\begin{aligned}\lambda_\ell &= \frac{1}{2}ac^2 \int_0^\infty \frac{1}{s+\ell^2}\frac{1}{(s+c^2)\sqrt{s+a^2}}\,\mathrm{d}s \\ &= ac^2 \int_a^\infty \frac{1}{(t^2+\ell^2-a^2)(t^2+c^2-a^2)}\,\mathrm{d}t \\ &= ac^2 \int_0^\infty \frac{1}{(t^2+2at+\ell^2)(t^2+2at+c^2)}\,\mathrm{d}t, \quad \ell \in \{a,c\}.\end{aligned}$$

For $\ell = a$, we decompose the integrand,

$$\begin{aligned}\lambda_a &= \frac{ac^2}{c^2-a^2}\int_0^\infty \frac{1}{(t+a)^2} - \frac{1}{t^2+2at+c^2}\,\mathrm{d}t \\ &= \frac{ac^2}{c^2-a^2}\left(\frac{1}{a} - \frac{1}{\sqrt{c^2-a^2}}\left\{\frac{\pi}{2} - \arctan\frac{a}{\sqrt{c^2-a^2}}\right\}\right) \\ &= \frac{1}{1-a^2/c^2}\left(1 - \frac{a/c}{\sqrt{1-a^2/c^2}}\operatorname{arccot}\frac{a/c}{\sqrt{1-a^2/c^2}}\right).\end{aligned}$$

To calculate λ_c, we use [69, 3.252 (1)],

$$\int_0^\infty \frac{1}{(\widetilde{a}x^2+2\widetilde{b}x+\widetilde{c})^n}\,\mathrm{d}x = \frac{(-1)^{n-1}}{(n-1)!}\frac{\partial^{n-1}}{\partial\widetilde{c}^{n-1}}\left[\frac{1}{\sqrt{\widetilde{a}\widetilde{c}-\widetilde{b}^2}}\operatorname{arccot}\frac{\widetilde{b}}{\sqrt{\widetilde{a}\widetilde{c}-\widetilde{b}^2}}\right], \qquad [\widetilde{a}>0,\ \widetilde{a}\widetilde{c}>\widetilde{b}^2], \tag{A.1}$$

which yields, with $n = 2, \widetilde{a} = 1, \widetilde{b} = a, \widetilde{c} = c^2$,

$$\begin{aligned}\lambda_c &= \frac{a}{2(c^2-a^2)}\left(\frac{c^2}{\sqrt{c^2-a^2}}\operatorname{arccot}\frac{a}{\sqrt{c^2-a^2}} - a\right) \\ &= \frac{1}{2(1-a^2/c^2)}\left(\frac{a/c}{\sqrt{1-a^2/c^2}}\operatorname{arccot}\frac{a/c}{\sqrt{1-a^2/c^2}} - \frac{a^2}{c^2}\right).\end{aligned}$$

The last case of interest is that of a prolate ellipsoid of revolution, $a = b < c$,

$$\begin{aligned}\lambda_\ell &= \frac{1}{2}a^2c \int_0^\infty \frac{1}{s+\ell^2}\frac{1}{(s+a^2)\sqrt{s+c^2}}\,\mathrm{d}s \\ &= a^2c \int_c^\infty \frac{1}{(t^2+\ell^2-c^2)(t^2+a^2-c^2)}\,\mathrm{d}t \\ &= a^2c \int_0^\infty \frac{1}{(t^2+2ct+\ell^2)(t^2+2ct+a^2)}\,\mathrm{d}t, \quad \ell \in \{a,c\}.\end{aligned}$$

To compute λ_a, we first note that (A.1) can used in the case $\widetilde{a}\widetilde{c} < \widetilde{b}^2$. Since

$$-\mathrm{i}\,\mathrm{arccot}(-\mathrm{i}\,z) = \operatorname{acoth} z, \quad z \in \mathbb{R},$$

we have

$$\int_0^\infty \frac{1}{(\widetilde{a}x^2 + 2\widetilde{b}x + \widetilde{c})^n}\,\mathrm{d}x = \frac{(-1)^{n-1}}{(n-1)!}\frac{\partial^{n-1}}{\partial \widetilde{c}^{n-1}}\left[\frac{1}{\sqrt{\widetilde{b}^2 - \widetilde{a}\widetilde{b}}}\operatorname{acoth}\frac{\widetilde{b}}{\sqrt{\widetilde{b}^2 - \widetilde{a}\widetilde{c}}}\right], \\ [\widetilde{a} > 0,\ \widetilde{b}^2 > \widetilde{a}\widetilde{c}].$$

Thus, with $n = 2, \widetilde{a} = 1, \widetilde{b} = c, \widetilde{c} = a^2$,

$$\begin{aligned}\lambda_a &= \frac{c}{2(c^2 - a^2)}\left(c - \frac{a^2}{\sqrt{c^2 - a^2}}\operatorname{acoth}\frac{c}{\sqrt{c^2 - a^2}}\right) \\ &= \frac{1}{2(1 - a^2/c^2)}\left(1 - \frac{a^2/c^2}{\sqrt{1 - a^2/c^2}}\operatorname{acoth}\frac{1}{\sqrt{1 - a^2/c^2}}\right).\end{aligned}$$

By the use of the partial fraction decomposition, we compute

$$\begin{aligned}\lambda_c &= \frac{a^2 c}{c^2 - a^2}\int_0^\infty \frac{1}{t^2 + 2ct + a^2} - \frac{1}{(t + c)^2}\,\mathrm{d}t \\ &= \frac{a^2 c}{c^2 - a^2}\left(\int_0^\infty \frac{1}{t^2 + 2ct + a^2}\,\mathrm{d}t - \frac{1}{c}\right) \\ &= \frac{a^2 c}{c^2 - a^2}\left(\frac{1}{\sqrt{c^2 - a^2}}\operatorname{acoth}\frac{c}{\sqrt{c^2 - a^2}} - \frac{1}{c}\right) \\ &= \frac{1}{1 - a^2/c^2}\left(\frac{a^2/c^2}{\sqrt{1 - a^2/c^2}}\operatorname{acoth}\frac{1}{\sqrt{1 - a^2/c^2}} - \frac{a^2}{c^2}\right).\end{aligned}$$

References

There are no answers, only cross-references.

(Norbert Wiener)

[1] J. E. Allen. "The plasma-sheath boundary: its history and Langmuir's definition of the sheath edge". In: *Plasma Sources Sci. T.* 18.014004 (2009) (cit. on p. 83).

[2] L. Anderegg et al. "Laser cooling of optically trapped molecules". In: *Nat. Phys.* 14 (2018), pp. 890–893 (cit. on p. 77).

[3] V. I. Arnol'd. *Mathematical Methods of Classical Mechanics*. Springer-Verlag, 1989 (cit. on pp. 11, 76).

[4] D. E. Baldwin and D. W. Ignat. "Resonant Absorption in Zero-Temperature Nonuniform Plasma". In: *Phys. Fluids* 12 (1969), pp. 697–701 (cit. on p. 74).

[5] J. Barnes and P. Hut. "A hierarchical $O(N \log N)$ force-calculation algorithm". In: *Nature* 324 (1986), pp. 446–449 (cit. on p. 55).

[6] M. Bebendorf. "Approximation of Boundary Element Matrices". In: *Numer. Math.* 86 (2000), pp. 565–589 (cit. on p. 58).

[7] M. Bebendorf. *Hierarchical Matrices*. Springer-Verlag, 2008 (cit. on pp. 55, 58, 60, 76).

[8] M. Bebendorf and S. Rjasanow. "Adaptive Low-Rank Approximation of Collocation Matrices". In: *Computing* 70 (2003), pp. 1–24 (cit. on p. 58).

[9] C. K. Birdsall and A. B. Langdon. *Plasma Physics via Computer Simulation*. Taylor & Francis, 1991 (cit. on p. 4).

[10] G. Birkhoff, M. H. Schultz, and R. S. Varga. "Piecewise Hermite Interpolation in One and Two Variables with Applications to Partial Differential Equations". In: *Numer. Math.* 11 (1968), pp. 232–256 (cit. on p. 41).

[11] A. Bogaerts, E. Neyts, R. Gijbels, and J. van der Mullen. "Gas discharge plasmas and their applications". In: *Spectrochim. Acta B* 57 (2002), pp. 609–658 (cit. on p. ix).

[12] D. Bohm and E. P. Gross. "Theory of Plasma Oscillations. A. Origin of Medium-Like Behavior". In: *Phys. Rev.* 75 (1949), pp. 1851–1864 (cit. on p. 63).

[13] D. Bohm and E. P. Gross. "Theory of Plasma Oscillations. B. Excitation and Damping of Oscillations". In: *Phys. Rev.* 75 (1949), pp. 1864–1876 (cit. on p. 63).

[14] L. Boltzmann. *Populäre Schriften*. Johann Ambrosius Barth Verlag, 1905 (cit. on p. 75).

[15] S. Börm. *Efficient Numerical Methods for Non-local Operators*. European Mathematical Society, 2010 (cit. on pp. 55, 59, 62).

[16] S. Börm and J. Bendoraityte. "Distributed $\mathcal{H}^2$-matrices for non-local operators". In: *Comput. Visual. Sci.* 11 (2008), pp. 237–249 (cit. on p. 75).

[17] S. Börm and S. Christophersen. “Approximation of integral operators by Green quadrature and nested cross approximation”. In: *Numer. Math.* 133 (2016), pp. 409–442 (cit. on p. 58).

[18] S. Börm and L. Grasedyck. “Hybrid cross approximation of integral operators”. In: *Numer. Math.* 101 (2005), pp. 221–249 (cit. on p. 58).

[19] S. Börm and L. Grasedyck. “Low-Rank Approximation of Integral Operators by Interpolation”. In: *Computing* 72 (2004), pp. 325–332 (cit. on p. 58).

[20] S. Börm, M. Löhndorf, and J. M. Melenk. “Approximation of Integral Operators by Variable-Order Interpolation”. In: *Numer. Math.* 99 (2005), pp. 605–643 (cit. on p. 58).

[21] P. Brémaud. *Markov Chains. Gibbs Fields, Monte Carlo Simulation and Queues*. 2nd ed. Springer-Verlag, 2020 (cit. on p. 86).

[22] S. C. Brenner and L. R. Scott. *The Mathematical Theory of Finite Element Methods*. 3rd ed. Springer-Verlag, 2008 (cit. on pp. 46, 47, 51).

[23] H. Brezis. *Functional Analysis, Sobolev Spaces and Partial Differential Equations*. Springer-Verlag, 2011 (cit. on p. 32).

[24] N. G. de Bruijn. *Asymptotic Methods In Analysis*. North-Holland Publishing, 1958. Reprinted by Dover, 2003 (cit. on p. 60).

[25] H. Bucerius. “Zu Dirichlets Ableitung des Ellipsoidpotential”. In: *Astron. Nachr.* 279 (1951), pp. 238–240 (cit. on p. 72).

[26] A. A. Buchheit and T. Keßler. *Singular Euler–Maclaurin expansion*. 2020. arXiv: 2003.12422 [math.NA]. In review (cit. on p. xi).

[27] A. A. Buchheit and T. Keßler. *Singular Euler–Maclaurin expansion on multidimensional lattices on multidimensional lattices*. 2021. arXiv: 2102.10941 [math.NA]. In review (cit. on p. xi).

[28] L. D. Carr, D. DeMille, R. V. Krems, and J. Ye. “Cold and ultracold molecules: science, technology and applications”. In: *New. J. Phys.* 11.055049 (2009) (cit. on p. 77).

[29] J. Carrier, L. Greengard, and V. Rokhlin. “A fast adaptive multipole algorithm for particle simulations”. In: *SIAM J. Sci. Statist. Comput.* 9 (1988), pp. 669–686 (cit. on p. 58).

[30] J. Céa. “Approximation variationelle des problèmes aux limites”. In: *Ann. I. Fourier* 14 (1964), pp. 345–444 (cit. on p. 41).

[31] F. F. Chen. *Introduction to Plasma Physics and Controlled Fusion*. Springer-Verlag, 2016 (cit. on pp. 1, 78).

[32] H. Cheng, L. Greengard, and V. Rokhlin. “A Fast Adaptive Multipole Algorithm in Three Dimensions”. In: *J. Comput. Phys.* 155 (1999), pp. 468–498 (cit. on p. 58).

[33] B. E. Cherrington. “The Use of Electrostatic Probes for Plasma Diagnostics—A Review”. In: *Plasma Chem. Plasma P.* 2 (1982), pp. 113–140 (cit. on p. 83).

[34] A. J. Christlieb, R. Krasny, J. P. Verboncoeur, J. W. Emhoff, and I. D. Boyd. “Grid-free plasma simulation techniques”. In: *IEEE T Plasma Sci* 34 (2006), pp. 149–165 (cit. on p. 4).

[35] E. W. Cliver. “The 1859 space weather event: Then and now”. In: *Adv. Space Res.* 38 (2006), pp. 119–129 (cit. on p. ix).

[36] E. W. Cliver and L. Svalgaard. “The 1859 Solar-Terrestrial Disturbance and the Current Limits of Extreme Space Weather Activity”. In: *Sol. Phys.* 224 (2004), pp. 407–422 (cit. on p. ix).

[37] M. Costabel. “Boundary Integral Operators on Lipschitz Domains: Elemtary Results”. In: *SIAM. J. Math. Anal.* 19 (1988), pp. 613–625 (cit. on pp. 33, 37).

[38] J. Dawson. “One-Dimensional Plasma Model”. In: *Phys. Fluids* 5 (1962), pp. 445–459 (cit. on p. 3).

[39] J. M. Dawson. “Particle simulation of plasmas”. In: *Rev. Mod. Phys.* 55 (1983), pp. 403–447 (cit. on p. 3).

[40] H. De Oliveira et al. “Langmuir probe electronics upgrade on the tokamak à configuration variable”. In: *Rev. Sci. Instrum.* 90.083502 (2019) (cit. on p. 83).

[41] D.-A. Deckert and V. Hartenstein. “On the initial value formulation of classical electrodynamics”. In: *J. Phys. A* 49 (2016), p. 445202 (cit. on p. 8).

[42] P. Degond. “Local Existence of Solutions of the Vlasov–Maxwell Equations and Convergence to Vlasov–Poisson Equations for Infinite Ligth Velocity”. In: *Math. Meth. in the Appl. Sci.* 8 (1986), pp. 533–558 (cit. on p. 2).

[43] P. Degond and P.-A. Raviat. “An analysis of the Darwin model of approximation to Maxwell’s equations”. In: *Forum Math.* 4 (1992), pp. 13–44 (cit. on p. 2).

[44] G. Dimarco and L. Pareschi. “Numerical methods for kinetic equations”. In: *Acta Numer.* 23 (2014), pp. 369–520 (cit. on p. 3).

[45] A. B. de Dios, J. A. Carrillo, and C.-W. Shu. “Discontinuous Galerkin Methods for the Multi-Dimensional Vlasov–Poisson Problem”. In: *Math. Mod. Meth. Appl. S.* 22.12 (2012), p. 1250042 (cit. on p. 3).

[46] W. Dittrich. *On Dirichlet’s Derivation of the Ellipsoid Potential*. 2016. arXiv: `1609.04709 [physics.hist-ph]` (cit. on p. 72).

[47] D. H. E. Dubin. “Displacement eigenmodes for cold-fluid and warm-fluid magnetized plasma oscillations”. In: *Phys. Plasmas* 12.042107 (2005) (cit. on p. 78).

[48] D. H. E. Dubin. “Effect of correlations on the thermal equilibrium and normal modes of a non-neutral plasma”. In: *Phys. Rev. E* 53 (1996), pp. 5268–5290 (cit. on pp. 63, 70).

[49] D. H. E. Dubin and T. M. O’Neil. “Trapped nonneutral plasmas, liquids, and crystals (the thermal equilibrium states)”. In: *Rev. Mod. Phys.* 71 (1999), pp. 87–172 (cit. on p. 77).

[50] V. Ehrlacher and D. Lombardi. “A dynamical adaptive tensor method for the Vlasov–Poisson system”. In: *J. Comput. Phys.* 339 (2017), pp. 285–306 (cit. on p. 3).

[51] L. Einkemmer. “Semi-Lagrangian Vlasov simulation on GPUs”. In: *Comput. Phys. Commun.* 254.107351 (2020) (cit. on p. 3).

[52] L. Einkemmer and C. Lubich. “A Low-Rank Projector-Splitting Integrator for the Vlasov–Poisson Equation”. In: *SIAM J. Sci. Comput.* 40 (2018), B1330–B1360 (cit. on p. 3).

[53] L. Einkemmer and A. Ostermann. “Convergence Analysis for Strang Splitting for Vlasov-Type Equations”. In: *SIAM J. Numer. Anal.* 52 (2014), pp. 140–155 (cit. on p. 3).

[54] A. Ern and J.-L. Guermond. *Theory and Practice of Finite Elements*. Springer-Verlag, 2010 (cit. on pp. 46, 47).

[55] L. C. Evans. *Partial Differential Equations*. 2nd ed. AMS, 2010 (cit. on pp. 10, 27).

[56] R. P. Feynman, R. B. Leighton, and M. Sands. *The Feynman Lectures on Physics*. New Millennium Edition. Basic Books, 2011 (cit. on p. 8).

[57] L. E. Fraenkel. *An Introduction to Maximum Principles and Symmetry in Elliptic Problems*. Cambridge University Press, 2000 (cit. on p. 27).

[58] F. G. Friedlander and M. Joshi. *Introduction to The Theory of Distributions*. 2nd ed. Cambridge University Press, 1998 (cit. on pp. 17, 23).

[59] N. Fusco, F. Maggi, and A. Pratelli. "The sharp quantitative isoperimetric inequality". In: *Ann. Math.* 168 (2008), pp. 941–980 (cit. on p. 68).

[60] P.-H. Fuss. *Correspondance Mathématiques et Physique. Tome II*. The St. Petersburg Academy, 1843 (cit. on p. 1).

[61] E. Gagliardo. "Caratterizzazioni delle tracce sulla frontiera relative ad alcune classi di funzioni in n variabili". In: *Rend. Semin. Mat. Univ. Padova* 27 (1957), pp. 284–305 (cit. on p. 33).

[62] K. Ganguly and H. D. Victory Jr. "On the convergence of particle methods for multidimensional Vlasov-Poisson systems". In: *SIAM J. Numer. Anal.* 26 (1989), pp. 249–288 (cit. on p. 13).

[63] C. F. Gauß. *Allgemeine Lehrsätze in Beziehung auf die verkehrten Verhältnisse des Quadrats der Entfernung wirkenden Anziehungs- und Abstossungs-Kräfte*. Weidmann, 1840 (cit. on p. 24).

[64] C. Geiger and C. Kanzow. *Theorie und Numerik restringierter Optimierungsaufgaben*. Springer-Verlag, 2002 (cit. on p. 66).

[65] I. M. Gel′fand and G. E. Shilov. *Generalized Functions. Volume 1: Properties and Operations*. AMS Chelsea Publishing, 1964 (cit. on p. 20).

[66] I. M. Gel′fand and G. E. Shilov. *Generalized Functions. Volume 4: Applications of Harmonic Analysis*. AMS Chelsea Publishing, 1964 (cit. on p. 32).

[67] D. Gilbarg and N. S. Trudinger. *Elliptic Partial Differential Equations of Second Order*. Reprint of the 1998 Edition. Springer, 2001 (cit. on pp. 5, 67).

[68] D. L. Goodstein and J. R. Goodstein. *Feynman's Lost Lecture. The Motion of Planets Around the Sun*. Vintage, 1997 (cit. on p. 76).

[69] I. S. Gradshteyn and I. M. Ryzhik. *Table of Integrals, Series and Products*. Ed. by A. Jeffrey and D. Zwillinger. 7th ed. Academic Press, 2007 (cit. on pp. 93, 94).

[70] L. Greengard and V. Rokhlin. "A fast algorithm for particle simulations". In: *J. Comput. Phys.* 73 (1987), pp. 325–348 (cit. on pp. 55, 58).

[71] L. Greengard and V. Rokhlin. "A new version of the Fast Multipole Method for the Laplace equation in three dimensions". In: *Acta Numer.* 6 (1997), pp. 229–269 (cit. on p. 58).

[72] L. Greengard and V. Rokhlin. "The rapid evaluation of potential fields in three dimensions". In: *Vortex Methods*. Ed. by C. Anderson and C. Greengard. Springer-Verlag, 1988, pp. 121–141 (cit. on pp. 55, 58).

[73] P. Grisvard. *Elliptic Problems in Nonsmooth Domains*. Pitman Publishing, 1985 (cit. on p. 30).

[74] W. Gropp, T. Hoefler, R. Thakur, and E. Lusk. *Using Advanced MPI. Modern Features of the Message-Passing Interface*. The MIT Press, 2014 (cit. on p. 75).

[75] W. Gropp, E. Lusk, and A. Skjellum. *Using MPI. Portable Parallel Programming with the Message-Passing Interface*. 3rd ed. The MIT Press, 2014 (cit. on p. 75).

[76] G. Grubb. *Distributions and Operators*. Springer-Verlag, 2009 (cit. on pp. 17, 24).

[77] R. Grzibovskis. *Integralgleichungen und Randelemente*. Lecture Notes. Department of Mathematics, Saarland University, 2017 (cit. on pp. 53, 71).

[78] W. Hackbusch. *Hierarchical Matrices: Algorithms and Analysis*. Springer-Verlag, 2015 (cit. on pp. 55, 62).

[79] W. Hackbusch and Z. P. Nowak. "On the Fast Matrix Multiplication in the Boundary Element Method by Panel Clustering". In: *Numer. Math.* 54 (1989), pp. 463–491 (cit. on p. 55).

[80] E. Hairer, C. Lubich, and G. Wanner. *Geometric Numerical Integration*. 2nd ed. Springer-Verlag, 2006 (cit. on p. 76).

[81] R. R. Hall and W. K. Hayman. "A Problem in the Theory of Subordination". In: *J. Anal. Math.* 60 (1993), pp. 99–111 (cit. on p. 68).

[82] R. R. Hall, W. K. Hayman, and A. W. Weitsman. "On Asymmetry and Capacity". In: *J. Anal. Math.* 56 (1991), pp. 87–123 (cit. on p. 68).

[83] R. E. Heath, I. M. Gamba, P. J. Morrison, and C. Michler. "A discontinuous Galerkin method for the Vlasov–Poisson system". In: *J. Comput. Phys.* 231 (2012), pp. 1140–1174 (cit. on p. 3).

[84] M. Hénon. "Vlasov Equation?" In: *Astron. Astrophys.* 114 (1982), pp. 211–212 (cit. on p. 2).

[85] A. Henrot, C. Nitsch, P. Salani, and C. Trombetti. "Optimal Concavity of the Torsion Function". In: *J. Optim. Theory. Appl.* 178 (2018), pp. 26–35 (cit. on p. 70).

[86] N. Hershkowitz. "Sheaths: More complicated than you think". In: *Phys. Plasmas* 12.055502 (2005) (cit. on p. 83).

[87] L. Hörmander. *The Analysis of Linear Partial Differential Operators I*. 2nd ed. Springer-Verlag, 1990 (cit. on pp. 17, 23).

[88] G. C. Hsiao and W. L. Wendland. "Boundary Integral Equations Recast as Pseudodifferential Equations". In: *Rend. Accad. Naz. Sci. XL Mem. Mat. Appl. (5)* XXX (124 2006), pp. 29–48 (cit. on p. 26).

[89] A. Iske. *Approximation Theory and Algorithms for Data Analysis*. Springer-Verlag, 2018 (cit. on p. 82).

[90] M. Izadi. "Parallel $\mathcal{H}$-matrix arithmetic on distributed-memory systems". In: *Comput. Visual. Sci.* 15 (2012), pp. 87–97 (cit. on p. 75).

[91] P. Jordan and J. von Neumann. "On Inner Products In Linear, Metric Spaces". In: *Ann. Math.* 36 (1935), pp. 719–723 (cit. on p. 18).

[92] A. U. Kennington. "Power Concavity and Boundary Value Problems". In: *Indiana Univ. Math. J.* 34 (1985), pp. 687–704 (cit. on p. 69).

[93] T. Keßler and S. Rjasanow. “Fully conservative spectral Galerkin-Petrov method for the inhomogeneous Boltzmann equation”. In: *Kinet. Relat. Mod.* 12 (2019), pp. 507–549 (cit. on p. xi).

[94] T. Keßler and S. Rjasanow. “Limit model for the Vlasov–Maxwell system with strong magnetic fields via gyroaveraging”. In: *St. Petersb. Math. J.* 32 (2021), pp. 753–765 (cit. on p. xi).

[95] T. Keßler, S. Rjasanow, and S. Weißer. “Vlasov–Poisson System Tackled by Particle Simulation Utilizing Boundary Element Methods”. In: *SIAM J. Sci. Comput.* 42 (2020), B299–B326 (cit. on pp. xi, 4).

[96] U. Kogelschatz. “Dielectric-barrier Discharges: Their History, Discharge Physics, and Indistridual Applications”. In: *Plasma Chem. Plasma P.* 23.1 (2003) (cit. on p. ix).

[97] H. Kokura, K. Nakamura, I. P. Ghanashev, and H. Sugai. “Plasma Absorption Probe for Measuring Electron Density in an Environment Soiled with Processing Plasmas”. In: *Jpn. Appl. Phys.* 38 (1999), pp. 5262–5266 (cit. on p. 63).

[98] K. Königsberger. *Analysis 2*. 5th ed. Springer-Verlag, 2004 (cit. on p. 57).

[99] K. Kormann. “A Semi-Lagrangian Vlasov Solver in Tensor Train Format”. In: *SIAM J. Sci. Comput.* 37 (2015), B613–B632 (cit. on p. 3).

[100] K. Kormann, K. Reuter, and M. Rampp. “A massively parallel semi-Lagrangian solver for the six-dimensional Vlasov–Poisson equation”. In: *Int. J. High Perform. C.* 33 (2019), pp. 924–947 (cit. on p. 3).

[101] K. Kormann and E. Sonnendrücker. “Sparse Grids for the Vlasov–Poisson Equation”. In: *Sparse Grids and Applications – Stuttgart 2014*. Ed. by J. Garcke and Pflüger. D. Springer-Verlag, 2016, pp. 163–190 (cit. on p. 3).

[102] R. Kriemann. “Parallel $\mathcal{H}$-Matrix Arithmetics on Shared Memory Systems”. In: *Computing* 74 (2005), pp. 273–297 (cit. on p. 75).

[103] H.-J. Kunze. *Introduction to Plasma Spectroscopy*. Springer-Verlag, 2009 (cit. on p. ix).

[104] L. Landau. “On the Vibrations of the Electronic Plasma”. In: *J. Phys.* 10 (1946), pp. 25–34 (cit. on p. 63). Reprinted on pp. 96–117 in: D. Ter Haar. *Men of Physics: L. D. Landau. Volume 2: Thermodynamics, Plasma Physics and Quantum Mechanics*. Pergamon Press, 1969.

[105] L. D. Landau and E. M. Lifshitz. *The Classical Theory of Fields. Course of Theoretical Physics. Volume 2*. Fourth Revised English Edition. Butterworth-Heinemann, 1975 (cit. on p. 7).

[106] S. Lang. *Real and Functional Analysis*. Springer-Verlag, 1993 (cit. on p. 27).

[107] T. K. Langin, G. M. Gorman, and T. C. Killian. “Laser cooling of ions in a neutral plasma”. In: *Science* 363 (2019), pp. 61–64 (cit. on p. 77).

[108] I. Langmuir. “Positive Ion Currents from the Positive Column of Mercury Arcs”. In: *Science* 58 (1502 1923), pp. 290–291 (cit. on p. 83).

[109] M. Lapke, T. Mussenbrock, and R. P. Brinkmann. “The multipole resonance probe: A concept for simultaneous determination of plasma density, electron temperature and collision rate in low-pressure plasmas”. In: *Appl. Phys. Lett.* 93.051502 (2008) (cit. on p. 63).

[110] D. Lazarovici and P. Pickl. “A mean field limit for the Vlasov–Poisson system”. In: *Arch. Ration. Mech. Anal.* 225 (2017), pp. 1201–1231 (cit. on pp. 14, 26).

[111] É Madaule, M. Restilli, and E. Sonnendrücker. “Energy conserving discontinuous Galerkin spectral element method for the Vlasov–Poisson system”. In: *J. Comput. Phys.* 279 (2014), pp. 261–288 (cit. on p. 3).

[112] R. de la Madrid. “Quantum Mechanics in Rigged Hilbert Space Language”. PhD thesis. University of Valladolid, 2001 (cit. on p. 32).

[113] W. C. H. McLean. *Strongly Elliptic Systems and Boundary Integral Equations*. Cambridge University Press, 2000 (cit. on pp. 28, 36).

[114] R. L. Merlino. “Understanding Langmuir probe current-voltage characteristics”. In: *Am. J. Phys.* 75 (2007), pp. 1078–1085 (cit. on p. 83).

[115] N. G. Meyers and J. Serrin. “H = W”. In: *PNAS USA* 51 (1964), pp. 1055–1056 (cit. on p. 29).

[116] S. E. Mikhailov. “Traces, extensions and co-normal derivatives for elliptic systems on Lipschitz domains”. In: *J. Math. Anal. Appl.* 378 (2011), pp. 324–342 (cit. on p. 33).

[117] I. Milch. *Successful second round of experiments with Wendelstein 7-X*. 2018. URL: https://www.ipp.mpg.de/4550215/11_18 (visited on 2021-07-15) (cit. on p. x).

[118] T. Möller and B. Trumbore. “Fast, Minimum Storage Ray-Triangle Intersection”. In: *J. Graph. Tools* 2 (1997), pp. 21–28 (cit. on p. 76).

[119] H. Neunzert. “An introduction to the nonlinear Boltzmann-Vlasov equation”. In: *Kinetic theories and the Boltzmann equation. Montecatini, Italy 1981)*. Ed. by C. Cercignani. Springer-Verlag, 1984, pp. 60–110 (cit. on pp. 13, 26).

[120] H. Neunzert and J. Wick. “Die Approximation der Lösung von Integro-Differentialgleichungen durch endliche Punktmengen”. In: *Numerische Behandlung nichtlinearer Integrodifferential- und Differentialgleichungen. Oberwolfach, Germany 1973*. Ed. by R. Ansorge and W. Törnig. Springer-Verlag, 1974, pp. 275–290 (cit. on p. 13).

[121] H. Neunzert and J. Wick. “Die Theorie der asymptotischen Verteilung und die numerische Lösung von Integrodifferentialgleichungen”. In: *Numer. Math.* 21 (1973), pp. 234–243 (cit. on p. 13).

[122] H. Neunzert and J. Wick. “Theoretische und numerische Ergebnisse zur nichtlinearen Vlasov-Gleichung”. In: *Numerische Lösung nichtlinearer partieller Differential- und Integrodifferentialgleichungen. Oberwolfach, Germany 1971*. Ed. by R. Ansorge and W. Tönig. Springer-Verlag, 1972, pp. 159–185 (cit. on p. 13).

[123] D. R. Nicholson. *Introduction to Plasma Theory*. Wiley, 1983 (cit. on p. 11).

[124] J. O’Rourke. *Computational Geometry in C*. 2nd ed. Cambridge University Press, 1998 (cit. on p. 76).

[125] G. Of, O. Steinbach, and W. L. Wendland. “Applications of a fast multipole Galerkin in boundary element method in linear elastostatics”. In: *Comput. Vis. Sci.* 8 (2005), pp. 201–209 (cit. on p. 58).

[126] G. Of, O. Steinbach, and W. L. Wendland. “The fast multipole method for the symmetric boundary integral formulation”. In: *IMA J. Numer. Anal.* 26 (2006), pp. 272–296 (cit. on p. 58).

[127] A. Pais. *Inward Bound. Of Matter and Forces in the Physical World*. Oxford University Press, 1986 (cit. on p. ix).

[128] M. Palmroth et al. "Vlasov methods in space physics and astrophysics". In: *Living Rev. Comput. Astrophys.* 4.1 (2018) (cit. on p. 3).

[129] W. K. H. Panofksy and M. Phillips. *Classical Electricity and Magnetism*. 2nd ed. Addison-Wesley, 1962. Reprinted by Dover, 2005 (cit. on pp. 8, 50).

[130] R. van der Pas, E. Stotzer, and C. Terboven. *Using OpenMP—The Next Step. Affinity, Accelerators, Tasking and SIMD*. The MIT Press, 2017 (cit. on p. 75).

[131] H. Rademacher. "Über partielle und totale Differenzierbarkeit von Funktionen mehrer Variablen und über die Transformation der Doppelintegrale". In: *Math. Ann.* 79 (1919), pp. 340–359 (cit. on pp. 31, 32).

[132] W. Reichel. "Characterization of balls by Riesz-potentials". In: *Ann. Mat. Pura Appl.* 188 (2009), pp. 235–245 (cit. on p. 27).

[133] K.-U. Riemann. "The Bohm criterion and sheath formation". In: *J. Phys. D: Appl. Phys.* 24 (1991), pp. 493–518 (cit. on p. 83).

[134] S. Rjasanow and O. Steinbach. *The Fast Solution of Boundary Integral Equations*. Springer-Verlag, 2007 (cit. on pp. 55, 58).

[135] W. Rudin. *Functional Analysis*. 2nd ed. McGraw-Hill, 1991 (cit. on p. 17).

[136] L. Rudischhauser et al. "The Langmuir probe system in the Wendelstein 7-X test divertor". In: *Rev. Sci. Instrum.* 91.063505 (2020) (cit. on p. 83).

[137] P. Rühmkopf. *Außer der Liebe nichts*. Rowohlt Taschenbuch Verlag, 1986 (cit. on p. 89).

[138] S. A. Sauter and C. Schwab. *Boundary Element Methods*. Springer-Verlag, 2011 (cit. on pp. 26, 36, 46).

[139] J. P. Sheehan and N. Hershkowitz. "Emissive probes". In: *Plasma Sources Sci. Technol.* 20.063001 (2011) (cit. on p. 83).

[140] A. N. Shiryavev. *Probability*. 2nd ed. Springer-Verlag, 1996 (cit. on pp. 13, 86).

[141] B. W. Silverman. *Density Estimation for Statistics and Data Analysis*. Chapman & Hall, 1986 (cit. on p. 84).

[142] A. Sommerfeld. *Vorlesungen über Theoretische Physik. Band I — Mechanik*. Verlag Harri Deutsch, 1994 (cit. on p. 63).

[143] E. Sonnendrücker, J. Roche, P. Bertrand, and A. Ghizzo. "The Semi-Lagrangian Method for the Numerical Resolution of the Vlasov Equation". In: *J. Comput. Phys.* 149 (1999), pp. 201–220 (cit. on p. 3).

[144] M. Spivak. *Physics for Mathematicians. Mechanics I*. Publish or Perish, 2010 (cit. on p. 76).

[145] H. Spohn. *Dynamics of Charged Particles and Their Radiation Field*. Cambridge University Press, 2004 (cit. on pp. 7, 8).

[146] H. Spohn. *Large Scale Dynamics of Interacting Particles*. Springer-Verlag, 1991 (cit. on p. 11).

[147] E. Stein. *Intégrales singulières et fonctions différentiables de plusieurs variables*. Lecture Notes. Publications Mathématiques d'Orsay, 1967 (cit. on p. 30).

[148] O. Steinbach. *Numerical Approximation Methods for Elliptic Boundary Value Problems*. Springer-Verlag, 2008 (cit. on pp. 37, 46–48, 50).

[149] S. Steinerberger. *Concavity of Solutions of the Poisson Equation In Sufficiently Round Planar Domains*. 2021. arXiv: 2103.17187 [math.AP] (cit. on p. 70).

[150] R. Stevenson and R. van Venetië. "Uniform preconditioners for problems of negative order". In: *Math. Comp.* 89 (2020), pp. 645–674 (cit. on pp. 50, 52).

[151] R. Stevenson and R. van Venetië. "Uniform preconditioners for problems of positive order". In: *Comput. Math. Appl.* 79 (2020), pp. 3516–3530 (cit. on pp. 49, 52).

[152] G. Strang. "Variational Crimes in the Finite Element Method". In: *The Mathematical Foundations of the Finite Element Method with Applications to Partial Differential Equations*. Ed. by A. K. Aziz. Academic Press, 1972, pp. 689–710 (cit. on p. 40).

[153] Texas Advanced Computing Center. *Stampede2 User Guide*. 2020. URL: https://portal.tacc.utexas.edu/user-guides/stampede2 (visited on 2020-12-11) (cit. on p. 3).

[154] P. Tittmann. *Einführung in die Kombinatorik*. 2nd ed. Springer-Verlag, 2014 (cit. on pp. 57, 60).

[155] P. Tol. *Colour Schemes*. Technical Note. SRON, 2018 (cit. on p. 107).

[156] L. Tonks and I. Langmuir. "Oscillations in Ionized Gases". In: *Phys. Rev.* 33 (1929), pp. 195–210 (cit. on pp. 7, 63, 73).

[157] Traueranzeige. Otto Braun. In: *Saarbrücker Zeitung* (2020-07-29) (cit. on p. x).

[158] F. Trèves. *Basic Linear Partial Differential Equations*. Academic Press, 1975. Reprinted by Dover, 2006 (cit. on pp. 17, 23, 24).

[159] F. Trèves. *Topological Vector Spaces, Distributions and Kernels*. Academic Press, 1967. Reprinted by Dover, 2006 (cit. on p. 17).

[160] J. P. Verboncoeur. "Particle simulation of plasmas: review and advances". In: *Plasma Phys. Contr. F.* 47 (2005), A231–A260 (cit. on p. 3).

[161] G. Verchota. "Layer Potentials and Regularity for the Dirichlet Problem for Laplace's Equation in Lipschitz Domains". In: *J. Funct. Anal.* 59 (1984), pp. 572–611 (cit. on p. 47).

[162] W. Voigt. "Über das Gesetz der Intensitätsverteilung innerhalb der Linien eines Gasspektrums". In: *Sitzber. Bayr. Akad.* 1912 (cit. on pp. 78, 79).

[163] Th. von Woedtke, S. Reuter, K. Masur, and K.-D. Weltmann. "Plasmas for medicine". In: *Phys. Rep.* 530 (2013), pp. 291–320 (cit. on p. ix).

[164] S. Wollman. "On the approximation of the Vlasov-Poisson system by particle methods". In: *SIAM J. Numer. Anal.* 37 (2000), pp. 1369–1398 (cit. on p. 13).

[165] A. Woo. "Fast Ray-Box Intersection". In: *Graphics Gems*. Ed. by A. S. Glassner. Academic Press, 1990, pp. 395–396 (cit. on p. 76).

The fonts used are Linux Libertine, Linux Biolinum, Inconsolata and MathTime Professional 2. This thesis was typeset with LuaLaTeX and the KOMA-Script class scrbook. The colour scheme for the plots is taken from Tol [155] and is specifically designed for colour-blind people.